Influence of Freeze-Thaw Dynamics and Spatial Contributions on Geochemical Loading from a Low Sulfide Waste-Rock Pile

by

Sean Andrew Sinclair

A thesis
presented to the University of Waterloo
in fulfilment of the
thesis requirement for the degree of
Master of Science
in
Earth Sciences

Waterloo, Ontario, Canada, 2014

Author's Declaration

I hereby declare that I am the sole author of this thesis. This is a true copy of the thesis, including any required final revisions, as accepted by my examiners.

I understand that my thesis may be made electronically available to the public.

Abstract

An experimental waste-rock pile (50m x 60m x 15m, 0.053 wt. % S) was constructed at the Diavik Diamond Mine, in the Northwest Territories, Canada to evaluate the generation of acid-rock drainage and the seasonal and annual release of various metals in drainage leachate. A dense internal instrumentation network enabled well resolved observations of temperature, air content, water content, fluid flow, microbiology, mineralogy and geochemistry within the waste-rock pile. Water samples were collected from soil water solution samplers (SWSSs) to measure core pore-water characteristics, from 4 m^2 to 16 m^2 scale basal collection lysimeters (BCLs) to measure core leachate characteristics, and from basal drains (3000 m^2 basal area) to measure aggregated leachate characteristics. Monitoring of pore-water geochemistry within the core of the test pile indicated an evolving weathering front characterized by changes in predominant acid-consuming mineral-dissolution reactions. Initially, acid neutralization occurred through dissolution of carbonate minerals. A subsequent decline in pH was limited by acid neutralization through dissolution of Al- and Fe-bearing minerals. This lower pH environment was accompanied by increasing concentrations of SO_4, Al, Fe, Ni, Co, Cu, Zn, Cd, Ca, Mg, K, Na and Si. Annual drainage cycles in the core of the test pile were characterized by distinct, high concentration 'spring flushes' followed by a steady decline of all dissolved constituents with minimums prior to freeze-up. Core trends were typical of freshets observed in polar environments and primarily explained by a combination of fluid residence time and the build-up of oxidation products over the winter. The opposite trend was observed in the aggregated pile drainage, whereby early-season low-concentration leachate was derived from snowmelt and batter flow and late-season high-concentration leachate was dominated by contributions from the core of the pile. Thermal data demonstrating the annual freeze-thaw cycle was used to delineate

core and batter subsystems within the pile. Mean annual solute concentrations and geochemical speciation modelling results revealed two different environments within these subsystems. Concentrations in the core of the test pile were 2.5 to 8.5 times greater than concentrations in the batter. Dilution through snowmelt contributions and shorter flow pathways were expected to control solute concentrations in the batter subsystem. Aggregated basal leachate loading exhibited a linear annual increase for all ARD reaction products, with the maximum annual release observed in 2012. Between 2007 and 2012 core flow accounted for 13 % of the total drainage volume; whereas 35 to 51 % of major and trace metal loads were attributed to this zone. Parameter correlation analysis and core contribution estimates were used to identify common source minerals for elements and infer mechanisms controlling the mobility of dissolved metals (sorption, co-precipitation and precipitation-dissolution). By 2012, the release of pyrrhotite oxidation products from the < 5 mm reactive fraction of waste rock reached as high as 5.1 %, 9.0 %, 7.2 % and < 0.1 % for S, Ni, Co and Fe respectively. The results of this study indicate that a comprehensive understanding of thermal cycling is imperative when estimating seasonal and annual releases of weathering products from waste rock. Observations of active zone dynamics and the temporal and spatial evolution of waste rock drainage loading recognized in this study will assist in the advancement of reactive transport models describing ARD in cold climates.

Acknowledgments

First and foremost I would like to acknowledge my supervisor, Dr. David Blowes for his extraordinary guidance and the wealth of knowledge he bestowed upon me throughout this journey. To my committee members: Dr. Richard Amos, for his open door and valuable perspective on the Diavik project; and to Dr. Carol Ptacek for her support and encouragement along the way. I would also like to thank Dr. Leslie Smith from the University of British Columbia and Dr. David Sego from the University of Alberta for their constructive comments at critical stages during the formation of my work.

Having joined in on the tail end of a near-decade long multidisciplinary research project, there are countless individuals whose hard work and determination laid the foundation for me to achieve all that was possible. First and foremost, thanks to previous graduate students Brenda Bailey and Stacey Hannam who took me under their wing and brought me up to speed on 'all things Diavik' that predated my arrival. Thanks to previous graduate students Nate Fretz, Nam Pham, Mandy Moore, Ashley Stanton and Steve Momeyer for all their earlier work; and of course thank you to graduate students Lianna Smith, Mike Gupton, Mike Moncur and Matt Neuner for the earliest work and constructing the test piles. I can imagine that was quite the task. Thanks to Jeff Bain for walking me through the Diavik field site early on and answering every question I could think to ask. Thanks to Laura Groza, Joy Hu and Julia Jamieson-Hanes for their hard work behind the scenes in the laboratory. Thanks to Andrew Krentz for fighting the good fight with me this last year. Thanks to Dr. Jeff Langman for his insight into my work and our ongoing collaborative efforts. To the next generation of graduate students: David Wilson, Sivaram Mullapudi, Steve Holland, Colleen Atherton and David Barsi; thanks for your support throughout this last period of my thesis, and good luck in the future. Finally, to the countless co-

ops, the mysterious workhorses of the project who largely remain hidden behind the curtain, we all owe you a grand thanks.

I would like to thank all my fellow graduate students and friends near and far. Thank you for my time outside the office. For all the good times in and around Waterloo. The Grad House. The camping trips. The climbing. The 'book club'. All the music. Really just for all the nights we will never forget and the others we never remembered.

And to Nadine. Thank you for making life awesome along the way. I look forward to our next adventure.

The Diavik Waste Rock Project is a joint research project by the University of Waterloo, the University of British Columbia and the University of Alberta. Funding for this research was provided by: Diavik Diamond Mines Inc.; a grant from the Natural Science and Engineering Research Council of Canada (NSERC) Collaborative Research and Development (CRD) program awarded to David Blowes, Principal Investigator; an award from the Canadian Foundation for Innovation (CFI) Innovation Fund awarded to James Barker, Principal Investigator; the Mine Environment Neutral Drainage (MEND) Program; the International Network for Acid Prevention (INAP); the Northern Scientific Training Program (NSTP); and the Ontario Graduate Scholarship (OGS) program.

Dedication

It is with the utmost gratitude and respect that I dedicate this thesis to those whom I should acknowledge most of all, my parents Andy and Julie. It was your unwavering support in my life's pursuits, academic and occasionally very much otherwise, that led me to this end.

Table of Contents

List of Figures x
List of Tables xiii
Chapter 1: Introduction 1
1.1 Research Objectives and Organization of Thesis 2
1.2 Background on the Problem 3
1.3 Present Research and the Diavik Waste Rock Project 5
Chapter 2: Influence of Freeze-Thaw Dynamics on Internal Geochemical Evolution of Low Sulfide Waste Rock 10
2.1 Executive Summary 11
2.2 Introduction 13
2.2.1 Site Description and Background 15
2.2.2 Test Pile Construction 16
2.3 Methodology 18
2.3.1 Hydrology 18
2.3.2 Geochemical Sampling and Analysis 19
2.3.3 Geochemical Modelling 21
2.3.4 Thermal Regime Monitoring 21
2.3.5 Subsystem Conceptual Model 21
2.3.6 Continuous Core and Total Drainage Geochemistry 22
2.4 Results and Discussion 23
2.4.1 Annual Freeze-Thaw Cycling 23
2.4.2 Pile Wet-up and First Flush of Matrix Pore Water 23
2.4.3 Internal Evolution of Geochemistry 25
2.4.4 Seasonal Variations in Core Geochemistry 30
2.4.5 Spatial Contributions to Drain Geochemistry 36
2.5 Conclusions 39
2.6 Figures 40

Chapter 3: Influence of Spatial Contributions to Geochemical Loading from a Low Sulfide Waste Rock Pile in a Permafrost Environment 53
3.1 Executive Summary 54
3.2 Introduction 56
3.2.1 Site Description and Background 58
3.2.2 Test Pile Construction 59
3.3 Methods 61
3.3.1 Hydrology 61
3.3.2 Geochemical Sampling and Analysis 62
3.3.3 Geochemical Load Estimates 63
3.3.4 Geochemical Modelling 66
3.3.5 Thermal Regime Monitoring 66
3.4 Results and Discussion 67
3.4.1 Water Balance and Method Evaluation 67
3.4.2 Spatial Variability in Waste-Rock Geochemistry 69
3.4.3 Spatial Contributions to Drainage Loading 74
3.4.4 Depletion of Sulfide Minerals 80
3.5 Conclusions 84
3.6 Figures 85
3.7 Tables 92
Chapter 4: Conclusions 103
4.1 Research Summary and Conclusions 104
References 108

List of Figures

Figure 2.1 - Location of the Diavik Diamond Mine on the East Island of Lac de Gras, in the Northwest Territories, Canada (64°29' N; 110°18' W) (from Smith, 2013)..... 40

Figure 2.2 - Instrumentation layout and data sources inside the Type III test pile. Total flow catchment is constrained to the area within the basal drains. 41

Figure 2.3 – Mean annual temperature of the Type III test pile (Image by Nam Pham, 2013).... 42

Figure 2.4 – Annual ground thawing index and ground freezing index for the Type III test pile (Image by Nam Pham, 2013) 43

Figure 2.5 – Freeze-thaw cycle based on mean monthly internal temperature data from 2012. Proposed spatial contributions to basal drain load in the Type III test pile: a) Winter; b) Spring; c) Summer; d) Early fall; e) Late fall. Diagram modified from thermal cross sections by Nam Pham, 2014. 44

Figure 2.6 – Vertical geochemical profiles in the test pile core display yearly mean values with error bars corresponding to the 95 % confidence interval on the mean value. Blasting residual and tracer evolution is consistent with physical observations of the matrix wet-up and the first flush of pore water. 45

Figure 2.7 – Vertical geochemical profiles in the test pile core display yearly mean values with error bars corresponding to the 95 % confidence interval on the mean value. In early years, pH is controlled by carbonate phase buffering to between pH 4.8 – 7.5. Following depletion of available carbonates by 2010, Al-hydroxide phase buffering occurs to between pH 4 – 4.5. Buffering from Al-hydroxide phases is overwhelmed and dissolution of Fe-hydroxide phases (pH 2.4 – 3.5) occurs concurrently with Al phases. Dynamic geochemical equilibrium is reached by 2012..... 46

Figure 2.8 – Vertical geochemical profiles in the test pile core display yearly mean values with error bars corresponding to the 95 % confidence interval on the mean value. Saturation indices for primary mineral phases which potentially control precipitation-dissolution reactions in the test pile core. 47
Figure 2.9 – Vertical geochemical profiles in the test pile core display yearly mean values with error bars corresponding to the 95 % confidence interval on the mean value. Release and accumulation of primary sulfide oxidation products, Ni and SO4, derived from pyrrhotite, and Ca and Mg from carbonate and silicate buffering. The transition to Mg dominated pore-water at depth is explained by an exhaustion of calcite phases and secondary loses of Ca to gypsum precipitation. 48
Figure 2.10 – Annual cycles of core and basal drainage geochemistry. Blue circles represent daily flow weighted mean concentrations from basal drainage network. Red triangles represent daily flow weighted mean concentrations from all currently flowing locations in the core BCL network. 49
Figure 2.11 – Results from 1-D temperature-depth variable sulfate release model (yellow stars), compared with flow weighted mean sulfate concentrations reported in the BCL network in 2011 and 2012 (red circles) and individual BCL sulfate concentrations (open circles). 50
Figure 2.12 – Trumpet diagrams demonstrating the annual freeze-thaw cycle observed in the Type III test pile core temperature (Pham, 2013) 51
Figure 2.13 – Seasonal trends observed in test pile pore-water geochemistry. Different symbols are representative of discrete SWSS locations ranging between 2 m and 9 m depth. Concentration build-up throughout season is primarily attributed to stagnant flow periods, brought on by intervals with minimal rainfall and infiltration. 52

Figure 3.1 – Location of the Diavik Diamond Mine on the East Island of Lac de Gras, in the Northwest Territories, Canada (64°29' N; 110°18' W) (from Smith, 2013). 85
Figure 3.2 – Instrumentation layout and data sources inside the Type III test pile. 86
Figure 3.3 – Daily outflow from the core (grey) and total drainage (black) systems. Highly variable mean ambient air temperature (grey) and stable core basal temperature (black) demonstrate freeze-thaw controls on internal water flow. Red boxes outline time periods when core basal temperatures are above zero. Blue boxes outline time periods when ambient air temperatures are above zero. Results supports core and batter scaling methodology. 87
Figure 3.4 – Internal flow summary for the Type III test pile. Daily flow from the full test pile (black) and the estimated contribution attributed to the core (grey) demonstrate spatial distributions in drainage throughout each year. Cumulative flow split between the core and batter subsystems demonstrate the overall prevalence of water derived from the test pile batter. 88
Figure 3.5 – Estimated infiltration (grey) as a proportion of measured rainfall (black) (dataset from Fretz 2013, updated by Krentz 2014). In general, rainfall events greater than 5 mm result in infiltration. Years with substantial rainfall and infiltration are moderately correlated with years of higher estimated core flow. 89
Figure 3.6 – Select annual box and whisker plots displaying results from saturation index modelling for calcite, gibbsite, ferrihydrite and gypsum from the total drainage (a), core drainage (b) and batter drainage (c) systems. 90
Figure 3.7 – Ni/Co molar ratio relationship over the full pH spectrum demonstrates an apparent retention of Co within the test pile when pH values rise above 5.5. 91

List of Tables

Table 3.1 - Water balance and validation of flow data sources in the Type III test pile. Total infiltration is scaled to each drainage area using infiltration estimates by Fretz (2013), updated by Krentz (2014). Total flow out is measured on site using calibrated tipping buckets (Fretz, 2013). Pore volume flushes are based on pore water being limited to the < 5 mm grain size fraction of waste rock. 92

Table 3.2 – Select results of annual and cumulative flow and loading in total drainage, core drainage and batter drainage systems. Infiltration estimates by Fretz 2013, updated by Krentz 2014..... 93

Table 3.3 – Select results of annual and cumulative core contributions to total drainage flow and loading. Infiltration estimates by Fretz 2013, updated by Krentz 2014..... 94

Table 3.4 – Select results of estimated total, core and batter drainage geochemistry concentrations calculated from annual and cumulative subsystem loading. 95

Table 3.5 – Pearson product-moment correlation analysis in the total drainage system. Significance testing for all results in black are at $P < 0.05$ level. Results in grey show no significant correlation. 96

Table 3.6 – Pearson product-moment correlation analysis in the core drainage system. Significance testing for all results in black are at $P < 0.05$ level. Results in grey show no significant correlation. 97

Table 3.7 – Pearson product-moment correlation analysis in the batter drainage system. Significance testing for all results in black are at $P < 0.05$ level. Results in grey show no significant correlation. 98

Table 3.8 – Full system control level results, modified from Pearson correlation analysis results for each scale of the test pile system (Core-Batter-Total). Results summarize the number of good correlations (> |0.7|) for a given parameter, divided by the total number of possible cases..... 99

Table 3.9 – Cross-environment control level results, modified from Pearson correlation analysis results for each test pile subsystem pair (Core-Batter-Total). Results summarize the number of good correlations (> |0.7|) for a given parameter which are consistent across subsystem environments, as a proportion of the total number of possible cases. 100

Table 3.10 – Estimated total mass of waste rock material, including the total mass of S, Ni, Co and Fe divided into the core, batter and total pile systems. Masses are further defined based on the < 5 mm waste rock fraction, < 50 mm waste rock fraction, and full grain size spectrum waste rock fraction. 101

Table 3.11 – Estimated annual and cumulative release of S, Ni, Co and Fe from the < 5 mm grain size fraction of waste rock. Results are presented as release from the total test pile system, and subdivided into the core and batter subsystems. 102

Chapter 1: Introduction

1.1 Research Objectives and Organization of Thesis

This thesis presents a multi-disciplinary approach to understanding acid rock drainage (ARD) in waste-rock systems. Foundations laid by previous researchers on the subjects of thermal cycling, unsaturated fluid flow, mineralogical characterization and geochemical characterization were built upon to reach the goal of fundamentally conceptualizing and quantifying waste rock drainage in a freeze-thaw governed environment. The contents of this thesis are divided into four chapters. The second and third chapter were prepared as stand-alone journal articles which could be submitted to a peer-reviewed journal. Chapter two examines the current state of the internal geochemical evolution of a 0.053 wt. % S test pile and conceptually evaluates the influence of freeze-thaw dynamics on the seasonal trends observed in the core and total drainage geochemistry. Chapter three quantitatively evaluates spatial contributions to drain loading, identifies varying element source, release and transport mechanisms and estimates the current state of sulfide-mineral depletion through observations of element release in the test pile. Chapter one and four present a global introduction and conclusion respectively.

1.2 Background on Acid Rock Drainage

The production of Acid Rock Drainage (ARD) caused by the oxidation of sulfide minerals can be an unfavourable by-product of some mining operations. During the mining process, often more than 90% of the extracted material is of an inadequate ore grade and defined as waste rock (Jamieson, 2011). This material is stored raw and unprocessed in vast waste-rock stockpiles. Material which is above the economically recoverable grade is processed through a series of steps to remove the desired minerals, with the remainder generally output as a water-rock slurry known as tailings. Tailings material is subsequently stored in engineered tailings impoundments. Environmental exposure of waste rock or tailings with a net acid generation potential can produce acidity through the oxidation of residual sulfide minerals by oxygen and water (Blowes *et al.*, 2003) (equation 1 & 2).

(1) $Pyyrhotite$: $Fe_{1-x}S + \left(2 - \frac{1}{2}x\right) O_2 + xH_2O \rightarrow (1-x)Fe^{2+} + SO_4^{2-} + 2xH^+$

(2) $Pyrite$: $FeS_2(s) + \frac{7}{2}O_2 + H_2O \rightarrow Fe^{2+} + 2SO_4^{2-} + 2H^+$

Fe(II) may be subsequently oxidized producing Fe(III) (equation 3) which can then result in the precipitation of Fe(III) oxyhydroxides, such as ferrihydrite [nominally $5Fe_2O_3 \cdot 9H_2O$] and goethite [αFeOOH] (equation 4) and the production of more acidity.

(3) $Fe^{2+} + \frac{1}{4}O_2 + H^+ \leftrightarrow Fe^{3+} + \frac{1}{2}H_2O$

(4) $Fe^{3+} + 3H_2O \leftrightarrow Fe(OH)_3 + 3H^+$

Fe(III) can also directly contribute to the oxidation of sulfides with emphasis as a major oxidant when pH < 4 (Nordstrom, 1982) (equation 5 and 6).

(5) $Pyrrhotite$: $Fe_{1-x}S\ (s) + (8-2x)Fe^{3+} + 4H_2O \leftrightarrow (9-3x)Fe^{2+} + SO_4^{2-} + 8H^+$

(6) $Pyrite$: $FeS_2(s) + 14Fe^{3+} + 8H_2O \leftrightarrow 15Fe^{2+} + 2SO_4^{2-} + 16H^+$

Drainage water with a declining pH and elevated concentrations of sulfate and various metals can be detrimental to local water resources and the surrounding environment (Blowes *et al.*, 2003). In many cases ARD has the potential to last thousands of years (Nordstrom & Alpers, 1999, Blowes & Jambor, 1990). Eventual remediation of ARD can be expensive and complex; the techniques of which are dictated by a number of environmental and economic factors (Johnson & Hallberg, 2005). Sufficient pre-mining characterization and post-closure projections of site specific physiochemical characteristics are required to achieve acceptable environmental performance in both the short and long term life of a mine (Amoah *et al.*, 2011).

1.3 Present Research and the Diavik Waste Rock Project

Extensive research has taken place to better understand the evolution of ARD in mine tailings (Moncur *et al.*, 2005, Al *et al.*, 1997, Blowes & Jambor, 1990, Lindsay *et al.*, 2009, Blowes *et al.*, 1998). Fewer studies exist which are related exclusively to understanding ARD evolution in waste rock (Smith *et al.*, 2013a, Marescotti *et al.*, 2010, Sracek *et al.*, 2004, Stockwell *et al.*, 2006); however studies related to mine tailings and associated column studies (Jurjovec *et al.*, 2002) provide a valuable comparison. Jurjovec et al., (2002) described the common sequence of acid-neutralization reactions which occur within mine tailings impoundments. pH plateaus representative of the following precipitation-dissolution reactions were recognized as: calcite (pH 6.5 - 7.5), siderite (pH 4.8 - 6.3), $Al(OH)_3$ (pH 4.0 - 4.5), $Fe(OH)_3$ (2.5 - 3.5) and Al_2SiO_5 (continuous at pH > 1.3). The capacity of each phase to neutralization acidity in the system depends on their relative distribution, availability and overall abundance in the material. Kinetically restrained, albeit continuous, aluminum silicate weathering (Gunsinger *et al.*, 2006b) results in limited acid neutralization from these phases. The effects of trace metal sorption on Fe- and Al-hydroxide phases and the strong dependence therein on pH conditions has been described in detail (Balistrieri *et al.*, 2003, Tonkin *et al.*, 2002, Paulson & Balistrieri, 1999, Dzombak & Morel, 1990). Results highlight the importance of these phases for the retention of trace metals in ARD systems, particularly when pH > 4.5.

A strategic approach to limit the oxidation rate of sulfide minerals in waste rock and tailings is to limit oxygen in the system. Submarine tailings disposal inherently limits oxygen diffusion at depth due to the water overlying the tailings mass. In the case of waste rock, the large grain-size range and volume of material involved generally makes submarine disposal unfeasible. Incorporating a cover system consisting of a till-like material with decreased air

permeability has been shown to significantly reduce oxygen diffusion and oxidation in waste-rock piles (Yanful *et al.*, 1993). In cold climates, incorporating a thermal cover and allowing tailings or waste rock to freeze through the upward aggradation of permafrost is considered one of the most advantageous approaches to decrease oxidation (Kyhn & Elberling, 2001).

A major challenge when predicting ARD in waste rock is the evaluation of fluid flow. Waste-rock piles often have extremely heterogeneous internal structures. Fluid flow is governed by complex unsaturated flow processes. The degree of heterogeneity, the spatial variability in grain-size distribution, and fluctuating rates of infiltration at the upper boundary control whether the flow system is driven by matrix or macropore flow. The presence of macropores can lead to significant variations in the timing and magnitude of solute loads (Beven & Germann, 1982) where contributions from macropore flow are generally connected to lower mass loading events when water largely by-passes grains rather than reacting. Macropores are expected to have a less significant impact in dryer soils, with increasing contributions as the soil matrix becomes saturated (Shipitalo & Edwards, 1996). Waste-rock flow systems are often controlled by a combination of both macropore and matrix flow processes, which exposes issues regarding the practicality of using models to effectively represent these systems (Nichol *et al.*, 2005). Comprehensive field scale studies have highlighted the challenges associated with the characterization of unsaturated flow in coarse, heterogeneous material and the particular difficulty of correlating flow data with geochemical results (Stockwell *et al.*, 2006). Despite a considerable research base on water flow in unsaturated waste-rock piles, very little is known about the hydraulic behaviour of waste-rock systems in cold climates and the impact freeze-thaw conditions have on water flow.

The impact of freeze-thaw cycles on the release of dissolved constituents from waste rock is a relatively new field and observations have been limited to the characterization of runoff (Søndergaard *et al.*, 2007, Søndergaard *et al.*, 2008). Geochemical trends characteristic of a high concentration spring flush followed by an abrupt or gradual decline in concentrations have been observed in these studies as well as at naturally exposed sulfide ore deposits (Søndergaard *et al.*, 2012). It is evident that freeze-thaw cycling has a strong effect on these annual geochemical trends; however the relative impact of the governing processes is hard to define. Laboratory studies have highlighted that the rate of sulfide oxidation is directly related to system temperature as described by a modified Arrhenius equation (Ahonen & Tuovinen, 1992). High ion concentrations in ARD can lower the freezing temperature of pore-water, which could subsequently allow sulfide oxidation to persist at sub-zero temperatures (Dawson & Morin, 1996). Laboratory studies have demonstrated that sulfide oxidation can occur at temperatures as low as -11 ^{o}C, whereby the persistence of sulfur oxidizing microbes is sustained within thin intergranular water films and pockets of liquid water which do not freeze due to the elevated solute concentrations characteristic of ARD (Elberling, 2005). Sustained winter oxidation with low or no flow conditions can lead to a build-up of oxidation products in solution. The subsequent remobilization of high concentration water at thaw can result in a release of substantial solute loads over short periods of time (Søndergaard *et al.*, 2007). Similar phenomena have been observed in arid climates where large solute loads are released following dry periods with limited water flow (Anawar, 2013).

Accurate prediction of the frequency and magnitude of high concentration flushes in ARD systems is challenging during the stages of mine closure planning. Cold climates appear to favour conditions which produce irregular and sizeable loading fluctuations and current research

lacks a comprehensive understanding of these processes in cold-climate waste rock. In addition, ecosystems in isolated cold climates are often very pristine and tend to be very sensitive, therefore the influence from mining operations can quickly become a major factor impacting overall ecosystem health.

Fundamentally, the goal of the Diavik Waste Rock Project is to provide a comprehensive basis for describing the geochemical, hydrological, microbiological, gas transport and thermal behaviour observed in waste rock in a freeze-thaw affected permafrost environment. An extension of this goal is to assess the utility and practicality of up-scaling laboratory tests to forecast full scale waste rock drainage characteristics. Present research at the Diavik site has focused on the initial characterization of the primary physiochemical waste rock pile properties (Bailey *et al.*, 2013, Chi *et al.*, 2013, Neuner *et al.*, 2013, Pham *et al.*, 2013, Smith *et al.*, 2013b, Smith *et al.*, 2013a, Amos *et al.*, 2009, Fretz, 2013, Hannam, 2012, Jambor, 1997) and early stage development of interpretative models for scaling and predicting waste rock behavior (Bailey, 2013, Pham, 2013).

The Diavik research site provides a unique opportunity to study the evolution of fresh waste rock as it evolves over annual freeze-thaw cycles. The dense internal instrumentation network at the Diavik site provides temporally and spatially resolved observations of temperature, air content, geochemistry and water flow within the waste-rock pile. The objective of this thesis is to approach ARD processes in waste-rock systems through a multidisciplinary approach; applying the essential foundations of previous Diavik waste-rock research to understand and quantify the direct and indirect effects freeze-thaw cycling has on the internal geochemical evolution, the spatial contributions to drain loading and the depletion of source minerals in the Diavik waste-rock system. An appreciation of the influence of freeze-thaw

cycling in waste rock will provide a strong foundation to assist in future prediction, up-scaling, and reactive transport modelling of waste-rock leachate in permafrost environments.

Chapter 2: Influence of Freeze-Thaw Dynamics on Internal Geochemical Evolution of Low Sulfide Waste Rock

2.1 Executive Summary

Between 2005 and 2006, a 15 m high heavily instrumented experimental waste rock pile (0.053 wt. % S) was constructed at the Diavik diamond mine, in the Northwest Territories, Canada to improve upon the understanding of physicochemical processes observed in waste rock. Ongoing monitoring since 2007 at the Diavik research site provided a unique opportunity to study the evolution of fresh run-of-mine waste rock as it evolved over six annual freeze-thaw cycles. The dense internal instrumentation network enabled well resolved observation of various physiochemical parameters across several scales within the waste rock pile. Samples were collected from soil water solution samplers to measure core pore-water properties, twelve 4 m^2 to 16 m^2 scale basal collection lysimeters to measure core basal leachate properties, and basal drains to measure aggregated total pile leachate properties. By 2012, monitoring of pore-water geochemistry within the core structure of the test pile revealed an apparent steady state with respect to a downward weathering front represented by a flush of pre-existing blasting residuals and applied tracers, a declining pH, a stepwise progression and subsequent equilibrium with acid-neutralizing phases (depletion of available carbonates; equilibrium with respect to aluminium hydroxide phases and subsequent iron(III) hydroxide phases) and concordant release of SO_4, major cations (Ca, Mg, K, Na, Si) and trace metals (Al, Fe, Ni, Co, Cu, Zn). Distinct, high concentration 'spring flushes' characteristic of drainage in northern environments and primarily explained by a combination of fluid residence time and the build-up of oxidation products over the winter were released from core drainage each season. Following the initial flush a steady decline in the concentrations of all dissolved constituents occurred; with distinct minimums prior to freeze-up. The opposite trend was observed in the cumulative pile drainage, whereby early season leachate dominated by snowmelt and batter flow had low concentrations

and late season leachate, dominated by contributions from the core of the pile (indicated by season-end merging of core and cumulative drainage geochemistry), had higher concentrations. This study demonstrates that northern waste rock pile drainage geochemistry is primarily controlled by freeze-thaw cycling and the resulting modification of core and batter subsystem contributions to total drainage. Results indicate that a comprehensive understanding of thermal cycling in waste-rock piles is an important component of temporal predictions of drainage water compositions based on up-scaling or reactive transport modelling.

2.2 Introduction

One of the most significant environmental obstacles facing many mining operations is the production of acid rock drainage (ARD) through the oxidation of sulfide minerals. During the mining process, rock is excavated from the earth on such a massive scale that the quantity of material involved is unmatched in magnitude by any other process in the world (ICOLD, 1996). Often more than 90% of the mined material is below the economically recoverable grade, and as such is stored indefinitely in vast stockpiles (Jamieson, 2011). Environmental exposure of waste rock with a net acid generation potential can result in drainage water with a declining pH and elevated concentrations of sulfate and various metals (Blowes *et al.*, 2003). The production of ARD can be detrimental to the environment and has the potential to last thousands of years (Nordstrom & Alpers, 1999, Blowes & Jambor, 1990).

The release and transport of oxidation products, progression of acid neutralization and pH as well as the appearance and evolution of major cations and trace metals in mine tailings (Moncur *et al.*, 2005, Al *et al.*, 1997, Blowes & Jambor, 1990, Lindsay *et al.*, 2009, Blowes *et al.*, 1998), and waste rock (Smith *et al.*, 2013a, Marescotti *et al.*, 2010, Sracek *et al.*, 2004, Stockwell *et al.*, 2006), is well documented. However, annual drainage dynamics resulting from the influence of freeze-thaw cycling in a permafrost environment are poorly understood.

The purpose of the Diavik waste rock project is to provide an improved scientific basis from which the geochemical, hydrological, microbiological, gas transport and thermal behaviours observed in waste rock in permafrost environments can be described. An extension of this goal is to assess the utility and practicality of up-scaling laboratory tests to forecast full scale waste rock drainage characteristics. Present research has focused on the initial characterization of the primary physiochemical properties (Bailey, 2013, Chi *et al.*, 2013, Neuner

et al., 2013, Pham *et al.*, 2013, Smith *et al.*, 2013b, Smith *et al.*, 2013a, Amos *et al.*, 2009) and early stage development of interpretative models for scaling and predicting waste rock behavior (Bailey, 2013, Pham, 2013). A detailed study (2007 to 2010) of the release and transport of oxidation products, source and attenuation of blasting residuals, progression of acid neutralization and pH as well as the appearance and evolution of major cations and trace metals within the Type III test pile basal drainage is presented by Bailey (2013).

Annual geochemical trends resulting from freeze-thaw cycling in waste rock have been observed at other Northern waste rock sites (Søndergaard *et al.*, 2007); however observations have been limited to the characterization of runoff. This limitation in the scale of observation is problematic when attempting to define the primary controls on annual drainage patterns. The Diavik research site provides a unique opportunity to study the evolution of fresh waste-rock material as it evolves over continuous annual freeze-thaw cycles. Additionally, the internal instrumentation network at the Diavik site provides temporally well resolved observations at several scales within the waste rock pile. For the purposes of this study, the evolution of select geochemical values between 2007 and 2012 were examined in detail with the intent of evaluating water flow and geochemical conditions within the test pile core and the total basal drainage.

A thorough understanding of the influence of freeze-thaw dynamics and spatial contributions to drainage geochemistry would allow for the creation of a comprehensive conceptual model of waste-rock evolution in a permafrost environment. An appreciation of the direct and indirect effects of freeze-thaw cycling in waste rock will provide a strong foundation to assist in future prediction, up-scaling, and reactive transport modelling of waste-rock leachate in permafrost environments.

2.2.1 Site Description and Background

Diavik Diamond Mine (Diavik) is located on a 20 km^2 island on Lac de Gras, in the Northwest Territories, Canada (64°29' N; 110°18' W, Figure 2.1). The mine site is approximately 220 km south of the Arctic Circle and 300 km North East of Yellowknife, within a semi-arid region of continuous permafrost. The annual precipitation is 280 mm per year; approximately 60% of which falls as snow. The mean annual temperature is -8.5^{o}C, with mean maximum temperatures of 18 ^{o}C in July and -31 ^{o}C in January/February (Environment Canada, 2012).

Since 2003, open pit and underground operations have been actively exploiting three diamondiferous kimberlite ore pipes. Current projections suggest operations will continue until 2020. The kimberlite pipes are hosted in primarily granite country rock (75%), with irregular veins of pegmatitic alkali-feldspar granite (14%), metasedimentary biotite schist (10%), and younger intrusive diabase dikes (1%) (Jambor, 1997). Compositionally, the granitic rocks contain negligible quantities of sulfides; thus, these rocks are expected to be non-acid generating with a very low potential to release metals (Smith *et al.*, 2013b, Blowes & Logsdon, 1998). In addition, the diabase dikes pose no environmental concern due to the inconsequential volume present (Jambor, 1997). Overall, the principal rock type of concern is the biotite schist, which contains locally distributed sulfides (0.02 to 0.42 wt. %), principally in the form of pyrrhotite [$Fe_{1-x}S$], and with traces of pyrite [FeS_2], chalcopyrite [$CuFeS_2$], and sphalerite [(Zn, Fe)S]) (Smith *et al.*, 2013a). Due to the low concentrations of carbonates and the kinetically limited acid neutralization potential from aluminosilicate phases, sulfide oxidation in the biotite schist is expected to have the potential for net generation of acidity and the release of metals from this rock type (Smith *et al.*, 2013b).

On-site, waste rock is categorized, segregated and stockpiled based on sulfur content: Type I (< 0.04 wt % S; primarily granitic country rock), Type II (0.04-0.08 wt % S; granitic country rock with limited biotite schist) and Type III (>0.08 wt % S; granitic country rock with a greater amount of biotite schist). This material was heaped in 60 m to 80 m high piles by push- and end-dumping techniques. Upon completion of mining it is estimated that there will be a total of 105 Mt of waste rock, of which 24 Mt could be Type III. The current closure plan indicates that the Type III batter slopes will be re-contoured to 18^{o} and a 1.5 m semi-permeable till layer and 3 m Type I thermal cover will be placed over the waste rock. Overall the full scale waste rock dump will cover up to 3.5 km^2 of the East Island of Lac de Gras.

2.2.2 Test Pile Construction

Three waste rock test piles (roughly 50 m by 60 m base, 15 m height) were constructed from 2005 to 2007 at the Diavik Waste Rock Research Facility (DWRRF) and heavily instrumented to monitor the geochemical, hydrological, microbiological, gas transport and thermal behaviour observed in waste rock. The Type I test pile was constructed with rock containing 0.035 wt. % sulfur and the Type III with rock containing 0.053 wt. % sulfur. Both piles were constructed by push- and end-dumping techniques. Batter slopes were established at the angle of repose of the waste rock during construction (~38^{o}, 1.3H:1V). The third Covered test pile was constructed with a Type III rock core containing 0.082 wt. % sulfur. The slopes on the Covered test pile were re-contoured to 18^{o} (3H:1V) and a 1.5 m till layer and 3 m Type I thermal cover were engineered to be representative of the current closure design for the full scale waste dump (Smith *et al.*, 2013c).

This paper focuses exclusively on data from the Type III test pile, including the internal water flow, acid generation and neutralization processes, release and attenuation of dissolved metals and freeze-thaw cycling.

2.3 Methodology

2.3.1 Hydrology

The primary basal drainage collection system consists of a graded (0.5 to 2 %) high-density polyethylene (HDPE) impermeable liner located at approximately 13.5 m depth below the test pile surface. The basal drainage system divides and directs water from the north and south halves of the test pile base to two separate drainage outflows. Each outflow was designed to be representative of a drainage area of approximately 1500 m^2 (25 m by 30 m) (Figure 2.2). Water is directed into heat traced PVC drainpipe, which leads to custom built and calibrated tipping buckets for flow measurements.

The basal drainage collection network includes six 4 m by 4 m and six 2 m by 2 m HDPE lined basal collection lysimeters (BCLs) located 12 m below the test pile surface, on top of the basal drainage liner (Figure 2.2). Drainage water from the BCL network is considered a subset of water reporting to the basal drains. Water is directed into heat traced PVC drainpipes which lead to dedicated tipping bucket rain gauges (Young Model 2202). The BCLs were designed to provide measurements of water flow and chemistry from smaller cross sectional areas through the test pile core.

Time domain reflectrometry (TDR) sensors calibrated to measured volumetric moisture content in the test pile matrix were used to assist in the examination of fluid flow within the piles. TDR sensors were located at depths ranging between 1 m and 9 m throughout the core of the pile.

2.3.2 Geochemical Sampling and Analysis

Water samples from the basal drains and BCLs were collected in 60 mL polyethylene (PE) bottles from dedicated flow through cells using PE tubing and sterile 60 mL PE syringes. Sample bottles and syringes were triple rinsed with sample before collection. Internal drainage networks and sample cells are open to the atmosphere, however, measured pore-gas concentrations of $O_2(g)$ and $CO_2(g)$ throughout the pile are constantly at atmospheric levels (Chi *et al.*, 2013) so the samples are representative of internal redox conditions. Samples from basal drains and lysimeters represent flux-averaged or integrative samples combining matrix and macropore flow.

In situ aqueous pore water samples were collected from soil water solution samplers (SWSSs) located in the core of the pile at depths ranging between 2 m and 9 m. SWSS samplers consist of a buried porous porcelain ceramic cup connected to a food grade PVC body with PE tubing access to the surface. A 50 to 60 cbar vacuum is applied to the unit, which creates a local hydraulic gradient in the matrix material around the porous cup. Suction was applied to the SWSS sampler for two days prior to sample collection. The sample chambers of the SWSS samplers were evacuated by applying positive pressure with nitrogen gas. Samples were collected at surface in a triple rinsed flow through cell and divided into 60 mL PE bottles as described above. Because the SWSS samplers collect pore water from the matrix material centimeters to tens of centimeters surrounding the porous cup, these samples are considered discrete point measurements and are representative of matrix water near the cup only.

Unfiltered samples were analyzed immediately on site to determine the pH, Eh, alkalinity, temperature and specific conductance. The pH measurements were made using a combination electrode (Orion ROSS Ultra® 8156BNUWP, Thermo Scientific, USA) calibrated

daily using three of pH 1.68, 4, 7, and 10 standard buffer solutions. The Eh measurements were made using a metallic combination redox electrode (Orion 9678BNWP, Thermo Scientific, USA), which was verified daily with ZoBell's (Nordstrom, 1977) and Light's solutions (Light, 1972) to ensure optimal functionality. Specific conductance and temperature measurements were made using an epoxy/graphite conductivity cell (Orion DuraProbe, Thermo Scientific, USA), which was calibrated with 100 µS/cm, 1413 µS/cm and 12.9 mS/cm solutions. Alkalinity measurements were conducted on 0.45 µm filtered samples with bromcresol green-methyl red indicator using a Hach digital titrator containing 0.1600 N H_2SO_4 (Hach method 8203).

Field analyses of NH_3-N (Hach method 10023/10031), H_2S (Hach method 8131), Fe^{2+} (Hach method 8146) and PO_4^{3-} (Hach method 8048) were conducted within one day of sampling on filtered (0.45um; cellulose acetate), unpreserved samples using a Hach DR/8400 Spectrophotometer.

Samples for major and minor cations were passed through a 0.45 µm cellulose acetate filter and preserved at a pH < 2 with Onmi Trace metal grade nitric acid (HNO_3) and stored below 4^{o}C until analysis. Major cations (Ca, K, Mg, Mn, Na, Si) were measured at the University of Waterloo by inductively coupled plasma optical emission spectrometry (ICP-OES; iCAP 6000, Thermo Scientific, USA). Minor and trace cations (Al, Be, B, P, Ti, V, Cr, Fe, Co, Ni, Cu, Zn, As, Se, Sr, Mo, Ag, Cd, Sn, Sb, Hg, Tl, Pb, U) were measured at the University of Waterloo by inductively coupled plasma-mass spectrometry (ICP-MS; XSeries 2, Thermo Scientific, USA). Samples for anions were also passed through a 0.45 µm cellulose acetate filter and stored below 4^{o}C until analysis. Anions (F^-, Cl^-, NO_3^-, NO_2^-, Br^-, SO_4^{2-}, PO_4^{3-}) were measured at the University of Waterloo by ion chromatography (IC; DX600, Dionex, USA).

Quality control and assurance procedures were employed in the field and laboratory in the form of field duplicates and blanks, as well as laboratory calibrations standards, instrument blanks, analytical replicates, and matrix spikes.

2.3.3 Geochemical Modelling

Geochemical speciation and saturation index (SI) modelling was completed in PHREEQCi (Parkhurst & Appelo, 1999) using the WATEQ4F geochemical database modified to include Co, and the mineral phases lepidocrocite, siderite (c), and schwertmannite. The final distribution of redox species and SI results are based on the initial elemental concentrations in solution and the principal geochemical parameters of pH, pe, and temperature. Based on these initial conditions, SI modelling results establish the mineral phases that are thermodynamically favoured to precipitate or dissolve. The SI results are used to evaluate hypotheses made about the seasonal and annual aqueous geochemical trends observed in the pile.

2.3.4 Thermal Regime Monitoring

The test pile was heavily instrumented with thermistors distributed along internal tipping faces, batter tipping faces, and within the bedrock underlying the test pile (Smith *et al.*, 2013c). Duplicate strings (separated by 5 m) of thermistor beads at 1 m depth intervals were installed down to 12 m on tipping faces 1, 2, and 4 of the Type III test pile core. Internal temperatures were recorded at all locations at 4 hour intervals.

2.3.5 Subsystem Conceptual Model

To identify the highly dynamic effect of freeze-thaw cycling on the test pile drainage geochemistry, the pile was divided into two subsystems: 1) the core system, and 2) the total system. The core subsystem was defined based on the ratio (bird's-eye view) of the test pile

crest and batter (Figure 2.2). This division was consistent with trends in the ground thawing index, ground freezing index, and mean temperature within the pile (Figure 2.3, Figure 2.4). Basal drainage representative of the entire test pile footprint is captured by two outlets representing the north and south halves of the pile. The combination of these outlets represents a mixture of water draining from all currently 'active' subsections of the pile (*ie*. total drainage). Samples of core drainage are captured by 12 small-scale (4 m^2 to 16 m^2) BCLs located under the test pile crest. The combination of these 12 outlets represents an average sampling of the fluid flow and geochemistry in the pile core (*ie*. core drainage). In addition, SWSSs located roughly above the BCLs between 2 m and 9 m depth provide a vertical profile of geochemical reactions and the evolution of the water chemistry within the pile core.

2.3.6 Continuous Core and Total Drainage Geochemistry

Geochemical samples were collected and analyzed from all active BCLs and basal drains every 2 to 7 days during the flow season. Intermediary geochemical values were interpolated for each BCL flow day as the mean value of the analysis results from the first sampling occurrence prior to and following that flow day. Based on a complete daily flow and geochemical dataset for all active BCLs, a daily flow weighted mean (L m^{-2} day^{-1}) geochemical dataset for the core of the pile was compiled. Similarly, intermediary geochemical values were interpolated for each basal drain flow day as the mean value of the analysis results from the first sampling occurrence prior to and following that flow day. Based on a complete daily flow and geochemical dataset for the north and south basal drains, a daily flow weighted mean (L m^{-2} day^{-1}) total drainage geochemical dataset was compiled. The total drainage geochemical dataset is representative of the aggregate drainage from the entire waste rock pile.

2.4 Results and Discussion

2.4.1 Annual Freeze-Thaw Cycling

The annual freeze-thaw cycle at Diavik causes significant seasonal variability in the internal flow and weathering rates observed in the Type III test pile drainage (Neuner *et al.*, 2013, Bailey, 2013, Fretz, 2013, Hannam, 2012). Annual freeze-thaw cycling continuously alters the mass of rock and internal region of the pile that can undergo active weathering and permit fluid flow into the drainage collection system. During each annual freeze-thaw cycle the pile reverts from being completely frozen between December and May (Figure 2.5a) to being completely thawed between August and October (Figure 2.5c). During the transitional months as summer approaches, a relatively uniform inward thawing front migrates from the pile surface to the base (Figure 2.5b). During the transitional months as winter approaches, a cooling front migrates inward from the pile surface (Figure 2.5d) with the late addition of an upward cooling front from the frozen bedrock below. The combination of these cooling processes produces a thermally isolated warm, hydrologically 'active' zone in the center of the pile between November and early December each year (Figure 2.5e).

2.4.2 Pile Wet-up and First Flush of Matrix Pore Water

At thaw, basal drain flow is dominated by batter sections of the pile due to shorter batter flow paths when compared to the longer core flow paths (Fretz, 2013). Three simulated rainfall events were applied to the Type III pile in 2006 and 2007 at rates equivalent to rainfall intervals of 5 – 35 years to expedite the core wet-up process (Neuner *et al.*, 2013). Volumetric moisture content (VMC) results from TDR sensors ranging in depth from 1 m to 9 m demonstrated a rapid wetting-up process within the pile. The wetting front reached the 9 m depth TDR sensors at

thaw in 2008, followed by core basal outflow (inferred from BCL flow) commencing with the basal thaw in August 2008 (Fretz, 2013).

Geochemical profiles of blasting residuals and tracers in SWSSs and underlying BCLs were evaluated to confirm the wetting-up timeline observed in the flow data and to develop a timeline for the first flush of matrix pore-water. During mining, the rock was blasted with ammonium nitrate/fuel oil (ANFO) explosives, which left blasting residuals distributed in the matrix material in the form of NO_3^-, NO_2^-, NH_4^+, Cl^- and ClO_4^-. Detailed analysis on the persistence of blasting residuals and the first flush of water in the early life of the Type III pile was studied by Bailey et al. (2013). In addition to the *in-situ* blasting residuals, Cl^- and Br^- tracers were applied during the 2007 applied rainfall event on the Type III crest (Fretz, 2013).

Figure 2.6 shows a rapid loss of NO_3^- and NH_4^+ throughout the Type III vertical profile. The downward movement of the NO_3^- and NH_4^+ is consistent with the understanding that the applied rainfall events of 2006 and 2007 initiated a prompt downward migration of the wetting front through the pile. This wetting front, and subsequent core outflow, led to a swift flush of the available blasting residuals by the end of 2010. Sulfide oxidation and the release and transport of solutes after 2010 can therefore be attributed to *in-situ* chemical processes rather than blasting (Bailey, 2013). In 2007, low Br^- concentrations represent background levels before the application of Br^- tracer. In 2008, vertical profiles of Cl^- and Br^- are in close agreement and demonstrate a relatively uniform vertical distribution of tracer in the test pile matrix. Subsequent years illustrate a downward displacement of tracer-rich water which migrated to a depth of 7 m by 2012. Low concentrations of Cl^- and Br^- detected in the 9 m SWSSs and BCL drainage in 2012 are primarily attributed to delayed returns from longer flow paths caused by heterogeneity in the pile core. Statistically insignificant (within 95 % confidence interval) variability in the

blasting residual and tracer geochemical profiles between 2011 and 2012 indicate that the first flush of matrix pore water has passed through the pile.

2.4.3 Internal Evolution of Geochemistry

A thorough understanding of the release and transport of oxidation products, progression of acid neutralization and pH as well as the appearance and evolution of major cations and trace metals throughout the pile core must be established before it is possible to evaluate the influence of annual freeze-thaw cycling on drainage geochemistry. Exposing rock with a net acid generation potential to water and oxygen can produce water with a declining pH and elevated concentrations of sulfate and various metals (Blowes *et al.*, 2003, Gunsinger *et al.*, 2006a). Overall, limited research has been completed examining the geochemical evolution of mine waste rock in profile (Sracek *et al.*, 2004, Bailey, 2013), however studies related to the evolution of mine tailings in profile (Moncur *et al.*, 2005, Al *et al.*, 1997, Blowes & Jambor, 1990, Lindsay *et al.*, 2009, Blowes *et al.*, 1998) provide a valuable comparison.

A conceptual model illustrating the common sequence of acid-neutralization reactions which occur within mine tailings impoundments was described by Jurjovec et al. (2002). Typically, the series can be recognized by pH plateaus which result from the following dissolution-precipitation reactions: calcite (pH 6.5 - 7.5), siderite (pH 4.8 - 6.3), $Al(OH)_3$ (pH 4.0 - 4.5), $Fe(OH)_3$ (2.5 - 3.5) and Al_2SiO_5 (pH > 1.3). The acid neutralization capacity of each phase will depend on the abundances of the acid-consuming minerals and the relative distribution and availability of each phase in the waste rock. Due to the strong kinetic limitations on aluminum silicate weathering (Gunsinger *et al.*, 2006b), acid neutralization from these phases is limited, albeit with continuous contributions of ions to solution.

In 2007, the pore-water pH from SWSSs in the core (Figure 2.7) ranged from pH 5 at 2 m depth to pH 7 at 9 m depth. During this time alkalinity was present at measureable concentrations but highly variable with mean values of ~10 mg L^{-1} as $CaCO_3$. Throughout 2008, core values stabilized between pH 5 at 2 m depth to pH 7 at 9 m depth. At thaw in 2008, significant flow began to report to the BCLs, indicating the wetting front had reached the base of the pile. At this time, the pH values observed in the BCL core drainage were lower (pH ~4.8) than measurements obtained from the SWSSs (pH 5 to 7) located within the pile. In 2008, alkalinity values in SWSSs and BCLs stabilized and remained between 5 to 10 mg L^{-1} as $CaCO_3$ throughout the entire thickness of the pile. This trend in pH and alkalinity suggests that in 2008 much of the H^+ generated by sulfide oxidation was consumed by the dissolution of carbonate minerals ($CaCO_3$ or $CaMg(CO_3)_2$). Measurements from 2009 and 2010 showed a gradual decrease in pH at all depths, concordant with a near depletion of alkalinity at all locations with the exception of the 9 m SWSSs. By 2011 and 2012 a front characterized by low pH and a depletion of alkalinity had migrated through the full thickness of the pile. Minimum pH values of ~3.5 were observed at 3 m and 5 m depths and pH values ranging from 4 to 5 were observed at all other depths. Geochemical modelling indicates that all depths within the pile were undersaturated with respect to all carbonate minerals including calcite ($CaCO_3$) (Figure 2.8), dolomite ($CaMg(CO_3)_2$) and siderite ($FeCO_3$) throughout the study period. These measurements suggest that by 2011 and 2012 consumption of available carbonates was complete within the majority of the pile, with limited carbonate buffering remaining at some 9 m depth locations.

In addition to alkalinity, Ca and potentially Mg are released during carbonate mineral dissolution. Mean concentrations of Ca remained relatively uniform throughout the pile over the study period. Mean concentrations of Ca in 2008 ranged from 500 mg L^{-1} to 1000 mg L^{-1}. From

2008 to 2012, mean Ca concentrations showed a gradual decrease across all depths with final concentrations ranging between 250 mg L^{-1} to 500 mg L^{-1}. Between 2007 and 2010, mean Mg concentrations were similar to mean Ca concentrations. In 2011 and 2012, mean concentrations of Mg gradually increased relative to Ca at 9 m and 12 m depths. Geochemical modelling indicates that the pore water samples at all locations within the pile were at equilibrium with respect to gypsum ($CaSO_4 \cdot 2H_2O$) for the duration of the study (Figure 2.8). The precipitation and dissolution of gypsum provides a secondary control on Ca concentrations, but not Mg concentrations and could explain the uniform distribution of Ca within the pile and the greater variability observed in dissolved Mg concentrations in 2011 and 2012.

Following carbonate depletion by 2010, a decrease in pH to values below 4.5 was concordant with a sudden increase in dissolved Al concentrations (Figure 2.7). In 2010, a linearly decreasing trend in mean Al concentration values was observed from ~20 mg L^{-1} at 3 m down to ~1 mg L^{-1} at 9 m. Subsequent years showed a significant increase in Al concentrations at all locations within the pile, with the exception of 9 m depth. By 2012, mean pore-water concentrations of Al reached ~45 mg L^{-1} at 7 m depth, and ranged between 20 mg L^{-1} to 45 mg L^{-1} at shallower depths. The observed downward front of Al is correlated to a decline in pH and is consistent with the expected acid neutralization sequence corresponding to the dissolution of aluminium hydroxide minerals such as gibbsite [$Al(OH)_3$] and amorphous $Al(OH)_3$. Geochemical modeling suggests that gibbsite could be a secondary source of Al in pore-water geochemistry (Figure 2.8). Throughout the study period, BCL drainage geochemistry exhibited a more gradual rise in mean Al concentrations from ~5 mg L^{-1} in 2009 to ~15 mg L^{-1} in 2012.

Prior to 2010, mean dissolved Fe concentrations (primarily derived from sulfide oxidation) in pore-water and basal drainage remained very low (< 1.0 mg L^{-1}) throughout the pile

core. Geochemical modelling suggests that the precipitation of secondary Fe(III) (oxy)hydroxides [$Fe(OH)_3$] and hydroxysulfates controlled the concentrations of dissolved Fe. By 2011, following a decrease in mean pH values to ~3.5 at 3 m and 5 m depths, an observed rise in mean Fe concentrations occurred (1.5 mg L^{-1} to 2.5 mg L-1) (Figure 2.7). Geochemical modelling conducted using measurements made in 2011 and 2012 suggests that the precipitation and subsequent dissolution of Fe(III) (oxy)hydroxides phases such as ferrihydrite could be regulating Fe concentrations in solution (Figure 2.8). The observed downward movement of rising Fe concentrations is indicative of a third component of an acid-neutralization sequence associated with the remobilization of ferric (oxy)hydroxide phases. The slight lag between the rise in Al and Fe suggests that initial acid consumption by Al(OH)3 phases was limited and was overwhelmed by dissolution of ferric (oxy)hydroxide phases.

In 2007, sulfide oxidation products derived from blasting (Bailey et al., 2013) were distributed fairly uniformly throughout the pile core (Figure 2.9). Mean SO_4 concentrations reported from SWSSs between 2 m and 7 m ranged between 1000 mg L^{-1} to 2000 mg L^{-1} and mean Ni concentrations were generally < 5 mg L^{-1}. From 2008 to 2012, measurements from all depths within the pile displayed a uniform and gradual rise in mean SO_4 concentrations reaching ~3000 mg L^{-1} by 2011. In 2012, mean SO_4 concentrations in 2012 began to decrease in shallow portions of the pile. Geochemical modelling suggests that the pore water in the internal portion of the pile was at equilibrium with respect to gypsum [$CaSO_4 \cdot 2H_2O$] for the duration of the study. Thus, it is anticipated that the precipitation and dissolution of gypsum limits Ca and SO_4 concentrations within the pile. From 2008 to 2012, mean Ni concentrations also increased gradually from < 5 mg L^{-1} at all locations up to 10 mg L^{-1} near the surface and 30 mg L^{-1} at the base. Under the pH conditions that prevail in most of the pile it is unlikely that Ni was strongly

affected by adsorption-complexation reactions (Gunsinger *et al.*, 2006b, Dzombak & Morel, 1990). In addition, geochemical modelling indicates that all pore-water and drainage is undersaturated with respect to all secondary Ni phases included in the WATEQ4F database. Under these conditions, Ni transport in the test pile provides the most appropriate indicator of sulfide (pyrrhotite) oxidation reactions occurring throughout the core. Furthermore, due to the relatively mobile nature of Ni under the conditions prevalent in the pile, concentrations appear to compound at each subsequent depth, with mean concentrations of 30 mg L^{-1} and maximum individual concentration measurements of 125 mg L^{-1} reaching the BCLs in 2012.

The principal mechanism of fluid flow in the test pile is matrix flow driven by the propagation of pressure waves during rainfall events (Neuner *et al.*, 2013, Fretz, 2013). In general, observations from the 9 m SWSS locations do not agree completely with the trends observed in the 2 m to 7 m SWSS and 12 m BCL profiles. This discrepancy can be attributed to a number of factors not limited to: 1) 75% of the 9 m SWSSs are located in a portion of the pile which falls within the Type I waste rock designation (< 0.04 wt. % S) (Smith *et al.*, 2013b); and 2) the 9 m SWSS locations are at a depth in the pile with the lowest mean temperature (Figure 2.3) and lowest yearly degree days (Figure 2.4). These elements highlight the fact that waste rock piles are extremely heterogeneous structures which are exceptionally difficult to characterize with limited sampling locations. Issues with drainage prediction derived from waste rock heterogeneity have been highlighted in other studies (Stockwell *et al.*, 2006).

A statistically insignificant difference in pore-water and drainage geochemistry at most locations throughout the pile between 2011 and 2012 (within 95 % confidence interval) suggests that the internal geochemical reactions have stabilized temporarily with on-going sulfide oxidation and acid neutralization through dissolution of Al and Fe hydroxide phases and

kinetically limited aluminosilicate dissolution. This hypothesis is consistent with the relatively stable internal pH, Al, Fe, SO_4 and related trace metals such as Ni and Co derived from pyrrhotite oxidation. Overall, observations on the internal geochemical evolution of the pile core are consistent with field observations at several mine tailings sites (Moncur *et al.*, 2005, Al *et al.*, 1997, Blowes & Jambor, 1990, Lindsay *et al.*, 2009, Blowes *et al.*, 1998). The consistency in pore-water composition within the pile core allows a more detailed examination of seasonal core drainage evolution, core-batter interactions and the effect of freeze-thaw dynamics on overall basal drainage geochemistry.

2.4.4 Seasonal Variations in Core Geochemistry

Annual freeze-thaw cycling continuously alters the mass of rock and internal structure of the pile which can undergo active weathering and permit fluid flow at any given time. The test piles present a unique opportunity to study this effect because they undergo one complete freeze-thaw cycle each year. Other studies focused on freeze-thaw dynamics in waste-rock drainage lack this control since they deal with larger piles where the active zone does not envelop the full pile (Søndergaard *et al.*, 2007, Søndergaard *et al.*, 2008).

The core geochemical dataset provides a comprehensive and unprecedented representation of the drainage from the interior of a waste rock pile (Figure 2.10). The trends in core effluent chemistry are most recognizable from 2010 onwards, following completion of the first flush of pore-water. Particular emphasis is placed on observations of core drainage in 2012 because the internal structure of the pile is presumed to have developed most fully with respect to flow and geochemistry. Core flow begins as the summer thawing front reaches the test pile base, which typically occurs in mid-August each year. Prior to the initiation of steady core flow in mid-August, it was not uncommon for low volume, low concentration flushes out of the BCL

drainage system to occur. Incidences of BCL flow prior to core thawing are primarily attributed to the release of water that was frozen at the end of the previous year and remained trapped in the drainage system. Thus, drainage reporting to the BCLs before August is probably representative of the geochemical conditions at the end of the previous year and is therefore excluded from further analysis.

In 2012, core outflow began in the second week of August. Initial concentrations of Ca, SO_4, and Ni ranged between 450 mg L^{-1} to 700 mg L^{-1}, 4200 mg L^{-1} to 4900 mg L^{-1}, and 37 mg L^{-1} to 59 mg L^{-1} respectively (Figure 2.10). The initial pH values ranged between 4.2 to 4.5. This steady low pH and high concentration flush of Ca, SO_4, and Ni (among others) lasted three to four weeks before concentrations gradually decreased until the termination of flow at the end of October. Pre-freeze values of Ca, SO_4, and Ni declined to concentrations of 230 mg L^{-1}, 1980 mg L^{-1}, and 16 mg L^{-1} respectively. The concentrations of Al and Fe were more variable than Ca, SO_4 and Ni, but are correlated with the variations in Ni concentrations. Trends of other trace metals derived from sulfide oxidation (Co; pyrrhotite, Cu; chalcopyrite, Zn, Cd; sphalerite) are also correlated with Ni concentrations. Trends in the concentrations of the major cations Mg, K, Si and Na are similar to those observed for Ca.

The trend of a high concentration early flush followed by an abrupt or gradual drop in concentrations has been observed at other arctic waste rock sites (Elberling *et al.*, 2007, Søndergaard *et al.*, 2008), the 2 m scale active zone lysimeter (AZL) experiments at Diavik (Bailey, 2013, Hannam, 2012), and naturally exposed sulfide ore deposits in arctic environments (Søndergaard *et al.*, 2012). At Diavik, it is not uncommon for concentrations of dissolved constituents to decrease by up by 50% in the AZLs (Bailey, 2013); a trend which is also observed in the BCLs (Figure 2.10).

Previous studies at the Diavik site have hypothesised that the observed temporal fluctuations in drainage geochemistry can be primarily explained by variations in flow path, temperature dependant reaction rates and dilution (Hannam, 2012, Bailey, 2013). It is possible that the increases and decreases in solute concentration result entirely from variations in flow rates; however, there is no correlation between flow rate and solute concentrations in the BCLs. This study suggests that the high solute concentrations in BCL drainage observed at the beginning of the season probably are derived from: 1) the fluid residence time in the pile, whereby water reaching the drainage system early in the season has resided longer allowing greater water-rock interactions relative to water exiting late in the season; and 2) solute loads accumulated from continued sulfide oxidation with limited water transport during the transitional seasons and over the winter.

2.4.4.1 Temperature History, Residence Time and Sulfate Release

To evaluate the potential influence of fluid residence time and temperature on solute release following a complete 12 m flow cycle in the test pile, a 1-D temperature-depth variable sulfate-release model was assembled. A database consisting of depth dependant daily mean temperatures (0 m to 14 m; 0.5 m intervals; 2008 to 2012) in the test pile core was compiled. Between 2008 and 2009, twenty 'water packages' were released onto a 4 m by 4 m cross section of the pile surface, saturating the matrix portion of that bulk section of waste rock to a depth of 0.5 m. Delivery of water packages was separated by two weeks; each representing an independent package of infiltrating water from an imagined rainfall event. A uniform downward flow velocity of 0.03 m day^{-1} (Neuner *et al.*, 2013) was used to describe downward movement of the water package through the waste-rock matrix for all days that the depth variable temperature was above zero ^{o}C. The water package was considered immobile when the temperature was

below zero ^{o}C. A mean daily sulfate release rate of 3.8 x 10^{-10} mol kg^{-1} s^{-1}, derived from the Diavik humidity cell experiments (Bailey, 2013), was applied to the water package as it travelled through the pile. The daily release rate was corrected to the daily depth dependant temperature according to a modified Arrhenius equation (Ahonen & Tuovinen, 1992). An activation energy describing pyrrhotite oxidation of 25 kJ mol^{-1}, also derived from the Diavik humidity cells (Bailey, 2013), and in agreement with other estimates (Ahonen & Tuovinen, 1992) was used. Sulfide oxidation was assumed to continue according to this relationship at temperatures below zero. The cumulative daily sulfate release was normalized to the mass of reactive matrix material within each unit volume of the test pile (4 m by 4 m by 0.5 m). The reactive matrix is defined as the < 5 mm grain-size fraction, which corresponds to approximately 14% of the waste rock in the test pile (Smith *et al.*, 2013b). The summation of daily sulfate release was converted to a final mass of sulfate contained within the water package. Finally, the total mass of sulfate within the water package was converted to a concentration of SO_4 in mg L^{-1} based on the volume of pore-water associated with one unit volume of the saturated fine-grained test pile matrix material (Neuner *et al.*, 2013). Modelling results were plotted against actual BCL sulfate concentrations in 2011 and 2012 (Figure 2.11). Reasonably close agreement between estimated and observed concentrations (with emphasis early in the flow season) was observed for both years. Agreement improved in 2012 after internal geochemical conditions had stabilized.

Pearson correlation analysis was completed for all model parameters. Significance testing indicated that SO_4 concentrations showed: 1) strong negative correlations with the Julian day that water entered and exited the pile; 2) strong positive correlations with total days spent in the pile and the depth of last freeze; and 3) no correlation with average water package temperature or cumulative degree days. The main findings uncovered in these analyses were: 1)

confirmation that water exiting the pile immediately after thaw is expected to have the highest SO_4 concentration throughout the season; and 2) unlike previously assumed, SO_4 concentrations do not appear to be related to the exit temperature, or the specific temperature history of the water package.

Following thaw, a mean decrease throughout the season of ~300 mg L^{-1} in SO_4 concentrations was observed. The model results did not capture the scale of seasonal SO_4 loss observed in the BCL drainage (~1000 mg L^{-1} to 2500 mg L^{-1}); however if the model combined the effect of stagnant-flow and freeze-concentration processes; and particularly secondary mineral precipitation-dissolution reactions (*e.g.* gypsum precipitation and dissolution), the agreement might improve. Additionally, this model assumes steady state uniform flow through the matrix only. Irregularities expected in the complex unsaturated flow system controlled by rapid snowmelt, and rainfall frequency and amplitude would invariably impact geochemical trends. As such, it is recommended that future research include a fully coupled reactive, 1-D unsaturated flow model with variable boundary conditions based on infiltration.

2.4.4.2 Impact of Sustained Winter Oxidation and Stagnant Flow on Core Drainage Geochemistry

Contours of mean annual temperature in the test pile (Figure 2.3) indicate the presence of a cold core (-10 ^{o}C avg.) surrounded by a warmer zone (-5 ^{o}C avg.). Contours of annual degree days within the pile core show a similar configuration (Figure 2.4). In general, the greatest variability in annual temperatures occurs at the surface of the test pile, with temperatures ranging from -25 ^{o}C in the winter to 15 ^{o}C in the summer (Figure 2.12). Conversely, the temperature at the test pile base is relatively uniform and unaffected by the highly variable surface temperatures, due to the insulating effect of the waste rock pile and the influence of the

permafrost below (Pham *et al.*, 2013). Under high TDS geochemical conditions, basal temperatures ranging between -8 ^{o}C and 1 ^{o}C have the potential to allow for sustained oxidation year round causing isolated accumulations of acidity and oxidation products near the pile base. High ion concentrations in ARD can lower the freezing temperature of pore-water (Dawson & Morin, 1996). Sulfide oxidation has been documented at temperatures as low as -11 ^{o}C, whereby the presence of sulfur oxidizing microbes is made possible by thin intergranular water films and pockets of liquid water which do not freeze due to the elevated solute concentrations characteristic of ARD (Elberling, 2005). Based on the typical ionic strength of pore-water found in the test pile core, the estimated freezing point depression and thus a potential for sustained winter oxidation is not expected to be significant at internal temperatures below -1.5 ^{o}C. However, during the freezing process, water will become increasingly concentrated and may allow for oxidation at temperatures below -1.5 ^{o}C.

Pore-water geochemical evolution in the test pile was evaluated over several annual freeze-thaw cycles. A systematic review of the temporal evolution of SO_4 from SWSSs in the test pile revealed a trend of increasing concentrations throughout the season at several discrete locations (Figure 2.13). The observed gradual build-up of solutes in pore-water throughout the season was amplified during stagnant flow periods. Drainage cycles characterized by high concentration spring flushes have been highlighted in other arctic waste rock pile studies; whereby the changeover results from the transition from non-steady state in the winter (oxidation rate overwhelms release rate due to no-flow conditions at sub-zero temperatures) to steady state in the summer (oxidation rate roughly equals release rate during steady flow). This process is characterized by a sudden flush of built-up oxidation products at thaw (Søndergaard *et al.*, 2007). Likewise, arid regions undergo a similar flush phenomenon after dry periods when internal flow

waned (Anawar, 2013). Solute accumulation during dry periods with a high solute release following the initiation of flow is considered analogous to the cycling observed during freeze-thaw phenomenon.

The principal mechanism of fluid flow in the test pile is matrix flow driven by the propagation of pressure waves during rainfall events (Fretz, 2013, Neuner *et al.*, 2013). As a result, periods with minimal precipitation will restrict flow and promote a gradual rise in solute concentrations within the pore-water. Trends are particularly strong in 2010 and 2012 when annual infiltration, and thereby internal flow, was minimal. Sampling attempts to capture pore-water geochemistry just before freeze-up (November to December) were not possible due to surface temperatures significantly below zero (-15 ^{o}C to -35 ^{o}C) instantaneously freezing sampling lines.

Overall, seasonal trends in BCL geochemistry are consistent with small scale field experiments, as well as studies of the active zone in other full scale waste-rock piles. Core cycles characterized by high concentration flushes at thaw followed by a steady decline in concentrations until freeze-up appear to be related to fluid residence time and an internal build-up of oxidation products during the winter which is amplified by periods of stagnant flow.

2.4.5 Spatial Contributions to Drain Geochemistry

Seasonal geochemical trends observed in the test pile basal drains are constantly evolving. Circum-neutral pH and low solute concentrations are observed during the spring flush, whereas lower pH and elevated solute concentrations are observed later in the fall with maximum values occurring just before freeze-up (Hannam, 2012, Bailey, 2013). The trends observed in the total basal drainage geochemistry are the inverse of those commonly observed in

the BCLs, AZLs (Hannam, 2012, Bailey, 2013) and other full scale waste-rock piles in arctic environments (Søndergaard *et al.*, 2008).

The complex spatial geometry of the test pile is intricately linked with freeze-thaw cycling and plays a critical role in the geochemical trends. Contrary to the SWSSs and BCLs, the fundamental assumptions of point source evolution or 1-D reactive transport culminating in observed drainage geochemistry are not appropriate. Freeze-thaw cycling continuously modifies the proportion of core and batter subsections of the test pile that contribute to total drainage. As the pile thaws from the surface inward, total drainage geochemistry begins exclusively as a representation of batter drainage (Figure 2.5b). Initial flow, characterized by circum-neutral pH and low solute concentrations (Figure 2.10), is primarily attributed to snow melt reporting to the drains as a result of by-pass flow through macropores. Low concentrations in by-pass flow result from a decrease in fluid residence time and limited contact with the reactive matrix material (Wagner *et al.*, 2006). Following the initial flush driven by snow melt, a slight rise in solute concentrations and decrease in flow suggests a transition from primarily by-pass flow to primarily matrix flow within the test pile batter (Figure 2.5b).

As the thawing front advances deeper into the pile, a thicker proportion of the test pile batter contributes to the total drainage. Increased contribution from thicker subsections of the test pile batter produces a gradual rise in total drainage concentrations and flow. As a result of a relatively uniform inward thawing front from the surface to the base of the pile (Pham *et al.*, 2013), a significant portion of the test pile base is expected to thaw simultaneously. Core basal thaw, inferred through temperature data and the initiation of BCL flow, is concordant with a prompt influx of high concentration water reported in the total basal drainage (Figure 2.10). This suggests that the additional input from core water to total drainage is the primary trigger of this

rise. Therefore, the concentration spike observed in the total drainage each season is primarily attributed to a transition from snow-melt batter-dominated geochemistry, to core-dominated geochemistry.

Following thawing of the core of the test pile, total drainage is representative of aggregated flow through all subsections of the test pile (Figure 2.5c). The increase in total drainage solute concentrations generally levels off as the system stabilizes in a core-dominated state. During the transitional months as winter approaches, the pile cools from the surface inward. Freeze-up of the test pile surface and batter produces total basal drainage largely derived of core flow (Figure 2.5d). This transition is reflected by a merging trend in the core and total effluent geochemistry (Figure 2.10). Sustained inward cooling from the surface further disconnects batter subsections of the test pile from total drainage. The temperature driven transition from batter-dominated to core-dominated geochemistry results in the similarity between the water chemistry from the BCLs draining the core of the test pile and the total basal drainage composition (Figure 2.10). At the end of each season, with increasing correlations from 2010 to 2012, total drainage water quality is very similar to the core water quality.

By late fall, sustained inward cooling combined with upward cooling from frozen bedrock produces a thermally isolated active zone within the pile core (Figure 2.5e). Following basal freeze-up, total basal drainage (13.5 m depth) terminates. Drainage from BCLs (12 m depth) persists for a short period of time (days to weeks) before freeze-up terminates the remaining core drainage. Prolonged internal flow and entrapment of oxidation products in the thermally isolated active core probably enhances the release of higher concentration core drainage at thaw in subsequent years.

2.5 Conclusions

The completion of six annual freeze-thaw cycles at the Diavik waste-rock research site revealed significant geochemical development of internal pore-water and outflow drainage from an experimental waste-rock pile. Concentrations of blasting residuals and applied tracers within the pile revealed an approximate timeline for the first flush of matrix pore-water. Furthermore, geochemical evolution characterized by a low pH front, a release of oxidation products and a stepwise progression through acid neutralization processes supported an approximate timeline for the establishment of apparent internal geochemical equilibrium. Following confirmation of quasi steady state flow and geochemical equilibrium within the test pile core, seasonal variations in total drainage geochemistry can be explained by the highly dynamic influence of freeze-thaw cycling on spatial contribution to drainage. Defining the active substructure of the pile which can undergo weathering and permit fluid flow allows for a more thorough understanding of temporal trends in total drainage effluent. Although oxidation can persist at sub-zero temperatures, observations suggest that physical isolation of the core of a waste rock pile would significantly limit effluent solute concentrations. In future waste rock pile designs, emphasis should be placed on the role of thermal covers and the aggradation of permafrost into pile cores. In addition, a comprehensive understanding of freeze-thaw cycling in a waste rock pile, derived from field observations or thermal modelling, will provide a strong foundation for the application of future up-scaling, and reactive transport modelling of drainage leachate in northern environments.

2.6 Figures

Figure 2.1 - Location of the Diavik Diamond Mine on the East Island of Lac de Gras, in the Northwest Territories, Canada (64°29’ N; 110°18’ W) (from Smith, 2013)

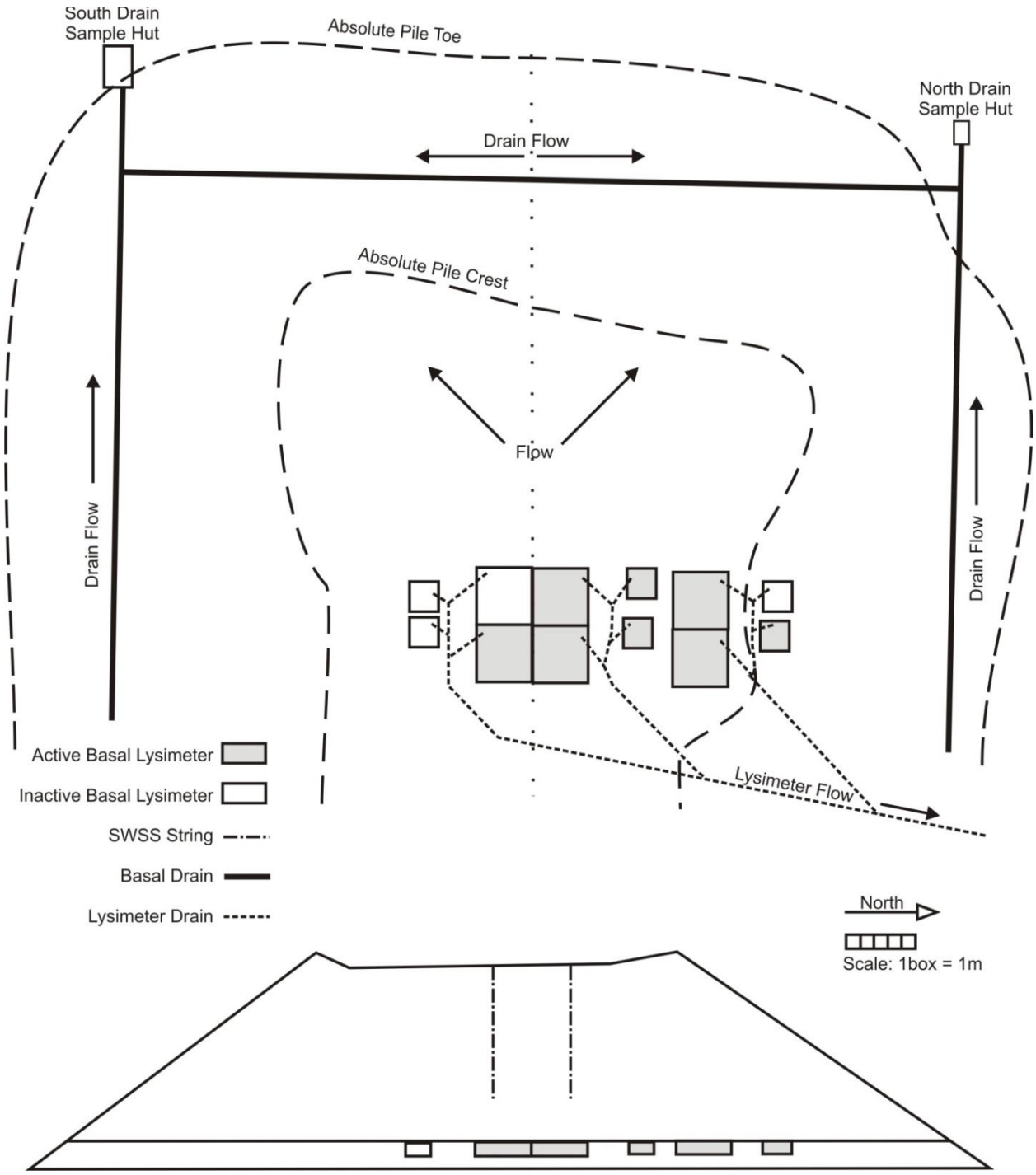

Figure 2.2 - Instrumentation layout and data sources inside the Type III test pile. Total flow catchment is constrained to the area within the basal drains.

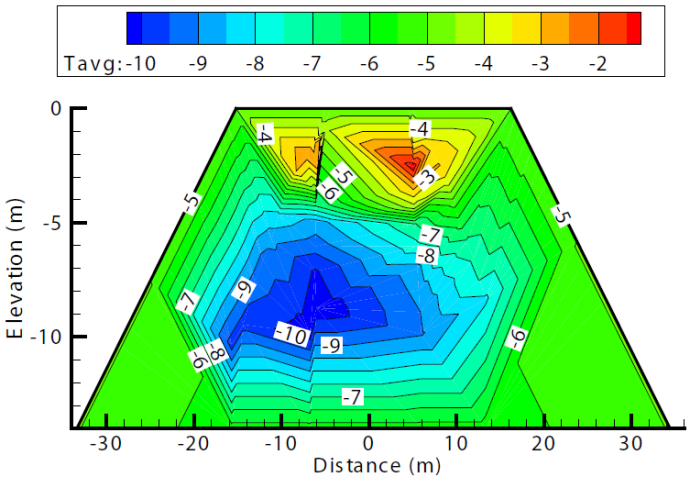

Figure 2.3 – Mean annual temperature of the Type III test pile (Image by Nam Pham, 2013)

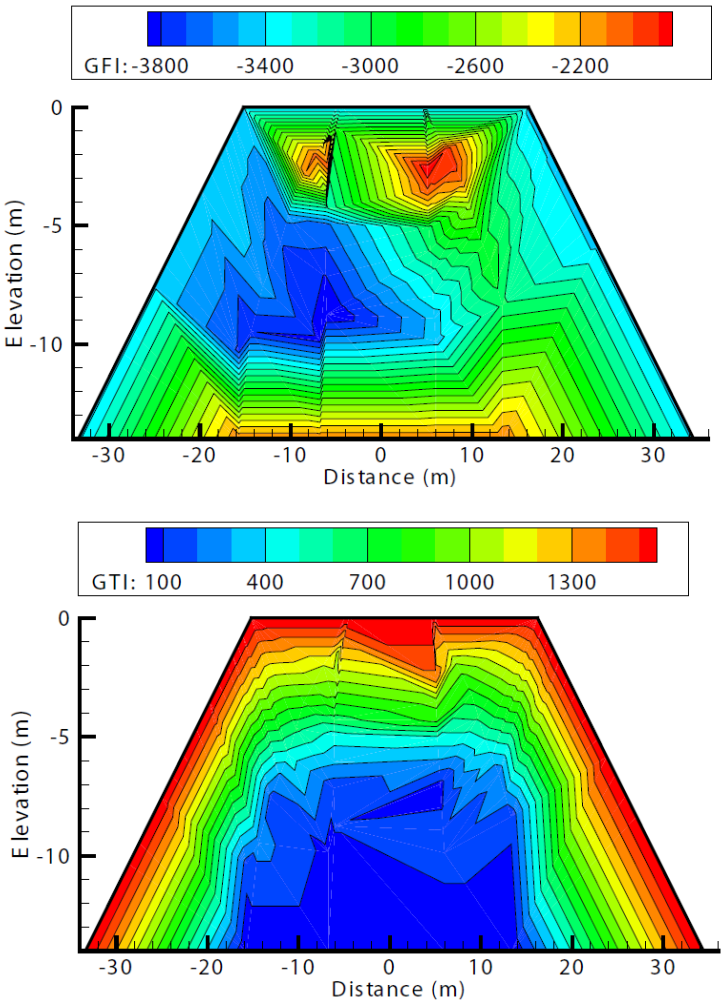

Figure 2.4 – Annual ground thawing index and ground freezing index for the Type III test pile (Image by Nam Pham, 2013)

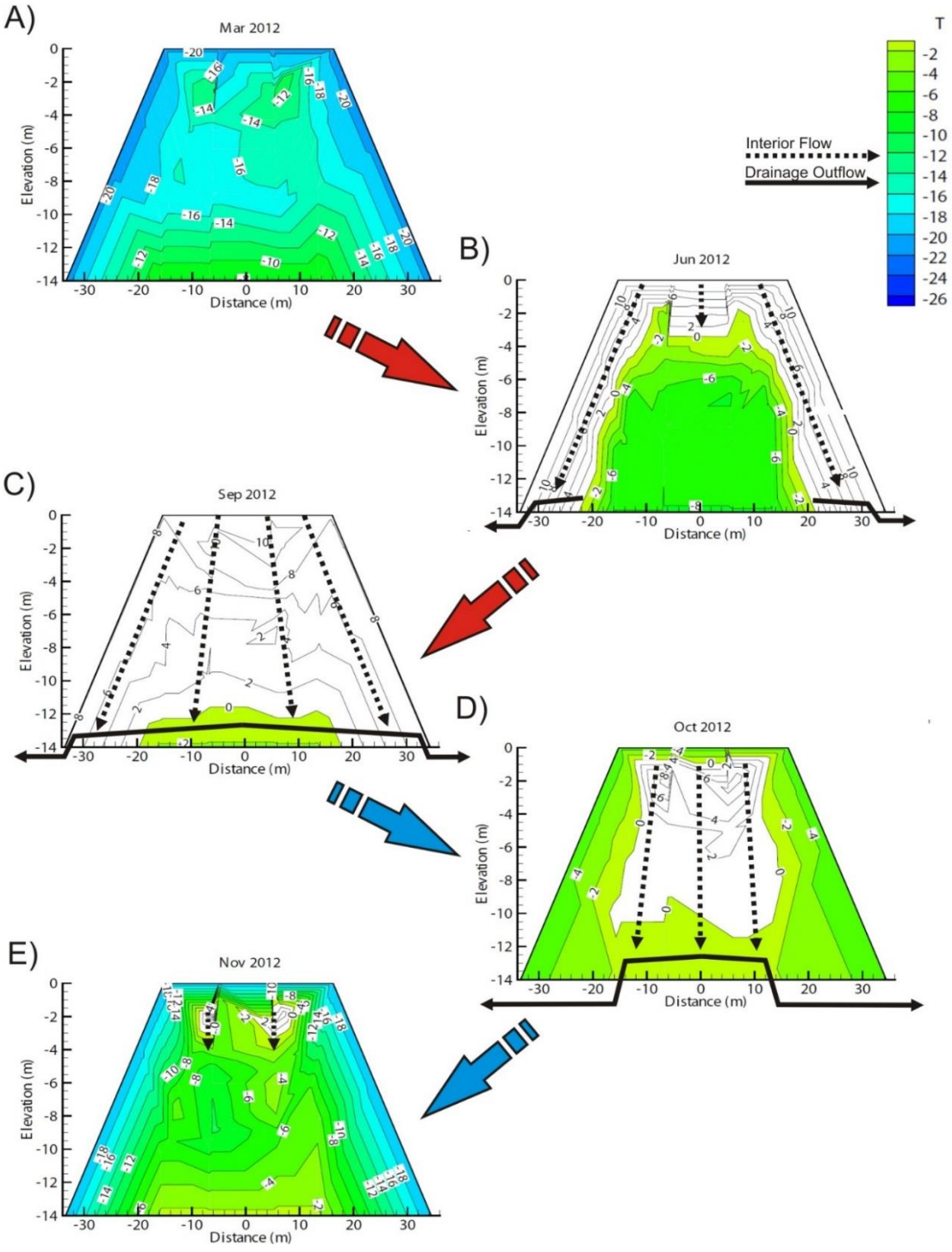

Figure 2.5 – Freeze-thaw cycle based on mean monthly internal temperature data from 2012. Proposed spatial contributions to basal drain load in the Type III test pile: a) Winter; b) Spring; c) Summer; d) Early fall; e) Late fall. Diagram modified from thermal cross sections by Nam Pham, 2014.

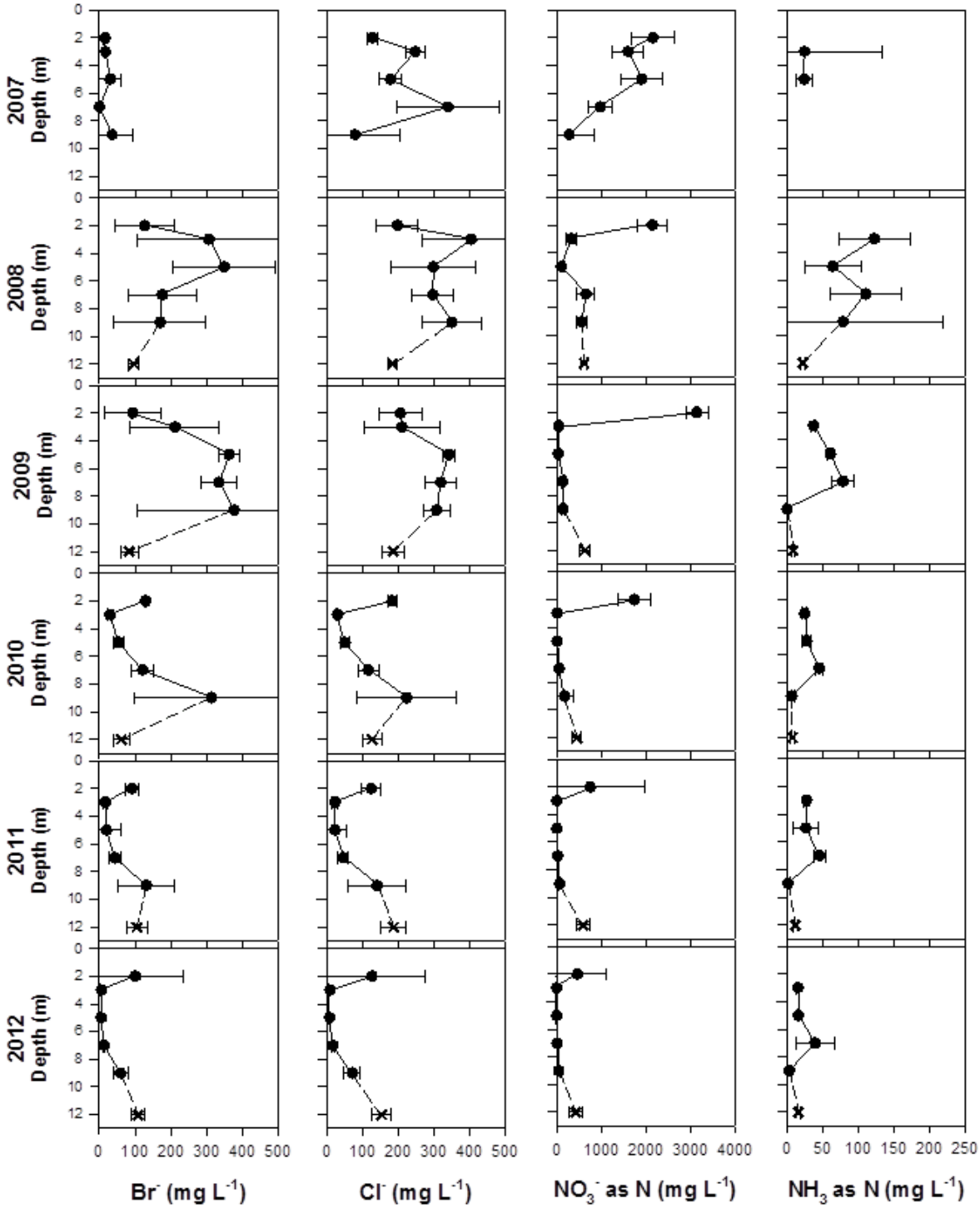

Figure 2.6 – Vertical geochemical profiles in the test pile core display yearly mean values with error bars corresponding to the 95 % confidence interval on the mean value. Blasting residual and tracer evolution is consistent with physical observations of the matrix wet-up and the first flush of pore water.

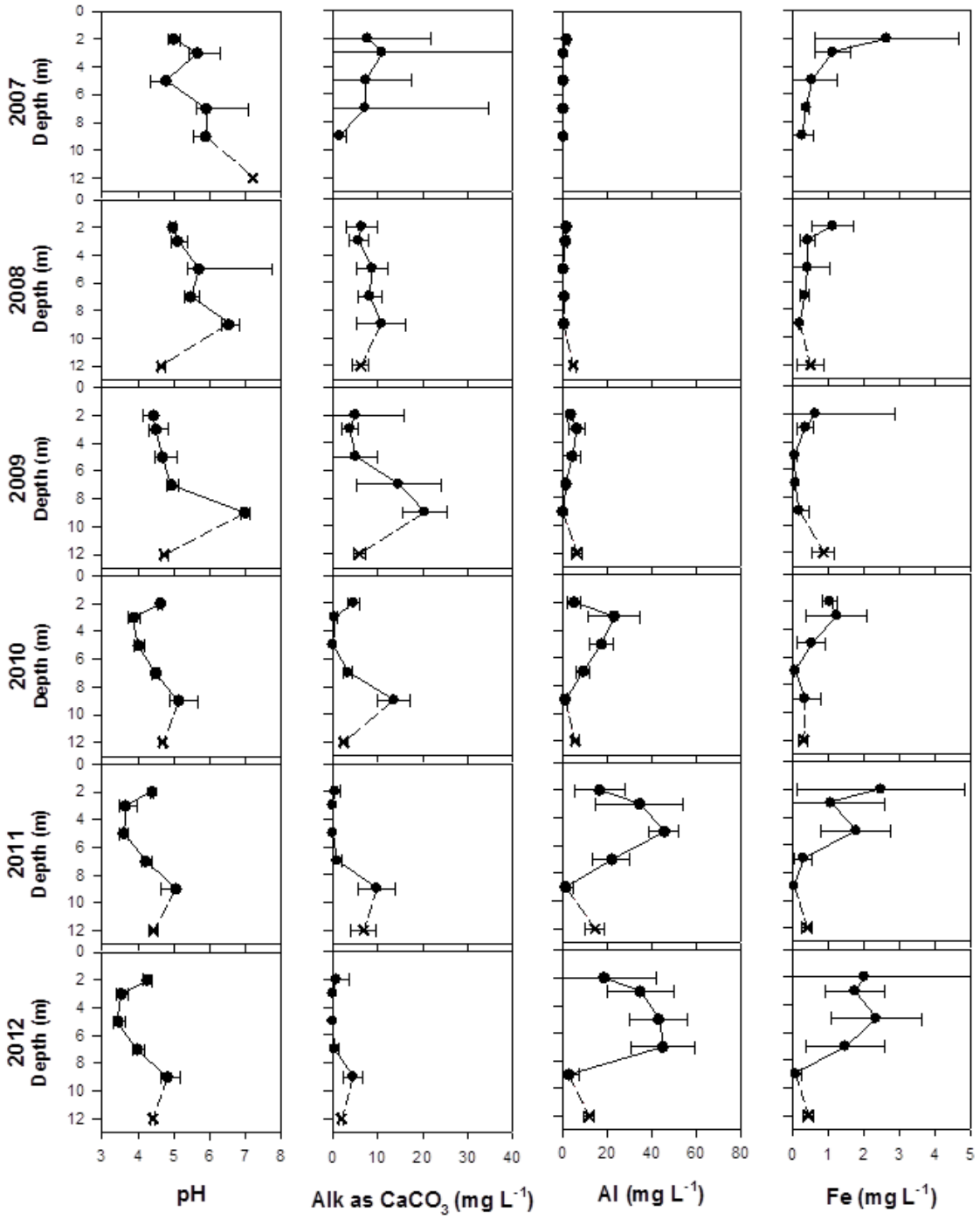

Figure 2.7 – Vertical geochemical profiles in the test pile core display yearly mean values with error bars corresponding to the 95 % confidence interval on the mean value. In early years, pH is controlled by carbonate phase buffering to between pH 4.8 – 7.5. Following depletion of available carbonates by 2010, Al-hydroxide phase buffering occurs to between pH 4 – 4.5. Buffering from Al-hydroxide phases is overwhelmed and dissolution of Fe-hydroxide phases (pH 2.4 – 3.5) occurs concurrently with Al phases. Dynamic geochemical equilibrium is reached by 2012.

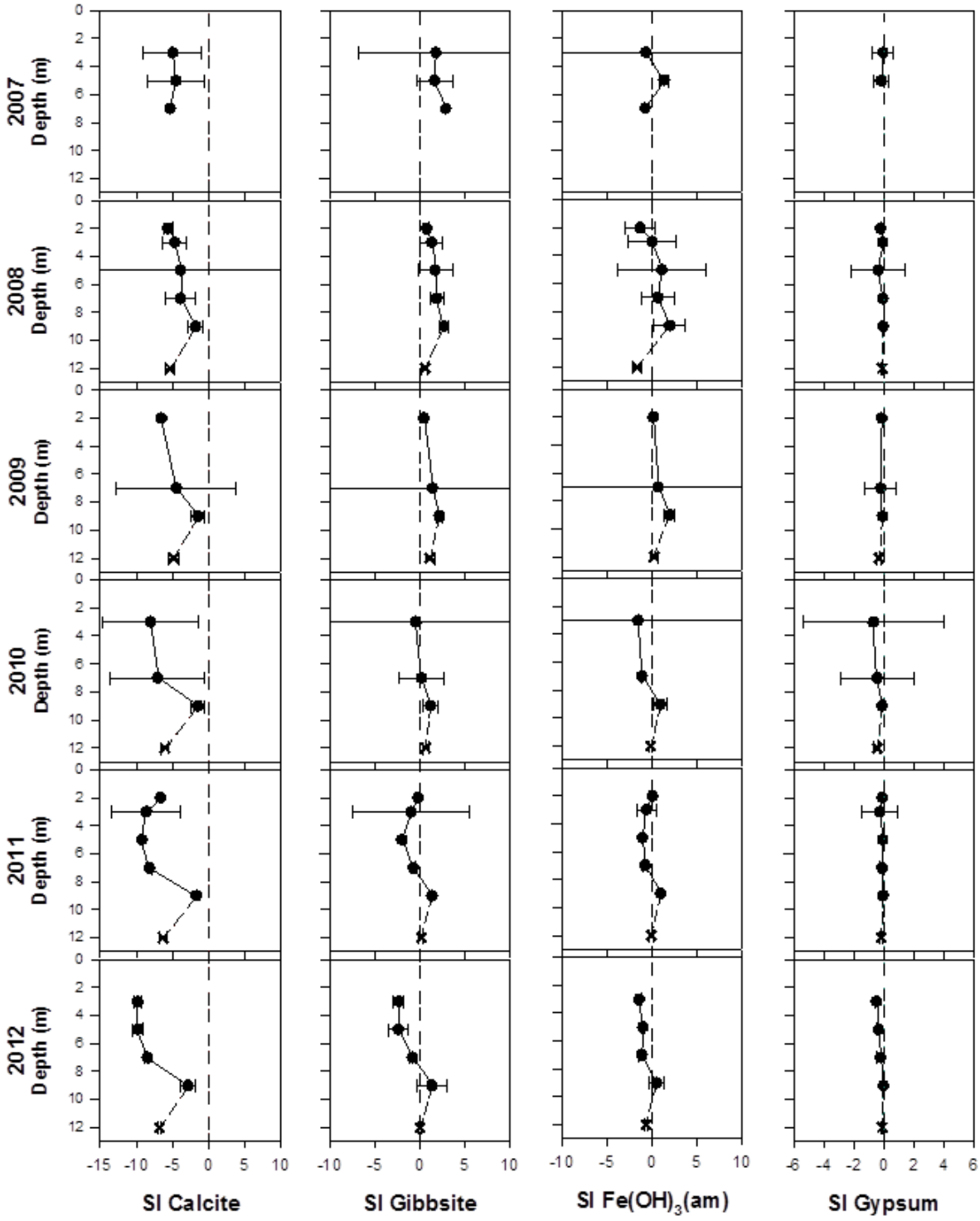

Figure 2.8 – Vertical geochemical profiles in the test pile core display yearly mean values with error bars corresponding to the 95 % confidence interval on the mean value. Saturation indices for primary mineral phases which potentially control precipitation-dissolution reactions in the test pile core.

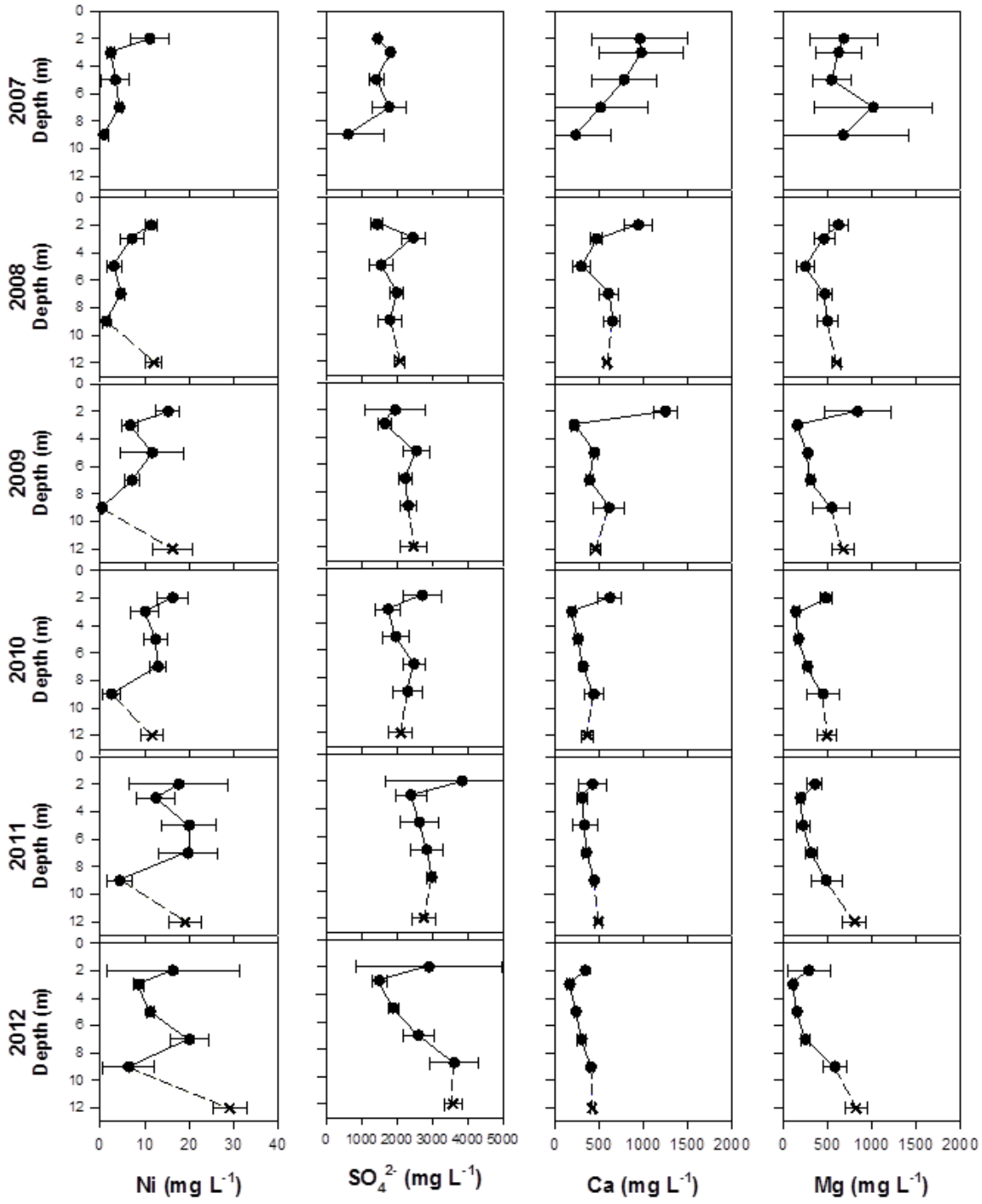

Figure 2.9 – Vertical geochemical profiles in the test pile core display yearly mean values with error bars corresponding to the 95 % confidence interval on the mean value. Release and accumulation of primary sulfide oxidation products, Ni and SO4, derived from pyrrhotite, and Ca and Mg from carbonate and silicate buffering. The transition to Mg dominated pore-water at depth is explained by an exhaustion of calcite phases and secondary loses of Ca to gypsum precipitation.

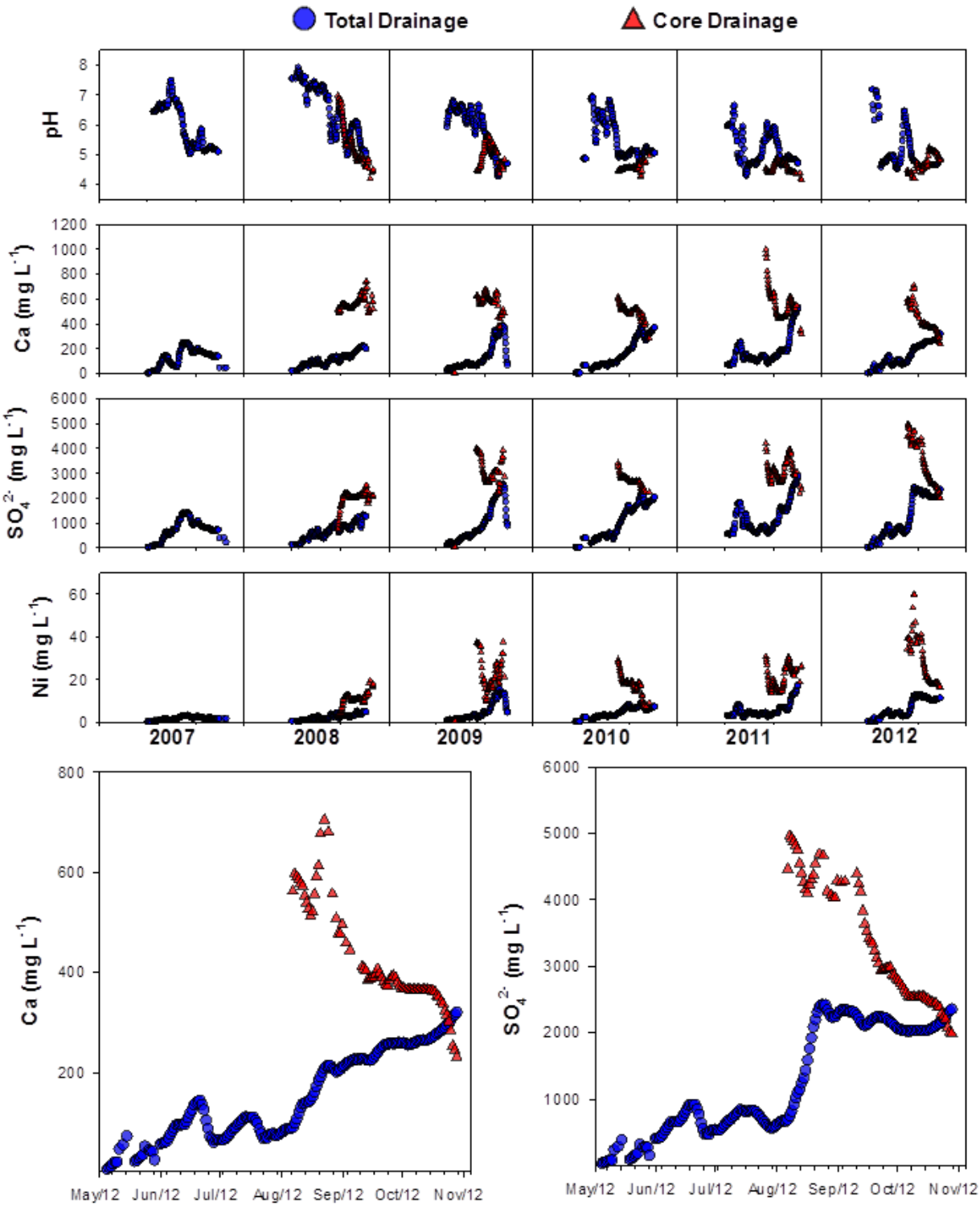

Figure 2.10 – Annual cycles of core and basal drainage geochemistry. Blue circles represent daily flow weighted mean concentrations from basal drainage network. Red triangles represent daily flow weighted mean concentrations from all currently flowing locations in the core BCL network.

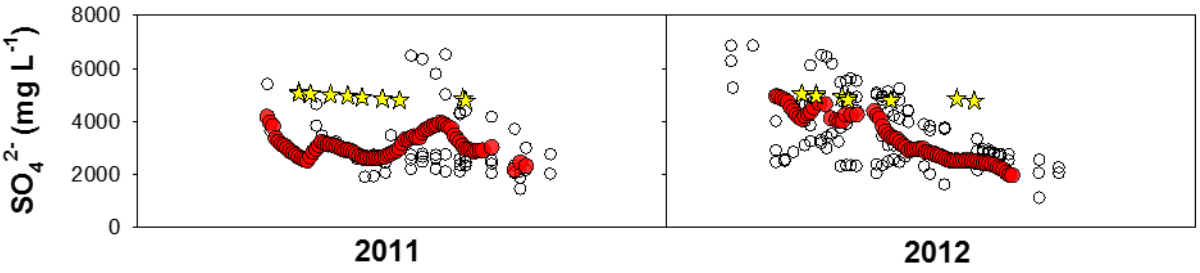

Figure 2.11 – Results from 1-D temperature-depth variable sulfate release model (yellow stars), compared with flow weighted mean sulfate concentrations reported in the BCL network in 2011 and 2012 (red circles) and individual BCL sulfate concentrations (open circles).

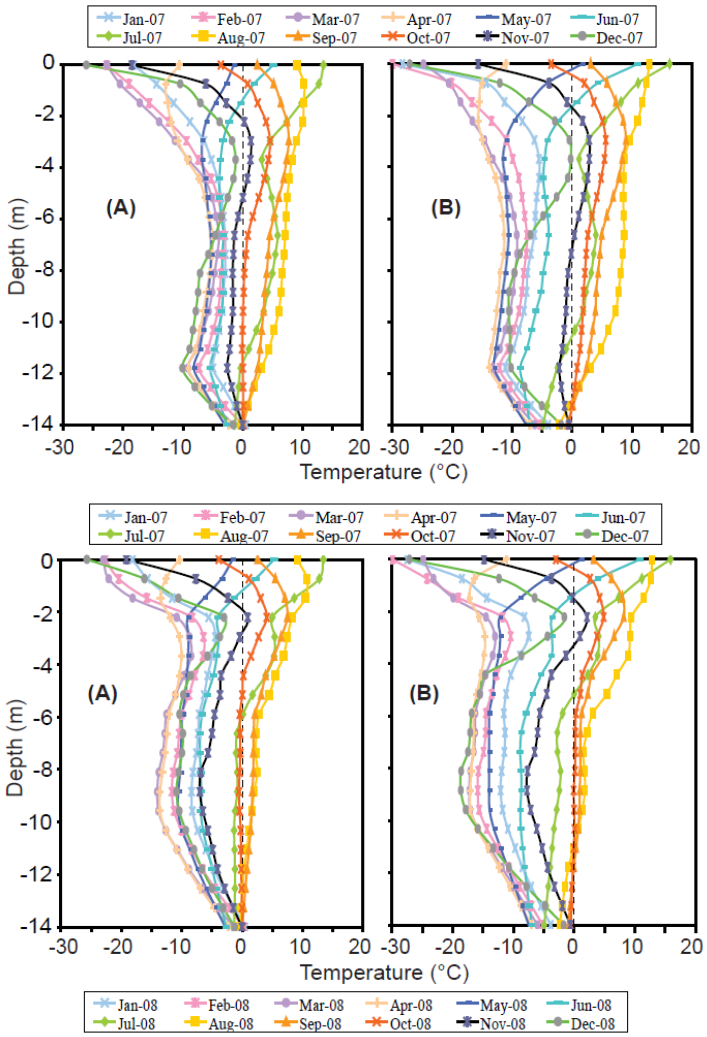

Figure 2.12 – Trumpet diagrams demonstrating the annual freeze-thaw cycle observed in the Type III test pile core temperature (Pham, 2013)

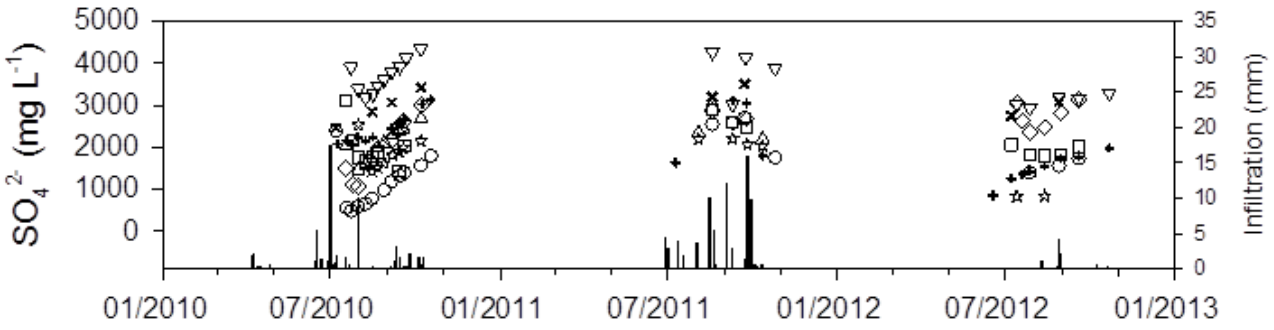

Figure 2.13 – Seasonal trends observed in test pile pore-water geochemistry. Different symbols are representative of discrete SWSS locations ranging between 2 m and 9 m depth. Concentration build-up throughout season is primarily attributed to stagnant flow periods, brought on by intervals with minimal rainfall and infiltration.

Chapter 3: Influence of Spatial Contributions to Geochemical Loading from a Low Sulfide Waste Rock Pile in a Permafrost Environment

3.1 Executive Summary

An experimental waste-rock pile (0.053 wt. % S) was constructed at the Diavik diamond mine, in the Northwest Territories, Canada to evaluate the generation of acid-rock drainage (ARD) and the seasonal and annual release of various metals in drainage leachate. A dense instrumentation network allowed for well resolved observations of spatially distributed leachate from within the core and batter of a waste-rock pile. Evaluation of the timing and retention of infiltrating water during the freeze-thaw cycles was combined with thermal data collected throughout the internal structure of the pile to separate it into distinct core and batter subsystems. Aggregated basal leachate was captured by a collection system underlying the entire waste-rock pile. Core drainage properties were estimated by up-scaling flow and chemistry data from 4 m^2 to 16 m^2 core basal collection lysimeters. Batter drainage properties were estimated using a mass balance approach through measurements of total drainage and core drainage. Monitoring of leachate loading from the test pile core and batter subsystems (2007 to 2012) produced sufficient geochemical data to quantitatively assess the timing and evolution of these spatially distributed contributions, and the effect of freeze-thaw cycles on the release and transport of metals in the test pile. Mean annual solute concentrations and geochemical speciation and saturation index modelling revealed two distinct environments in the core and batter subsystems. Concentrations in the core of the test pile were generally 2.5 to 8.5 times greater than concentrations in the batter. Scaling results indicated that core flow accounted for 13 % of the total drainage volume; while it was estimated that 35 to 51 % of major and trace metal loads were attributed to this zone. Parameter correlation analysis and core contributions were used to identify common source minerals for elements and assess the mechanisms (sorption and precipitation-dissolution) controlling metal mobility in the core and batter subsystems. By 2012, the release of pyrrhotite

oxidation products in the < 5 mm reactive fraction of waste rock was as high as 5.1 %, 9.0 %, 7.2 % and < 0.1 % for S, Ni, Co and Fe respectively. Results indicate that a comprehensive understanding of thermal cycling is imperative when estimating seasonal and annual releases of weathering products from waste rock. Thermal isolation of the core of the test pile through the upward aggradation of permafrost could significantly decrease the expected range of drainage concentrations and the predicted range of daily and annual drainage solute loadings. Evolution of waste-rock drainage loading determined through this study will assist in the advancement of reactive transport models describing ARD in permafrost environments.

3.2 Introduction

Metal leaching and acid rock drainage (ARD) can be an undesirable environmental impact of mining operations of any scale. The vast majority of material that is mined from the earth is of an inadequate grade to attempt mineral recovery and is subsequently stored in massive waste-rock piles (Jamieson, 2011). With no mitigation, the resulting environmental exposure of waste rock with a net acid generation potential can result in drainage water with a low pH and elevated concentrations of sulfate and trace metals (Blowes *et al.*, 2003). It is advantageous to dispose of sulfide-bearing waste materials under water to limit oxidation processes; however in the case of waste rock, the volume of material involved often makes this option unfeasible. Incorporating a thermal cover and allowing waste rock to freeze through the upward aggradation of permafrost is considered one of the most advantageous approaches in cold climates (Kyhn & Elberling, 2001).

ARD generation results from a coupling of numerous physical and biogeochemical processes. In order to understand and eventually predict ARD, it is essential to properly identify and describe all the factors which contribute to its occurrence. The physical processes within a waste-rock pile which govern oxygen supply, the boundary conditions which govern fluid flow and the mechanisms which regulate unsaturated flow are as important as the geochemical processes which describe acid production, neutralization, and the release and transport of solutes. The thermal state of the system governs fluid flow and also effects mineral reaction rate kinetics and microbiological community input. Inadequate characterization of ARD risks and preparation prior to the production of a mineral resource can detrimentally impact local water resources with results persisting for thousands of years (Nordstrom & Alpers, 1999, Blowes & Jambor, 1990).

Extensive research has taken place to better understand the evolution of ARD in mine tailings (Moncur *et al.*, 2005, Al *et al.*, 1997, Blowes & Jambor, 1990, Lindsay *et al.*, 2009, Blowes *et al.*, 1998) and to describe the processes which govern trace metal mobility in ARD systems (Balistrieri *et al.*, 2003, Tonkin *et al.*, 2002, Paulson & Balistrieri, 1999). Fewer studies are related exclusively to understanding ARD evolution in waste rock (Smith *et al.*, 2013a, Marescotti *et al.*, 2010, Sracek *et al.*, 2004, Stockwell *et al.*, 2006). In general, there is an absence of comprehensive multi-disciplinary studies coupling the physical and biogeochemical components of ARD which control waste-rock leachate loading. In addition, the complex influence of a polar climate producing annual freeze-thaw cycles has remained relatively unquantified.

The purpose of the Diavik waste-rock project is to improve our understanding of the geochemical, hydrological, microbiological, gas transport and thermal behaviours observed in waste rock. Specific to the Diavik project is the objective to identify the effect of freeze-thaw and permafrost conditions on the evolution of these physiochemical characteristics. Present research has resulted in early stage development of interpretative models for predicting thermal and chemical behaviours in waste rock (Bailey, 2013, Pham, 2013), while earlier work focused on the initial characterization of the primary physiochemical properties (Amos *et al.*, 2009, Chi *et al.*, 2013, Neuner *et al.*, 2013, Pham *et al.*, 2013, Smith *et al.*, 2013b, Smith *et al.*, 2013a). Studies have highlighted yet unresolved issues with the extrapolation of simple laboratory studies to the complex and heterogeneous field scale (Malmström *et al.*, 2000). Identification of spatially variable field-scale processes which influence the geochemical evolution and trace metal mobility within a waste-rock pile are essential in the pursuit of identifying parameters required for reactive transport models. For advanced reactive transport modelling of arctic

waste-rock piles to be successfully executed as a predictive tool, comprehensive multi-disciplinary research, with the focus of quantifying the physiochemical processes, including freeze-thaw cycling, is required. The Diavik research site provides a unique opportunity to study the evolution of fresh waste-rock material as it evolves over continuous annual freeze-thaw cycles. The experimental waste-rock piles at Diavik can be considered well-constrained systems, with clearly defined initial conditions (Smith *et al.*, 2013b), instrumentation to quantify changes to the internal and external physiochemical environments and a data collection system to continuously monitor drainage effluent at discrete locations (Smith *et al.*, 2013c).

3.2.1 Site Description and Background

Diavik Diamond Mine (Diavik) is located on a 20 km^2 island on Lac de Gras, in the Northwest Territories, Canada (64°29' N; 110°18' W; elevation 440m; Figure 3.1). The site falls within a semi-arid region which contains continuous permafrost. Open pit and underground mining provides access to three diamondiferous kimberlite ore bodies. Mean historical precipitation is 280 mm per year; of which approximately 60% falls as snow. Mean annual temperatures range between 18 ^{o}C in July and -31 ^{o}C in January/February, with an overall mean of -8.5 ^{o}C (Environment Canada, 2012).

The kimberlite ore bodies intruded into Archean host rock primarily composed of granite (75%), with pegmatitic alkali-feldspar granite (14%), irregular xenoliths of metasedimentary biotite schist (10%), and younger intrusive diabase dikes (1%) (Jambor, 1997). The primarily granitic rocks contain an insignificant mass of sulfides; thus, these rocks have a very low potential to release metals and are expected to be non-acid generating (Smith *et al.*, 2013b). The diabase dikes pose no environmental concern due to the negligible mass present (Jambor, 1997). The major rock type of concern is the biotite schist (0.02 to 0.42 wt. % S), which contains locally

disseminated sulfides predominantly in the form of pyrrhotite [$Fe_{1-x}S$, with Ni, Co replacement], and with traces of pyrite [FeS_2], chalcopyrite [$CuFeS_2$], and sphalerite [(Zn, Fe)S, trace Cd]) (Smith *et al.*, 2013a). Due to the low abundance of carbonates (0.027 wt. % C) and the kinetically restricted acid neutralization potential from aluminosilicate phases, sulfide oxidation in the biotite schist is expected to have the potential for net generation of acidity and the release of metals (Smith *et al.*, 2013b).

Due to the irregular distribution of biotite schist units within the granite, waste rock is segregated based on mean sulfur content: Type I (< 0.04 wt % S; primarily granitic country rock), Type II (0.04-0.08 wt % S; granitic country rock with limited biotite schist) and Type III (> 0.08 wt % S; granitic country rock with a greater amount of biotite schist). Operational forecasting suggests mining will continue until 2020. At closure, there will be a total of 105 Mt of waste rock, of which up to 24 Mt will be the higher sulfide Type III material. Waste rock stockpiles will be 60 m to 80 m high and will cover up to 3.5 km^2 of the East Island of Lac de Gras. The current closure plan for the Type III waste rock requires that the batter slopes be re-contoured to 18^o and a 1.5 m low permeability till layer and 3 m Type I layer will be placed over the waste rock as a thermal cover. An expected result of this plan is the enhanced aggradation of permafrost into the waste-rock core, isolating the vast majority of material from environmental exposure.

3.2.2 Test Pile Construction

Between 2005 and 2006, an instrumented waste-rock test pile (roughly 50 m by 60 m base, 15 m height) was constructed at the Diavik Waste Rock Research Facility (DWRRF). The test pile was constructed with rock containing on average 0.053 wt. % sulfur. The pile was constructed by push- and end-dumping techniques over four successive tipping faces with batter

slopes established at the angle of repose of the waste rock (~38^{o}, 1.3H:1V) (Smith *et al.*, 2013c). Instrumentation was installed during construction to monitor the geochemical, hydrological, microbiological, gas transport and thermal behaviour observed within the pile.

This study builds on previous work describing the influence of freeze-thaw dynamics on the internal geochemical evolution of the test pile (Chapter 2). This work integrates data on the internal flow, the thermal regime and on the acid generation and neutralization processes, to quantify the effect of spatial variations in these characteristics on dissolved metal loading and to predict the current stage of solute release from the test pile system.

3.3 Methods

3.3.1 Hydrology

Rainfall was measured on-site by three tipping bucket rain gauges (Young Model 2202). Net infiltration calculations between 2007 and 2010 were conducted by Fretz (2013) and updated until 2012 by Krentz (In Progress). Infiltration was estimated using the FAO-56 Penman-Monteith method (Allen *et al.*, 1998). The accuracy and applicability of using this method to estimate infiltration at the test piles was checked against a water balance from 2008 to 2011. Testing demonstrated the ability of the FAO-PM method to reasonably predict net infiltration on a flat waste-rock surface in a northern climate (Fretz, 2013). Estimates of net infiltration on the flat test pile crest were extended onto the sloped batter sections of the test pile. Some error is expected in this extrapolation; however infiltration estimates were only used as a qualitative estimation tool for the internal flow regime; therefore, the absolute magnitude of infiltration values do not affect the results of this study.

A high-density polyethylene (HDPE) impermeable liner (50 m by 60 m) underlies the test pile at approximately 13.5 m depth. A graded basal surface (0.5 to 2 %) divides and directs total basal leachate between the north and south halves of the pile. The north and south catchment zones were each designed to drain an area of approximately 1500 m^2 (25 m by 30 m), however field measurements suggest that a greater proportion of the flow is directed to the south basal drain (Figure 3.2). At the pile boundaries, water is directed into heat traced PVC drain pipes and channelled directly into sampling huts. Continuous flow measurements are recorded by custom built and calibrated tipping buckets.

Six 4 m by 4 m and six 2 m by 2 m HDPE-lined basal collection lysimeters (BCLs) located at approximately 12 m depth collect a subset of the total drainage leachate in the test pile core (Figure 3.2). Outflow from each BCL is continuously monitored by dedicated tipping bucket rain gauges (Young Model 2202).

3.3.2 Geochemical Sampling and Analysis

Drain lines within the test pile direct water into dedicated flow through sampling cells. Water samples were collected with dedicated PE tubing, sterile polyethylene (PE) syringes and 60 mL PE bottles. All sampling equipment was triple rinsed with sample before collection. Drainage lines and flow through cells are open to the atmosphere, which is consistent with the atmospheric conditions within the pile (Amos *et al.*, 2009, Chi *et al.*, 2013).

pH, alkalinity, Eh, temperature and specific conductance were analyzed immediately on unfiltered samples. A combination electrode (Orion ROSS Ultra® 8156BNUWP, Thermo Scientific, USA), calibrated daily using three of pH 1.68, 4, 7, and 10 standard buffer solutions, was used to take pH measurements. Filtered samples were used to conduct alkalinity measurements using bromcresol green-methyl red indicator and a Hach digital titrator containing 0.1600 N H_2SO_4 (Hach method 8203). A platinum combination redox electrode (Orion 9678BNWP, Thermo Scientific, USA), verified daily with ZoBell's (Nordstrom, 1977) and Light's solutions (Light, 1972) was used to take Eh measurements. An epoxy/graphite conductivity cell (Orion DuraProbe, Thermo Scientific, USA), which was calibrated with 100 uS/cm, 1413 uS/cm and 12.9 mS/cm solutions, was used to take specific conductance and temperature measurements.

Field analysis was conducted on filtered (0.45um; cellulose acetate), unpreserved samples within one day of sample collection. A Hach DR/8400 Spectrophotometer was used to measure NH_3-N (Hach method 10023/10031), H_2S (Hach method 8131), Fe^{2+} (Hach method 8146) and PO_4^{3-} (Hach method 8048).

Samples for major cation, minor cation, and anion concentrations were passed through a 0.45 µm cellulose acetate filter and stored below 4°C until analysis. Additionally, cation samples were preserved with trace metal grade nitric acid (HNO_3) at a pH < 2. Anions (F^-, Cl^-, NO_3^-, NO_2^-, Br^-, SO_4^{2-}, PO_4^{3-}) were measured at the University of Waterloo by ion chromatography (IC; DX600, Dionex, USA). Major cations (Ca, K, Mg, Mn, Na, Si) concentrations were measured at the University of Waterloo by inductively coupled plasma optical emission spectrometry (ICP-OES; iCAP 6000, Thermo Scientific, USA). Minor cations and trace element concentrations (Al, Be, B, P, Ti, V, Cr, Fe, Co, Ni, Cu, Zn, As, Se, Sr, Mo, Ag, Cd, Sn, Sb, Hg, Tl, Pb, U) were measured at the University of Waterloo by inductively coupled plasma-mass spectrometry (ICP-MS; XSeries 2, Thermo Scientific, USA).

Field duplicates (10 %) and blanks (5 %), as well as laboratory calibration standards, instrument blanks (>10 %), analytical replicates (>10 %), and matrix spikes were employed for quality control and assurance.

3.3.3 Geochemical Load Estimates

3.3.3.1 Total Test Pile Load Estimate

Daily flow and geochemical data from the North and South basal drains was used to calculate daily loading (mg day^{-1}) of various solutes. Flow from the North and South basal drains represents an aggregate of spatially distributed leachate which has undergone reactive

transport through varying thicknesses of waste rock (0 m to 13.5 m) over freeze-thaw cycles; or specifically drainage reporting from all 'active' or thawed subsections of the test pile. Geochemical samples were collected and analyzed from the basal drains every 2 to 7 days. Intermediary geochemical values were interpolated for each basal drain flow day as the mean value of the analysis results from the first sampling occurrence prior to and following that flow day. Daily loading was normalized to the representative cross sectional areas of each drain (mg m^{-2} day^{-1}). Based on a complete daily load dataset for both basal drains, a mean drain load (mg m^{-2} day^{-1}) dataset was compiled. Mean basal drain loading (mg m^{-2} day^{-1}) was combined with the full area of the test pile footprint (3000 m^2) to calculate mass loadings. Mean annual and cumulative solute concentrations (mg L^{-1}) were calculated based on loading and flow data.

3.3.3.2 Test Pile Core Load Estimate

Drainage from small-scale (4 m^2 to 16 m^2) BCLs represents water which has undergone reactive transport through 12 m of waste rock over several freeze-thaw cycles. Water flow is anticipated to travel vertically downward through the internal structure of the pile underlying the crest, therefore flow and geochemical results from BCLs can be scaled to the test pile core area (1350 m^2). Based on a complete daily load dataset for all BCLs, a mean BCL load (mg m^{-2} day^{-1}) dataset, which accounted for all currently flowing and dry locations, was compiled. Mean BCL load (mg m^{-2} day^{-1}) was then scaled to the cross sectional area of the test pile core (1350 m^2). The core subsystem was delineated based on the ratio (bird's-eye view) of the test pile crest and batter (Figure 3.2). This core – batter division was also identified in annual trends of ground thawing index, ground freezing index, and mean temperature within the pile (Chapter 2, Pham *et al.*, 2013). Daily, annual and cumulative solute concentrations (mg L^{-1}) in the core were calculated based on loading and flow data.

Throughout the project, eight out of 12 BCLs yielded water. The four remaining inactive BCLs produced little to no water (< 500 ml). For the purpose of determining representative BCL flow and geochemical loading, two separate approaches were considered: 1) the four inactive BCLs were assumed defective and excluded from future calculations and 2) the four inactive BCLs were assumed to be functioning, but had not yielded water due to spatial heterogeneity in the flow system. The results from each approach represent the minimum and maximum expected range of values (36% difference in range); however the higher core flow estimate was expected to be more accurate and was adopted for future calculations. The equipment failure rate (~ 40%) applied in the maximum estimate is consistent with the construction survivability of other test pile instrumentation networks (Smith *et al.*, 2013c). Between August 22nd and September 10th, 2012, electrical malfunctions caused a total loss of BCL flow data. For this period, available flow and loading data collected from the total basal drainage network was allocated to the core and batter subsystems based on mean historical parameter specific contributions from each subsystem during that time period each year.

3.3.3.3 Test Pile Batter Load Estimate

The batter load (mg day^{-1}) was calculated using a mass-balance approach. Batter load was calculated daily as the difference between the total load (mg day^{-1}) and the core load (mg day^{-1}). These estimates disregard deviations expected to result from differences in travel times for water reporting to the total basal drainage and BCL networks. Daily, annual and cumulative solute concentrations (mg L^{-1}) were calculated based on daily load, flow and a batter area of 1650 m^2.

3.3.4 Geochemical Modelling

Geochemical speciation and saturation index (SI) calculations were completed using PHREEQCi (Parkhurst & Appelo, 1999) using the WATEQ4F geochemical database modified to include Co, and the mineral phases lepidocrocite, siderite (c), and schwertmannite. Redox species distribution and SI values were based on solute concentrations, pH, pe and temperature.

3.3.5 Thermal Regime Monitoring

The internal structure of the test pile was instrumented with 150 thermistors distributed along tipping faces in the core and batter, and within the bedrock underlying the test pile (Smith *et al.*, 2013c). Temperatures were recorded at 4 hour intervals to provide a continuous record of thermal cycling within the pile.

3.4 Results and Discussion

3.4.1 Water Balance and Method Evaluation

Flow data evaluation is essential before scaling methods can be employed. A mass-balance approach equating measured outflow from basal drains and core lysimeters to predicted outflow based on net infiltration estimates demonstrated strong correlations across the flow system (Table 3.1). Daily net infiltration (mm) (Fretz, 2013, Krentz, In Progress) for the test pile areas was applied to the cross sectional area of each drainage system. Pore-volume saturation was assumed to be constrained to within the fine fraction (< 5 mm) material (Neuner *et al.*, 2013). This assumption had direct implications on the estimated number of pore-volume flushes; and results should be weighed accordingly. In late 2011 and 2012, one of the eight active BCLs (3BNClys2E; 4 m^2) began yielding disproportionately large volumes of water. On average, this BCL registered thirty-one times more flow per unit drainage area than the other BCLs. Drainage from this BCL was probably an amalgamation of flow from a larger drainage area (> 4 m^2) resulting from broken drain lines.

Water recovery and pore-volume flushes were evaluated separately for basal drains and active BCLs. Estimates from basal drainage showed significant recovery overall at 78 % of infiltration (Table 3.1). BCLs showed lesser recovery, with an average recovery of 25 % (SD 17 %) of infiltration (Table 3.1). Recovery from basal drains suggests the full test pile has undergone an 83 % pore volume flush (Table 3.1). Recovery from BCLs suggests that on average the core of the pile has undergone a 23 % (SD 16 %) pore volume flush (Table 3.1). These estimates suggest that the batter of the pile has undergone a 159 % pore volume flush. Consistency in the results between discrete BCLs suggests that collectively, they provide a

representative estimate of flow conditions in the test-pile core; thus scaling of BCL flow data to the core area generates accurate predictions of overall core drainage.

Daily flow from the test-pile core and batter subsystems was used to identify annual and cumulative flow trends. Drainage outflow from the test pile batter system was constrained to periods when mean ambient air temperatures were above 0 ^{o}C (Figure 3.3). Core outflow was constrained to periods when core basal temperatures were above 0 ^{o}C (Figure 3.3). Annual outflow from the test pile ranged between 111,000 L to 213,000 L (Table 3.2). Based on scaling of contributions from the core of the test pile, the annual core drainage volume ranged between 10,000 L and 46,000 L. Annual batter drainage ranged between 107,000 L and 204,000 L (Table 3.2). Rainfall and infiltration rates influenced the spatial distributions to outflow drainage. Annually, infiltration ranged between 14 % and 60 % of rainfall values (Fretz, 2013, Krentz, In Progress). Estimates of annual core contributions to drainage ranged between 5 % and 26 %, with a cumulative contribution of roughly 13 % (Table 3.3). In general, periods of weeks or months with increased infiltration resulted in increased core flow (Figure 3.4, Figure 3.5).

The impact of snow melt and enhanced infiltration on batter slopes is expected to have a significant influence on annual flow trends. Monitoring of water content in the test pile core revealed the arrival of a wetting front in the basal core at the end of 2008 (Fretz, 2013). Following wet-up, it was hypothesized that fluid flow within the test pile is primarily driven by the propagation of pressure waves through the matrix during significant infiltration events (Neuner *et al.*, 2013) and that flow is generally associated with periods of increased infiltration. A mass balance (infiltration vs. outflow) of the test pile core, batter and total systems between 2009 (post primary wet-up) and 2012 revealed a surplus mass release in the total pile and batter systems, and mass retention in the core system. Excess mass release attributed to the batters is

primarily derived from snow melt contributions (not included in infiltration calculations). Mass storage in the core system is attributed to permanent ice formation with a potential influence from secondary wet-up of unsaturated matrix zones. Results suggest that between 2009 and 2012, snow melt contributed 35 % to the total system outflow, and 59 % to the batter system outflow. Results indicate that snowmelt contributions are not significant in the core system; however as much as 110,000 L of water may be entrapped in the form of ice. If this ice is limited to the < 5 mm waste-rock fraction, it would occupy 2300 m^3 of bulk waste-rock material; constituting a 1.65 m thick zone of ice throughout the entire core subsystem (1350 m^2). Estimates of core and batter snowmelt contributions are consistent with field observations describing an annual buildup of snow on the batters of the pile and scouring of snow on the crest of the pile. Thermal monitoring in the core of the test pile identified basal regions which may allow for ice accumulation. More detailed flow system analysis including measurements of oxygen isotopes, batter tracers and snowmelt and ice formation modelling would help refine these estimates.

3.4.2 Spatial Variability in Waste-Rock Geochemistry

A detailed evaluation of geochemical results obtained from total basal drainage, estimated core drainage and estimated batter drainage was conducted to illustrate spatial variations within the geochemical environment of the test pile. Cumulative annual loading from each subsystem was used to calculate flow-weighted mean annual concentrations (Table 3.4). Using this approach, estimates of mean concentrations in the core and total drainage systems were in excellent agreement with concentrations from direct measurements of basal drain and BCL water.

A comparison of mean annual concentrations in the core and batter of the test pile revealed two distinctly different and contrasting environments (Table 3.4). Relative to the batter, the mean concentrations of trace metals associated with sulfide oxidation (Ni, Co, Cd, Zn, Cu, Fe) in the contributions from the core of the test pile were generally 3.6 to 6.9 times greater than the concentrations in the batter contributions; while the mean sulfate concentration was 2.8 times greater. Mean concentrations of cations derived from acid consuming reactions (Ca, Mg, Al, Na, Si, K) were 2.5 to 4.6 times greater in the core than in the batter contributions. Concentrations of blasting residuals (Cl^-, NH_3, NO_2^-, NO_3^-) were much higher in the core (6.3 to 8.4); an observation which is principally attributed to disproportionately rapid flushing of pre-existing blasting residuals from the test pile during tracer tests initiated in 2007. Concentrations of tracers (Br^-, Cl^-) were also much greater in the core (17.7 and 6.3 respectively) than in the batter components. Exceedingly high concentrations of Br^- in the core were expected because Br^- tracer was deposited exclusively over the core region of the test pile. A lower relative concentration of Cl^- in the core indicates that non-tracer sources of Cl^- appear to be significant in the test pile system.

In the test-pile basal drainage, mean concentrations of various solutes rose annually with strong positive correlations between mean concentration and year. Basal drainage development was primarily attributed to the progressively evolving water chemistry in the core of the test pile, and increasing contributions from the core to the total drainage (Chapter 2). In the core subsystem, mean annual concentrations also rose annually with strong positive correlations between mean concentration and year. Core drainage development was attributed to the progressively evolving weathering front within the core of the test pile (Chapter 2). In the batter

subsystem, mean annual concentrations were more uniform between years, which was consistent with the hypothesis that the geochemical system in the pile batters is more mature and stable.

A Pearson product-moment correlation analysis was completed independently for each of the test pile subsystem datasets (Total Drainage, Core Drainage and Batter Drainage; for each pair of: Flow, Air Temperature, Core Temperature, pH, EC, Cl^-, NO_3^-, SO_4^{2-}, Ca, Mg, Na, Si, K, Al, Fe, Co, Ni, Cu, Zn, Cd; Table 3.5, Table 3.6, Table 3.7) to help explain contrasting geochemical trends observed between the core of the test pile and the batters. Pearson correlation coefficients (PCCs) quantify the strength (0 to 1) and direction (positive or negative) of a linear relationship between two variables. Results were used for the identification of common mechanisms that control the distribution of different elements throughout the test pile. Variations in the concentrations of dissolved metals with the same predicted source were often highly correlated.

The PCC between Ni and Co was consistently greater than 0.98 within all subsystems of the test pile. The strong correlation between Ni and Co concentrations is consistent with the assumption that they are exclusively derived from pyrrhotite [$Fe_{0.852}Ni_{0.004}Co_{0.001}S$] oxidation and that both metals were uniformly affected (or not affected) by secondary mineral precipitation-dissolution reactions or surface complexation processes. Additionally, the correlation between Ni, Co and other sulfide-mineral oxidation products, Zn and Cd from sphalerite [(Zn, Fe)S; with trace Cd replacement] and Cu from chalcopyrite [$CuFeS_2$] were consistently strong (PCC = 0.73 to 0.98). Strong correlations in trace metal concentrations are consistent with the hypothesis that oxidation of all sulfide minerals occurred concurrently. The lower range of correlations observed between Cu, Zn, Cd and Ni, Co (PCC = 0.73 to 0.98) was probably caused by sorption on hydroxide minerals (Dzombak & Morel, 1990, Balistrieri *et al.*,

2003, Dyer *et al.*, 2004) with greater sorption expected on Fe-hydroxide phases than Al-hydroxide phases (Paulson & Balistrieri, 1999). The PCCs between Ca, Mg, Na and K were generally greater than 0.85 within all subsystems of the test pile. Strong correlations among major cation concentrations are consistent with the hypothesis that these elements were primarily released through the dissolution of carbonate and aluminosilicate phases. Correlations between Si, Fe and Al concentrations were generally lower (PCC = 0.3 to 0.7). Poor correlations between Si concentrations and those of the major cations were probably due to the precipitation of quartz [SiO_2], with additional retention by Si surface complexation at higher pHs (Hiemstra *et al.*, 2007). Poor correlations between Fe and Al concentrations were probably due to successive secondary mineral precipitation-dissolution reactions resulting in progressive accumulation and depletion of Al and Fe hydroxide and hydroxysulfate phases (Gunsinger *et al.*, 2006b, Jurjovec *et al.*, 2002, Moncur *et al.*, 2005) (Figure 3.6). Saturation index calculations demonstrated occasional thermodynamically favourable conditions for the secondary precipitation of montmorillonite [$Ca_{0.165}Al_{2.33}Si_{3.67}O_{10}(OH)_2$] and illite [$K_{0.6}Mg_{0.25}Al_{2.3}Si_{3.5}O_{10}(OH)_2$], which commonly occur as alteration products of muscovite and feldspar. These secondary precipitation-dissolution controls are expected to impact the concentrations of these major cations. Water flow, ambient air temperature, and core temperature were very poorly correlated with all parameters; however, after 2009, when a steady state flow system was established in the interior of the test pile and after the internal geochemical system stabilized in 2012, a modest trend to increasing correlations was observed.

Between the test pile subsystems, the batter component consistently exhibited equal or higher PCCs, with the exception of Si and Cd. Low PCCs for these two parameters were attributed to mobility constraints through surface complexation reactions (Haines & Lloyd, 1985,

Hiemstra *et al.*, 2007) at the higher pH conditions prevalent in the batter. Stronger PCCs were expected in the batter because this subsystem has flushed the most water, was influenced by more instantaneous and less complex freeze-thaw cycling and has developed the most stable geochemistry. Weaker PCCs were expected in the core because this subsystem has not flushed as much water as the batter and has less developed and less stable geochemistry. Total drainage geochemical conditions varied significantly throughout each year due to the effect of freeze-thaw cycling on the timing of spatial contributions to drainage (Chapter 2), which was expected to have a negative impact on PCCs.

Elements which routinely have high PCCs are likely to have fewer factors controlling their release and attenuation. In contrast, low PCCs are anticipated for parameters which are likely to be affected by more complex secondary controls on mobility (sorption, precipitation-dissolution). A 'full system control level', defined as the percentage of good PCCs (> |0.7|) for a given parameter was calculated within each subsystem. Parameters were ranked within each subsystem, and cumulatively (Table 3.6) to determine which components produced consistently high PCCs. Freeze-thaw cycling, fluid flow rates, and the pH environment differ significantly between the core, batter and complete test pile systems. A 'cross-environment control level', defined as the percentage of good PCCs that were also roughly equivalent at two levels in the subsystem hierarchy (*eg.* $PCC_{CoreNi} \approx PCC_{BatterNi} > |0.7|$), was calculated for each parameter-subsystem pair. Parameters were ranked in each subsystem pair, and cumulatively (Table 3.7) to determine which components produced consistently high PCCs across varying spatial scales. This ranking identified parameters for which the release and attenuation mechanisms are consistent irrespective of the subsystem within the test pile.

Nickel, Co, Mg, Na and SO_4 consistently ranked high using both system correlation ranking schemes. This observation suggests that the mechanisms which control the distribution of these parameters can be explained by more uniform geochemical dynamics; and thereby they can likely be reproduced using simplified methods. This also suggests that the mechanisms which control the source, release and attenuation of these parameters are similar in the core and batter; therefore the differences in temperature cycling, fluid flow rates, reactive pathway length and the pH environment do not significantly impact the correlation coefficients. Iron, Si and pH were consistently very low in both subsystem ranking schemes. Poor correlations suggest that a complex combination of mechanisms may affect the distribution of these elements, including surface complexation and secondary mineral precipitation-dissolution reactions. Advanced reactive transport modelling would likely be required to describe these reaction sequences and provide meaningful predictions of the distribution of these elements. Parameters which demonstrated moderate overall correlations under both ranking schemes included: Cd, Al, Ca, Cl, Cu, NO_3^-, Zn, and K.

3.4.3 Spatial Contributions to Drainage Loading

Contrasting physiochemical environments in the core and batter of the test pile combined with the influence of freeze-thaw cycling on water transport to the basal drainage system has the potential to generate predictable fluctuations in the annual loading cycles. Daily, annual and cumulative loadings of all chemical parameters were examined in the core, batter, and total drainage systems (Table 3.2). Despite minor flow contributions from the core of the test pile, core loads often comprised a much larger proportion of the total drainage load (Table 3.3). Emphasis was placed on the evaluation of: 1) parameters which routinely produced strong correlations in the core and batter subsystems and are thus likely to have simple reaction

sequences controlling their release and attenuation (Ni, Co, Mg, SO_4^{2-}), 2) parameters that are derived from sulfide oxidation and acid neutralization processes (Al, Ca, Fe); and 3) parameters which are linked to blasting practices and the 2007 tracer tests (Cl^-, NO_3^-).

The wetting front reached the base of the central portion of test pile in August 2008. Therefore, basal outflow throughout 2007, which reached 111,000 L, was entirely derived from the test pile batters. The cumulative annual loading of various dissolved constituents in the 2007 basal drainage was the lowest observed throughout the life of the project (SO_4: 8.77×10^4 g; Cl^-: 2.65×10^3 g; NO_3^-: 4.67×10^4 g; Ca: 1.49×10^4 g; Mg: 1.56×10^4 g; Ni: 1.68×10^2 g; Co: 3.21×10^1 g; Al: 1.09×10^1 g; Fe: 2.14 g). In subsequent years a steady linear annual increase in the cumulative basal drainage loading was observed for all parameters, with a maximum annual release in 2012 (SO_4: 3.01×10^5 g; Cl^-: 9.15×10^3 g; NO_3^-: 8.71×10^4 g; Ca: 3.19×10^4 g; Mg: 5.98×10^4 g; Ni: 1.54×10^3 g; Co: 2.98×10^2 g; Al: 1.22×10^3 g; Fe: 5.24×10^1 g), with the exception of Cl^- and NO_3^- which peaked in 2011. Diminishing concentrations of tracers and blasting residuals is expected as the initial pore water continues to flush. Retention of Al and Fe, in the early stages of geochemical evolution, is attributed to the precipitation of Al and Fe hydroxides and hydrosulfates, similar to reaction sequences observed in mine tailings impoundments (Gunsinger *et al.*, 2006b, Jurjovec *et al.*, 2002, Moncur *et al.*, 2005). A downward weathering front represented by a decrease in pH and subsequent progression through acid-neutralization phases (Chapter 2) resulted in rising loads from remobilized Al and Fe (albeit very limited). Annual rainfall and infiltration, which varied greatly between years, did not appear to directly control annual basal drainage flow or geochemical loading. Incorporating the unresolved impact of snowmelt contributions on the internal flow regime could improve this correlation and should be considered in future studies.

Annual loadings of dissolved constituents from the core of the test pile were less uniform and less predictable than the total test pile drainage loading. Years with substantial rainfall and infiltration had moderate positive correlations with years of increased core flow. Stronger positive correlations between infiltration and loading were expected in the core subsystem given that snowmelt is insignificant. A substantial flux of elements from the core of the test pile was coincident with the arrival of a wetting front at the base of the pile in August 2008. The initial release of pore water from the core of the pile occurred during a period with high annual rainfall (179.7 mm) and infiltration (104.5 mm) (Fretz, 2013), and the second highest volume of annual core flow (31,000 L). Annual core solute loading in 2008 was the third highest observed during the life of the project (SO4: 4.6 x 104 g; Cl-: 4.5 x 103 g; NO3-: 5.1 x 104 g; Ca: 1.3 x 104 g; Mg: 1.2 x 104 g; Ni: 2.2 x 102 g; Co: 4.1 x 101 g; Al: 1.0 x 102 g; Fe: 1.7 x 101 g) in spite of the immature development of the geochemical system in the core of the test pile (Chapter 2). The high flux of solutes in 2008 was primarily attributed to the initial flush of oxidation products related to the blasting of waste-rock material (Bailey *et al.*, 2013). Subsequent years exhibited a linear increase in the cumulative core loading of most chemical parameters. Solute release from the core peaked in 2011 (SO_4: 1.2 x 10^5 g; Cl^-: 7.1 x 10^3 g; NO_3^-: 1.1 x 10^5 g; Ca: 2.0 x 10^4 g; Mg: 3.1 x 10^4 g; Ni: 7.9 x 10^2 g; Co: 1.7 x 10^2 g; Al: 5.0 x 10^2 g; Fe: 2.2 x 10^1 g) which was coincident with a year of significant infiltration (83.1 mm) and the maximum estimated core basal outflow (46,000 L). Despite low rainfall (56.3 mm), infiltration (8.9 mm) and moderate core outflow (24,000 L) in 2012, solute release (SO_4: 9.2 x 10^4 g; Cl^-: 3.4 x 10^3 g; NO_3^-: 5.3 x 10^4 g; Ca: 1.2 x 10^4 g; Mg: 2.4 x 10^4 g; Ni: 6.7 x 10^2 g; Co: 1.3 x 10^2 g; Al: 4.2 x 10^2 g; Fe: 1.3 x 10^1 g) was similar to the peak release observed in 2011.

Patterns of annual batter loading are consistent with the hypothesis that the geochemical system in the pile batters is more mature and stable, resulting in more uniform solute concentrations. Mean annual solute loadings from the batters exhibited irregular variations between 2007 and 2012 (Table 3.2), with weak inter-annual trends. Batter solute release peaked in 2012 (SO_4: 2.1 x 10^5 g; Cl^-: 5.8 x 10^3 g; NO_3^-: 3.4 x 10^4 g; Ca: 2.0 x 10^4 g; Mg: 3.6 x 10^4 g; Ni: 8.7 x 10^2 g; Co: 1.7 x 10^2 g; Al: 8.0 x 10^2 g; Fe: 3.9 x 10^1 g), which was coincident with a year of limited infiltration (8.9 mm) and moderate estimated batter outflow (145,000 L). Overall, batter flow had no correlation with rainfall or infiltration, which was fundamentally caused by the unresolved control of snowmelt on batter flow. Batter loading demonstrated moderate negative correlations with rainfall and infiltration. The observed negative correlation between batter load and infiltration was explained by: 1) kinetic limitations on element release caused by decreased residence time near the base of the batter, where the large grain sizes are predominant and residence times are low, during periods of rapid flow (snowmelt and high rainfall); and 2) an artifact of snowmelt contributions to batter drainage which were not captured by rainfall or infiltration estimates.

Mean subsystem loading datasets provide well-constrained measurements of aggregated daily loading from 'active' subsections of the pile. Analyzing the geochemical loading data in terms of relative contributions of the core drainage to the total drainage has two main benefits: 1) it provides a quantitative estimate of the spatial contributions to drainage loading, which will assist in the development of reactive transport models; and 2) it offers a novel approach to assist in the identification of geochemical processes within waste-rock systems. The integration of the spatial contribution analysis with PCC analysis can further clarify mechanisms that control the distribution of solutes in waste-rock piles. The core contributions of all constituents were

computed annually and cumulatively (Table 3.3). Despite modest annual core contributions to flow (5 % to 26 %); annual core contributions of various solute loads ranged between 9 % and 85 %; representing contributions much greater than expected due to flow variability. This is consistent with the idea that snowmelt dilution greatly affects batter geochemistry but is not significant in the core system.

Annual core contributions of Ni and Co ranged between 14 % and 85 %, with a cumulative contribution estimated at roughly 45 %. Contributions of Ni and Co persisted in excellent agreement throughout the life of the project. Strong PCCs between these dissolved metals, combined with the similar ranges of contribution results strongly suggest that Ni and Co are solely derived from pyrrhotite oxidation. The similarity of the cumulative core contributions of Cd and Zn (35 % and 37 % respectively), combined with strong PCCs between Zn and Cd concentrations, suggests that these elements are derived from sphalerite oxidation. Surface complexation models (Dzombak & Morel, 1990) predict a preference for Cd and Zn sorption, relative to Ni and Co, at lower pHs. These results could partially explain the retention of Zn and Cd in the core of the test pile. Dissolved Cu is probably derived from the oxidation of chalcopyrite. The contributions of Cu associated with the core drainage (51 %) relative to drainage derived from the batters was greater than observed for the other trace metals. Higher core contributions of Cu were likely related to more extensive sorption of Cu in the batters (Dzombak & Morel, 1990). Heterogeneous oxidation of sulfide minerals may also have contributed to the observed variability in trace metal contributions attributed to the core drainage; however the strong PCCs between the trace metal concentrations is consistent with concurrent dissolution of sulfide phases. In addition, a recent study found that the surface complexation constants of Dzombak and Morel underestimated adsorption of Cd, Zn, Ni, Co and

other trace metals on Fe-oxides when concentrations significantly exceeded the availability of surface binding sites (Balistrieri *et al.*, 2003).

Sulfate is also derived from sulfide-mineral oxidation. Sulfate contributions associated with core drainage ranged between 9 % and 56 %, with an estimated cumulative contribution of 29 %. Lower than expected contributions of SO_4 from the core of the test pile were probably due to precipitation of secondary S phases (Figure 3.6). Thermodynamic calculations conducted using PHREEQCi on water samples from the test pile drainage systems indicated that the core system, and to a lesser extent the batter system, are often saturated or supersaturated with respect to the secondary S phases: gypsum, jarosite (ss), jarosite-K and alunite. Annual core contributions of constituents derived from aluminosilicate weathering (Ca, Mg, Al, Na) were observed at relatively uniform core: total ratios based on annual loading calculations, particularly in the later, more geochemically-developed years. Annual core contributions of these major cations generally ranged between 12 % and 84 %, with an overall core contribution of roughly 40 %. Core contributions of Al were slightly higher than those of Ca, Mg and Na, which is primarily attributed to the dissolution of Al-hydroxide phases as the pH of the core effluent declined to pH < 4.5 (Figure 3.6).

Core contributions of blasting residuals (NO_3^-, NH_3, Cl^-) and tracers (Cl^-, Br^-), which peaked during the first flush of core water in 2008 (at greater than 1000 % for Br), remained very high throughout each year with cumulative contributions ranging between 48 % and 72 %. High contributions of tracers were largely explained by the historically unbalanced distribution on the pile crest, which was further amplified by accelerated water flushing during the tracer tests.

3.4.4 Depletion of Sulfide Minerals

The total mass of S, Ni, Co and Fe contained within each of the test pile subsystems was estimated using: 1) the waste rock volumes overlying the basal liner (total: 31930 m^3; core: 18230 m^3 or 57 % of the total; batter 13700 m^3 or 43 % of the total (Smith, 2006); 2) a waste-rock porosity of 0.25 (Neuner *et al.*, 2013), 3) a particle density of 2.7 g cm^{-3} (Neuner *et al.*, 2013), 4) the grain-size distribution and S content data (Smith *et al.*, 2013b), 5) the global test pile wt. % S of 0.053% (Smith *et al.*, 2013b); and 6) the known composition of sulfide minerals in the waste rock (Jambor, 1997). Values for grain-size fraction specific S content in the less than 50 mm grain size fractions were scaled to the global test pile S content of 0.053 %. Sulfur content in the grain-size fractions larger than 50 mm were extrapolated assuming that the mean S content in the 1.25 to 50 mm grain size fractions (0.046 wt. % S) was representative for all larger grain sizes. The estimated S content of the > 50 mm grain size fractions were expected to be accurate since the range of mean S contents within the 1.25 to 40 mm grain size fractions were statistically equivalent at the 95 % confidence interval. Measured values of S were assumed to be derived entirely from the rapidly oxidizing mineral pyrrhotite [$Fe_{0.852}Ni_{0.004}Co_{0.001}S$]. The associated mass of Fe, Ni and Co was estimated based on the molar ratio determined for Diavik pyrrhotite (Jambor, 1997).

The very fine fraction (less than 0.25 mm) of waste-rock material can contribute to up to 80 % of sulfide oxidation products (Strömberg & Banwart, 1999). The less than 5 mm fraction of the Diavik waste rock also has the greatest potential to store and transmit matrix pore water (Neuner *et al.*, 2013). Due to elevated sulfide contents in the finer fraction material, 20 % of the total mass of sulfur was distributed within the less than 5 mm range, while only representing 14 % of the waste rock by weight. The total test pile mass of S, Ni, Co and Fe was estimated within

the full spectrum of grain sizes (S: 33000 kg, Ni: 240 kg, Co: 61 kg, Fe: 49000 kg), the less than 50 mm grain size fraction (S: 13000 kg, Ni: 97 kg, Co: 24 kg, Fe: 20000 kg), and the less than 5 mm grain size fraction (S: 6700 kg, Ni: 49 kg, Co: 12 kg, Fe: 9900 kg). Results were further subdivided between the core and batter subsystems (Table 3.10). The less than 5 mm grain size fraction was believed to contribute the greatest amount to overall metal release. The less than 50 mm grain size fraction was considered to contain the majority of sulfides potentially available for long-term oxidation processes.

Focus was placed on the annual and cumulative depletion of S, Ni, Co and Fe in the less than 5 mm grain-size fraction after six years of weathering (Table 3.11). By 2012, the full test pile had released 341 kg of S, 4.39 kg of Ni, 0.885 kg of Co, and 0.150 kg of Fe, which corresponded to a net depletion of 5.1 %, 9.0 %, 7.2 % and 0.0 % respectively. By 2012, the core of the test pile had released approximately 99 kg of S, 2.0 kg of Ni, 0.39 kg of Co, and 0.067 kg of Fe, which corresponded to a net depletion of 2.6 %, 7.0 %, 5.6 % and 0.0 % respectively. By 2012, the batter of the test pile had released approximately 240 kg of S, 2.4 kg of Ni, 0.49 kg of Co, and 0.083 kg of Fe, which corresponded to a net depletion of 8.4 %, 11.6 %, 9.4 % and 0.0 % respectively. Under the geochemical conditions which prevail in the test pile system, Ni release can be considered the most mobile tracer of sulfide oxidation processes (Dzombak & Morel, 1990, Gunsinger *et al.*, 2006b). Mean annual release of Ni in 2011 and 2012 was 2.5 %, 2.6 %, and 2.4 % in the total, core and batter systems respectively. If release rates persist at these levels, depletion of sulfides in the < 5 mm fraction could be complete within 37 years. Investigation of element release rates from the Diavik humidity cell experiments indicated that release rates began to exhibit an exponential decline after a 15 % depletion of S from the system (Langman, In Progress). Declining release rates were attributed to the

accumulation of secondary minerals on the surface of sulfide mineral grains. Based on humidity cell results, the test pile release rates are likely approaching a maximum (Langman, In Progress); thus exhaustion of S in the < 5 mm fraction could take significantly more than 37 years.

Following six years of weathering in a system with limited metal retention – as observed with Ni – a net release of roughly 9.0 %, 7.0 % and 11.6 % of all sulfide oxidation products (Ni, Co, S and Fe) would be expected in the total, core, and batter systems respectively. Differences observed relative to the release of Ni can be attributed to secondary controls on element mobility including precipitation-dissolution reactions and sorption on hydrous ferric oxides. Co release was 7.2 %, 5.6 % and 9.4 % in the total, core, and batter systems respectively. Observations of the Ni to Co ratio in drainage samples remained between 3-6_{Ni}:1_{Co} at pH values below 5.5; however this relationship was found to break down and increase as high as 30_{Ni}:1_{Co} as pH values increased up to pH 8 (Figure 3.7). Despite these results, Co did not show preferential retention in the higher pH batter subsystem. Divergence between Ni and Co release estimates may therefore be related to an imprecise 4_{Ni}:1_{Co} molar ratio estimate for pyrrhotite [$Fe_{0.852}Ni_{0.004}Co_{0.001}S$], for which aqueous geochemical results propose a ratio closer to 5_{Ni}:1_{Co}. Total S release was 5.1 %, 2.6 % and 8.4 % in the total, core, and batter systems respectively. Lower than expected release of S, relative to Ni, was probably due to secondary mineral formation. A larger decrease in S release was observed in the core subsystem relative to the batter subsystem. Nonconformity between core and batter S release variations and the release rate expected based on the Ni results may be due to the precipitation of gypsum and some hydrous sulfates (Jarosite (ss), Jarosite-K). Saturation with respect to these phases was observed throughout the core subsystem, and to a lesser extent throughout the batter subsystem (Figure 3.6). Fe release was 0.0 % in all test pile systems. Despite an available reactive mass of roughly

9.9 tons of Fe (from pyrrhotite only), 150 g was released from the entire test pile by the end of 2012. Nearly complete retention of Fe within the test pile was attributed to the formation of several secondary minerals. Geochemical modelling suggests that the conditions prevalent throughout the test pile often favour the precipitation of ferrihydrite, goethite, lepidocrocite, schwertmannite and hematite. These secondary Fe phases account for the vast majority of trace metal scavenging which occurs in the system (Paulson & Balistrieri, 1999). Conformity between the core and batter Fe release ratios with the Ni standard suggests that Fe in not being preferentially retained in the core or batter subsystems.

3.5 Conclusions

Fluid flow and solute loading from the base of a waste-rock test pile can be divided into discrete core and batter subsystems by scaling data from representative core lysimeters and using a mass balance approach to estimate batter characteristics. Evaluation of loading estimates revealed distinct and contrasting geochemical environments within the core and batter subsystems. Estimated solute concentrations in the core were much higher than those in the batter. Concentration variance between these subsystems was partially explained by the effect of snowmelt dilution in the batter. Despite minor contributions to drainage outflow, up to 50 % of many solute loads were attributed to the core. Combining results from a Pearson product-moment correlation analysis and the quantitative evaluation of spatial contributions to drainage loading assisted in the identification of the release and transport mechanisms that control the mobility of several trace and major elements in the test pile system. Element release and depletion estimates from the test pile core and batter subsystems suggest that the application of a low sulfide cover layer would promote the thermal isolation of the core of the test pile through the upward aggradation of permafrost in the bedrock. Isolation of the core could lead to a significant decrease in the reactive mass of waste rock available for ARD processes. In addition, a shift to a batter dominated system would significantly decrease the expected range of leachate concentrations and a related decrease in the predicted range of daily and annual drainage solute loadings.

3.6 Figures

Figure 3.1 – Location of the Diavik Diamond Mine on the East Island of Lac de Gras, in the Northwest Territories, Canada (64°29’ N; 110°18’ W) (from Smith, 2013).

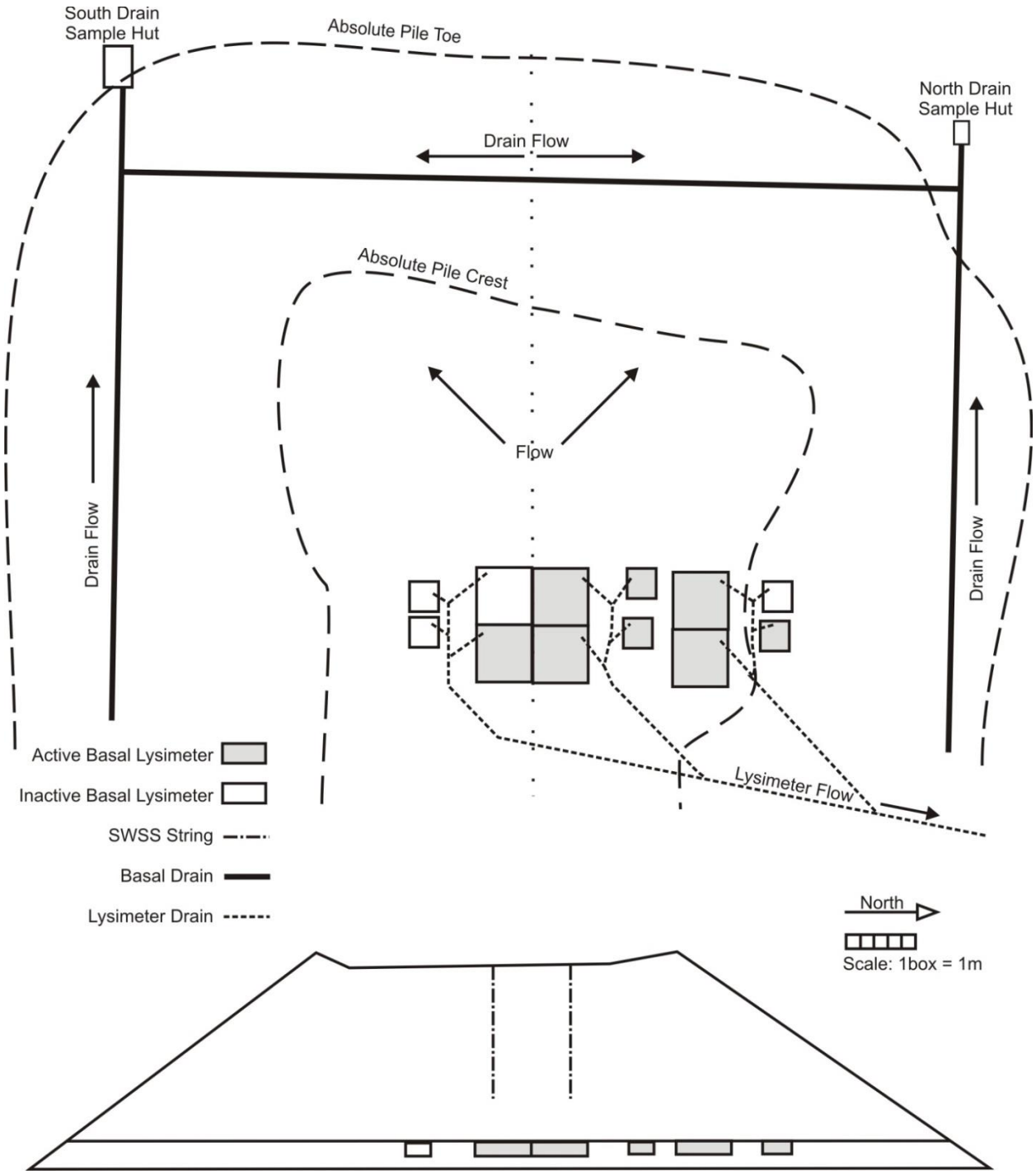

Figure 3.2 – Instrumentation layout and data sources inside the Type III test pile.

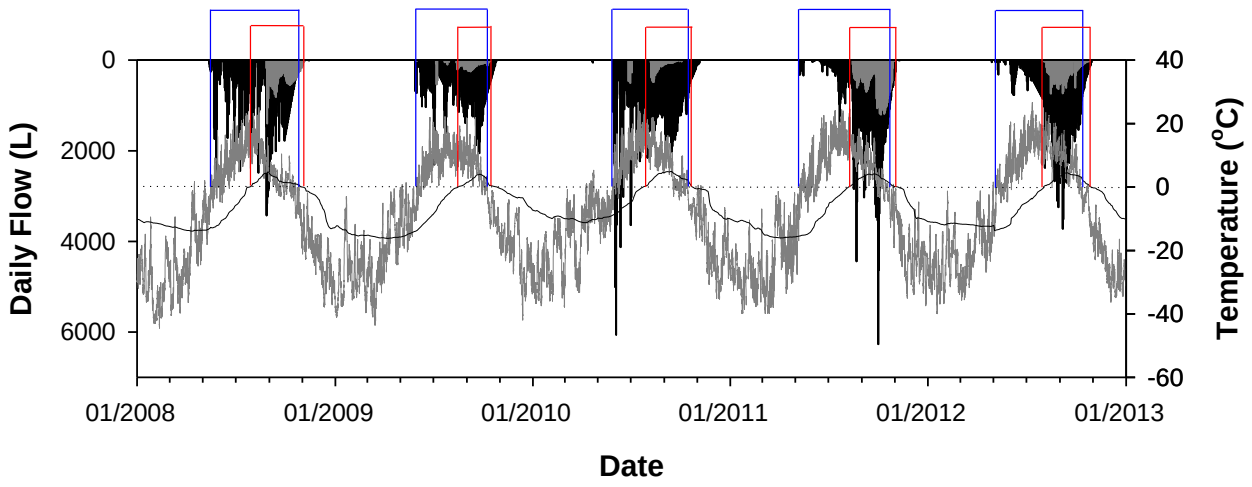

Figure 3.3 – Daily outflow from the core (grey) and total drainage (black) systems. Highly variable mean ambient air temperature (grey) and stable core basal temperature (black) demonstrate freeze-thaw controls on internal water flow. Red boxes outline time periods when core basal temperatures are above zero. Blue boxes outline time periods when ambient air temperatures are above zero. Results supports core and batter scaling methodology.

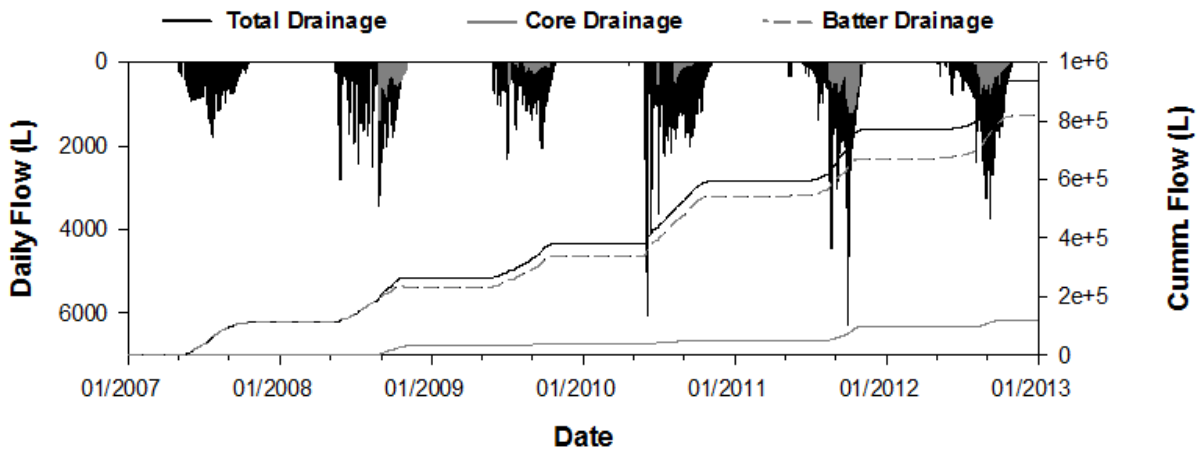

Figure 3.4 – Internal flow summary for the Type III test pile. Daily flow from the full test pile (black) and the estimated contribution attributed to the core (grey) demonstrate spatial distributions in drainage throughout each year. Cumulative flow split between the core and batter subsystems demonstrate the overall prevalence of water derived from the test pile batter.

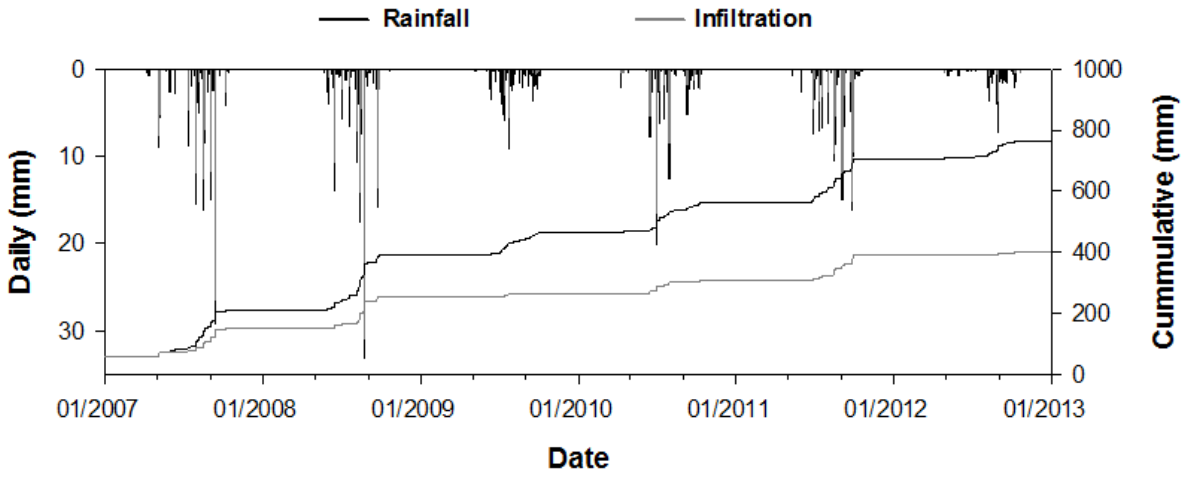

Figure 3.5 – Estimated infiltration (grey) as a proportion of measured rainfall (black) (dataset from Fretz 2013, updated by Krentz 2014). In general, rainfall events greater than 5 mm result in infiltration. Years with substantial rainfall and infiltration are moderately correlated with years of higher estimated core flow.

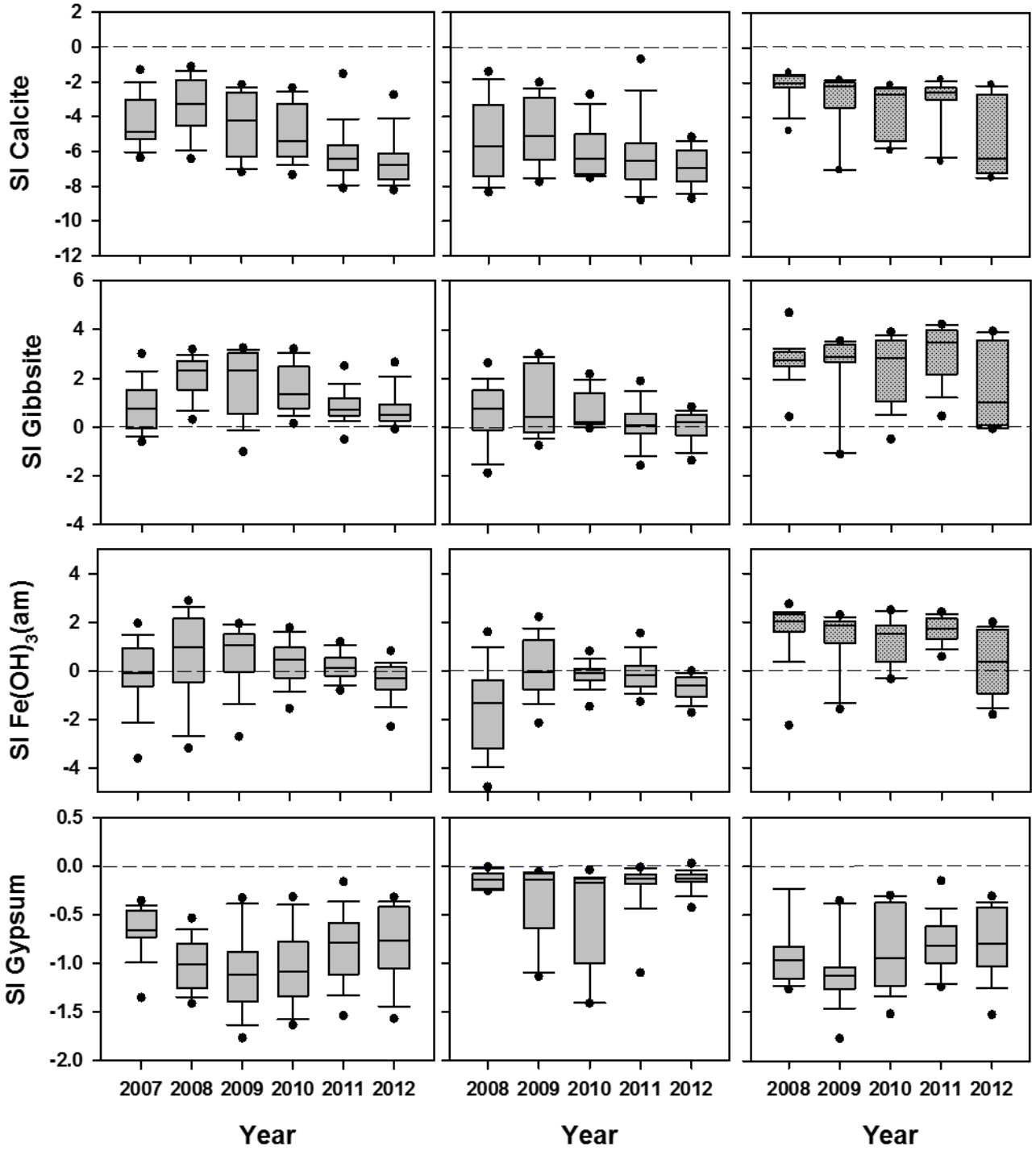

Figure 3.6 – Select annual box and whisker plots displaying results from saturation index modelling for calcite, gibbsite, ferrihydrite and gypsum from the total drainage (a), core drainage (b) and batter drainage (c) systems.

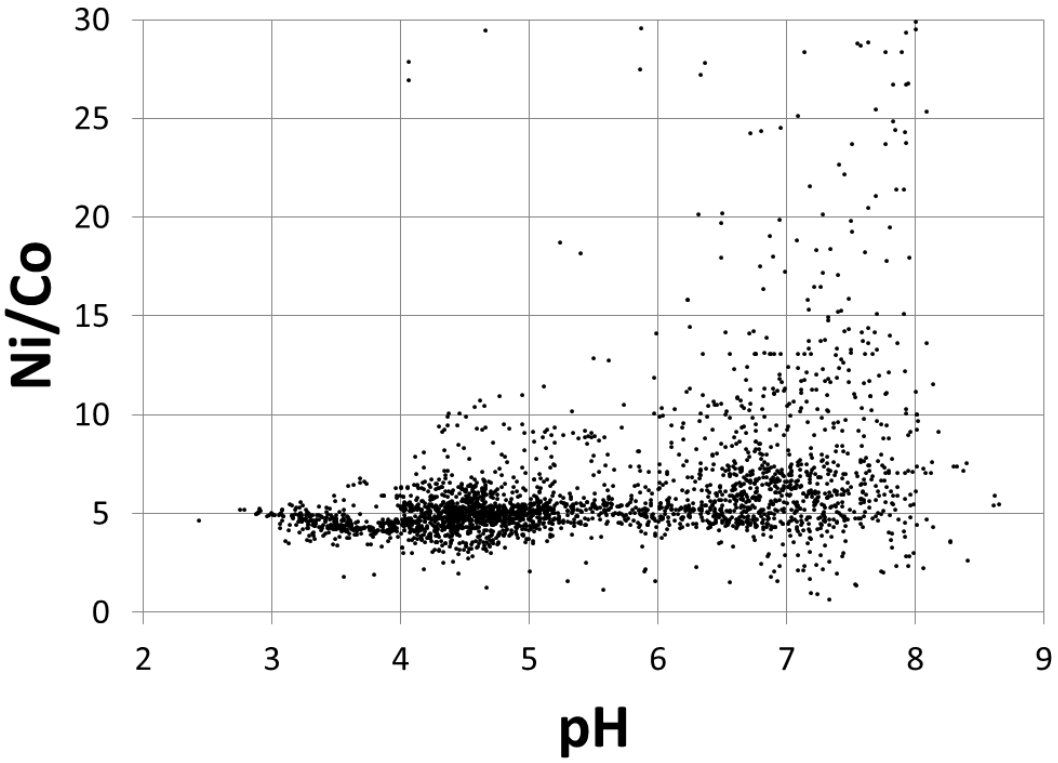

Figure 3.7 – Ni/Co molar ratio relationship over the full pH spectrum demonstrates an apparent retention of Co within the test pile when pH values rise above 5.5.

3.7 Tables

Table 3.1 - Water balance and validation of flow data sources in the Type III test pile. Total infiltration is scaled to each drainage area using infiltration estimates by Fretz (2013), updated by Krentz (2014). Total flow out is measured on site using calibrated tipping buckets (Fretz, 2013). Pore volume flushes are based on pore water being limited to the < 5 mm grain size fraction of waste rock.

	Lysimeters						Drains		Full Pile
	2x2m 3BNClys2E	2x2m 3BNBlys2E	4x4m 3BNBlys4W	4x4m 3BSClys4E	4x4m 3BNClys4E	4x4m 3BNClys4W	25x60m 3BSxdrn15	25x60m 3BNxdrn15	50x60m T3 Pile
Tot Infiltration (L)	*1599*	*1599*	*6397*	*6397*	*6397*	*6397*	*599758*	*599758*	*1199517*
Tot Flow Out (L)	*12275*	*235*	*2108*	*752*	*3536*	*647*	*831962*	*106529*	*938491*
Recovery	768%	15%	33%	12%	55%	10%	139%	18%	78%
Pore Volume Flush	718%	14%	31%	11%	52%	9%	146%	19%	83%

Excluding 3BNClys2E			
AVG % Recovery	*25%*	Stdev	*17%*
Pore Volume Flush	*23%*	Stdev	*16%*

Table 3.2 – Select results of annual and cumulative flow and loading in total drainage, core drainage and batter drainage systems. Infiltration estimates by Fretz 2013, updated by Krentz 2014.

			Total Drainage									
	Rainfall (mm)	Infiltration (mm)	Flow (m^3)	SO_4 (g)	Cl (g)	NO_3 (g)	Ca (g)	Mg (g)	Ni (g)	Co (g)	Al (g)	Fe (g)
2007	*152.7*	*92.2*	*111.1*	*8.77E+04*	*2.65E+03*	*4.67E+04*	*1.49E+04*	*1.56E+04*	*1.68E+02*	*3.21E+01*	*1.09E+01*	*2.14E+00*
2008	*179.7*	*104.5*	*152.5*	*1.01E+05*	*1.60E+03*	*2.43E+04*	*1.59E+04*	*1.60E+04*	*2.95E+02*	*5.94E+01*	*3.97E+01*	*1.83E+01*
2009	*74.0*	*10.3*	*116.3*	*1.19E+05*	*4.51E+03*	*7.40E+04*	*1.64E+04*	*2.56E+04*	*5.76E+02*	*1.11E+02*	*2.48E+02*	*2.42E+01*
2010	*97.6*	*43.0*	*213.3*	*2.00E+05*	*7.93E+03*	*1.08E+05*	*3.00E+04*	*4.05E+04*	*8.80E+02*	*1.70E+02*	*3.04E+02*	*2.04E+01*
2011	*145.5*	*83.1*	*175.7*	*2.13E+05*	*1.06E+04*	*1.16E+05*	*2.98E+04*	*4.42E+04*	*9.26E+02*	*2.15E+02*	*8.53E+02*	*3.28E+01*
2012	*56.3*	*8.9*	*168.6*	*3.01E+05*	*9.15E+03*	*8.71E+04*	*3.19E+04*	*5.98E+04*	*1.54E+03*	*2.98E+02*	*1.22E+03*	*5.24E+01*
Total	**764**	**400**	**937.4**	**1.02E+06**	**3.65E+04**	**4.55E+05**	**1.39E+05**	**2.02E+05**	**4.39E+03**	**8.85E+02**	**2.68E+03**	**1.50E+02**

			Core Drainage									
	Rainfall (mm)	Infiltration (mm)	Flow (m^3)	SO_4 (g)	Cl (g)	NO_3 (g)	Ca (g)	Mg (g)	Ni (g)	Co (g)	Al (g)	Fe (g)
2007	*152.7*	*92.2*	*0*	*0.0E+00*	*0.0E+00*	*0.0E+00*	*0.0E+00*	*0.0E+00*	*0.0E+00*	*0.0E+00*	*0.0E+00*	*0.0E+00*
2008	*179.7*	*104.5*	*31*	*4.6E+04*	*4.5E+03*	*5.1E+04*	*1.3E+04*	*1.2E+04*	*2.2E+02*	*4.1E+01*	*1.0E+02*	*1.7E+01*
2009	*74.0*	*10.3*	*10*	*2.2E+04*	*1.8E+03*	*2.6E+04*	*4.3E+03*	*6.2E+03*	*1.5E+02*	*2.9E+01*	*6.3E+01*	*9.8E+00*
2010	*97.6*	*43.0*	*10*	*1.9E+04*	*8.7E+02*	*1.8E+04*	*3.5E+03*	*4.8E+03*	*1.3E+02*	*2.4E+01*	*6.3E+01*	*4.8E+00*
2011	*145.5*	*83.1*	*46*	*1.2E+05*	*7.1E+03*	*1.1E+05*	*2.0E+04*	*3.1E+04*	*7.9E+02*	*1.7E+02*	*5.0E+02*	*2.2E+01*
2012	*56.3*	*8.9*	*24*	*9.2E+04*	*3.4E+03*	*5.3E+04*	*1.2E+04*	*2.4E+04*	*6.7E+02*	*1.3E+02*	*4.2E+02*	*1.3E+01*
Total	**764**	**400**	**121**	**3.0E+05**	**1.8E+04**	**2.5E+05**	**5.2E+04**	**7.8E+04**	**2.0E+03**	**3.9E+02**	**1.2E+03**	**6.7E+01**

			Batter Drainage									
	Rainfall (mm)	Infiltration (mm)	Flow (m^3)	SO_4 (g)	Cl (g)	NO_3 (g)	Ca (g)	Mg (g)	Ni (g)	Co (g)	Al (g)	Fe (g)
2007	*152.7*	*92.2*	*111*	*8.8E+04*	*2.7E+03*	*4.7E+04*	*1.5E+04*	*1.6E+04*	*1.7E+02*	*3.2E+01*	*1.1E+01*	*2.1E+00*
2008	*179.7*	*104.5*	*121*	*5.5E+04*	*-2.9E+03*	*-2.7E+04*	*2.5E+03*	*3.8E+03*	*7.4E+01*	*1.8E+01*	*-6.4E+01*	*1.2E+00*
2009	*74.0*	*10.3*	*107*	*9.7E+04*	*2.7E+03*	*4.8E+04*	*1.2E+04*	*1.9E+04*	*4.3E+02*	*8.2E+01*	*1.9E+02*	*1.4E+01*
2010	*97.6*	*43.0*	*204*	*1.8E+05*	*7.1E+03*	*9.0E+04*	*2.7E+04*	*3.6E+04*	*7.5E+02*	*1.5E+02*	*2.4E+02*	*1.6E+01*
2011	*145.5*	*83.1*	*129*	*9.5E+04*	*3.5E+03*	*1.0E+04*	*1.0E+04*	*1.3E+04*	*1.4E+02*	*4.3E+01*	*3.5E+02*	*1.1E+01*
2012	*56.3*	*8.9*	*145*	*2.1E+05*	*5.8E+03*	*3.4E+04*	*2.0E+04*	*3.6E+04*	*8.7E+02*	*1.7E+02*	*8.0E+02*	*3.9E+01*
Total	**764**	**400**	**817**	**7.2E+05**	**1.9E+04**	**2.0E+05**	**8.6E+04**	**1.2E+05**	**2.4E+03**	**4.9E+02**	**1.5E+03**	**8.3E+01**

Table 3.3 – Select results of annual and cumulative core contributions to total drainage flow and loading. Infiltration estimates by Fretz 2013, updated by Krentz 2014.

			Core Contribution									
	Rainfall (mm)	Infiltration (mm)	Flow	SO_4	Cl	NO_3	Ca	Mg	Ni	Co	Al	Fe
2007	*152.7*	*92.2*	*0%*	*0%*	*0%*	*0%*	*0%*	*0%*	*0%*	*0%*	*0%*	*0%*
2008	*179.7*	*104.5*	*20%*	*46%*	*278%*	*211%*	*84%*	*76%*	*75%*	*69%*	*260%*	*94%*
2009	*74.0*	*10.3*	*8%*	*18%*	*40%*	*35%*	*26%*	*24%*	*26%*	*26%*	*25%*	*40%*
2010	*97.6*	*43.0*	*5%*	*9%*	*11%*	*16%*	*12%*	*12%*	*14%*	*14%*	*21%*	*24%*
2011	*145.5*	*83.1*	*26%*	*56%*	*67%*	*91%*	*66%*	*71%*	*85%*	*80%*	*59%*	*68%*
2012	*56.3*	*8.9*	*14%*	*31%*	*37%*	*61%*	*36%*	*39%*	*44%*	*42%*	*35%*	*25%*
Total	**764**	**400**	**13%**	**29%**	**48%**	**56%**	**38%**	**39%**	**45%**	**44%**	**43%**	**45%**

Table 3.4 – Select results of estimated total, core and batter drainage geochemistry concentrations calculated from annual and cumulative subsystem loading.

	Mean Total Concentration (mg L^{-1})								
	SO_4	Cl	NO_3	Ca	Mg	Ni	Co	Al	Fe
2007	*790*	*24*	*420*	*130*	*140*	*1.50*	*0.30*	*0.10*	*0.00*
2008	*660*	*11*	*160*	*100*	*100*	*1.90*	*0.40*	*0.30*	*0.10*
2009	*1000*	*39*	*640*	*140*	*220*	*5.00*	*1.00*	*2.10*	*0.20*
2010	*940*	*37*	*500*	*140*	*190*	*4.10*	*0.80*	*1.40*	*0.10*
2011	*1200*	*60*	*660*	*170*	*250*	*5.30*	*1.20*	*4.90*	*0.20*
2012	*1800*	*54*	*520*	*190*	*350*	*9.10*	*1.80*	*7.30*	*0.30*
Total	**1100**	**39**	**490**	**150**	**220**	**4.70**	**0.90**	**2.90**	**0.20**

	Mean Core Concentration (mg L^{-1})								
	SO_4	Cl	NO_3	Ca	Mg	Ni	Co	Al	Fe
2007	*n/a*	*n/a*	*n/a*	*n/a*	*n/a*	*n/a*	*n/a*	*n/a*	*n/a*
2008	*1500*	*140*	*1600*	*430*	*390*	*7.10*	*1.30*	*3.30*	*0.60*
2009	*2200*	*190*	*2700*	*440*	*640*	*15.00*	*3.00*	*6.50*	*1.00*
2010	*1900*	*90*	*1800*	*360*	*490*	*13.00*	*2.40*	*6.50*	*0.50*
2011	*2600*	*150*	*2300*	*430*	*670*	*17.00*	*3.70*	*11.00*	*0.50*
2012	*3800*	*140*	*2200*	*480*	*980*	*28.00*	*5.30*	*18.00*	*0.50*
Total	**2400**	**150**	**2100**	**430**	**640**	**16.00**	**3.20**	**9.50**	**0.60**

	Mean Batter Concentration (mg L^{-1})								
	SO_4	Cl	NO_3	Ca	Mg	Ni	Co	Al	Fe
2007	*790*	*24*	*420*	*130*	*140*	*1.50*	*0.30*	*0.10*	*0.00*
2008	*450*	*-20*	*-200*	*21*	*32*	*0.60*	*0.20*	*-1.00*	*0.00*
2009	*910*	*25*	*450*	*110*	*180*	*4.00*	*0.80*	*1.70*	*0.10*
2010	*890*	*35*	*440*	*130*	*180*	*3.70*	*0.70*	*1.20*	*0.10*
2011	*730*	*27*	*79*	*77*	*100*	*1.10*	*0.30*	*2.70*	*0.10*
2012	*1400*	*40*	*240*	*140*	*250*	*6.00*	*1.20*	*5.50*	*0.30*
Total	**890**	**23**	**250**	**110**	**150**	**3.00**	**0.60**	**1.90**	**0.10**

Table 3.5 – Pearson product-moment correlation analysis in the total drainage system. Significance testing for all results in black are at $P < 0.05$ level. Results in grey show no significant correlation.

	Air Temp	Core Temp	pH	EC	Cl	NO_3-N	SO_4	Ca	Mg	Na	Si	K	Al	Fe	Co	Ni	Cu	Zn	Cd
Flow	*0.56*	*0.65*	*0.06*	*0.17*	*0.11*	*0.04*	*0.26*	*0.14*	*0.18*	*0.14*	*0.32*	*0.21*	*0.34*	*0.31*	*0.28*	*0.27*	*0.15*	*0.32*	*0.23*
Air Temp		*0.54*	*0.29*	*0.35*	*0.43*	*0.43*	*0.32*	*0.39*	*0.40*	*0.42*	*0.09*	*0.29*	*0.06*	*0.05*	*0.30*	*0.31*	*0.03*	*0.17*	*0.33*
Core Temp			*0.23*	*0.50*	*0.37*	*0.33*	*0.60*	*0.53*	*0.49*	*0.47*	*0.73*	*0.59*	*0.44*	*0.33*	*0.53*	*0.53*	*0.29*	*0.51*	*0.49*
pH				*0.33*	*0.33*	*0.31*	*0.36*	*0.31*	*0.37*	*0.33*	*0.24*	*0.25*	*0.41*	*0.14*	*0.40*	*0.39*	*0.32*	*0.39*	*0.41*
EC					*0.95*	*0.94*	*0.95*	*0.96*	*0.98*	*0.97*	*0.66*	*0.91*	*0.58*	*0.44*	*0.87*	*0.88*	*0.53*	*0.71*	*0.88*
Cl						*0.97*	*0.87*	*0.92*	*0.95*	*0.96*	*0.59*	*0.84*	*0.52*	*0.37*	*0.83*	*0.83*	*0.50*	*0.66*	*0.85*
NO_3-N							*0.82*	*0.91*	*0.92*	*0.94*	*0.53*	*0.83*	*0.40*	*0.33*	*0.75*	*0.76*	*0.42*	*0.54*	*0.77*
SO_4								*0.93*	*0.97*	*0.93*	*0.73*	*0.90*	*0.69*	*0.51*	*0.93*	*0.93*	*0.58*	*0.81*	*0.92*
Ca									*0.95*	*0.96*	*0.67*	*0.92*	*0.50*	*0.35*	*0.82*	*0.83*	*0.48*	*0.66*	*0.85*
Mg										*0.98*	*0.66*	*0.91*	*0.63*	*0.48*	*0.92*	*0.93*	*0.56*	*0.77*	*0.93*
Na											*0.59*	*0.92*	*0.52*	*0.40*	*0.85*	*0.86*	*0.45*	*0.67*	*0.86*
Si												*0.70*	*0.65*	*0.47*	*0.74*	*0.72*	*0.66*	*0.75*	*0.74*
K													*0.50*	*0.44*	*0.81*	*0.81*	*0.47*	*0.65*	*0.80*
Al														*0.65*	*0.82*	*0.81*	*0.79*	*0.91*	*0.80*
Fe															*0.59*	*0.60*	*0.51*	*0.59*	*0.54*
Co																*0.99*	*0.73*	*0.94*	*0.98*
Ni																	*0.71*	*0.92*	*0.97*
Cu																		*0.82*	*0.72*
Zn																			*0.93*

Table 3.6 – Pearson product-moment correlation analysis in the core drainage system. Significance testing for all results in black are at $P < 0.05$ level. Results in grey show no significant correlation.

	Air Temp	Core Temp	pH	EC	Cl	NO_3-N	SO_4	Ca	Mg	Na	Si	K	Al	Fe	Co	Ni	Cu	Zn	Cd
Flow	*0.24*	*0.48*	*0.08*	*0.04*	*0.19*	*0.08*	*0.15*	*0.20*	*0.12*	*0.09*	*0.06*	*0.11*	*0.09*	*0.09*	*0.07*	*0.03*	*0.02*	*0.11*	*0.12*
Air Temp		*0.54*	*0.15*	*0.07*	*0.02*	*0.02*	*0.01*	*0.07*	*0.07*	*0.09*	*0.23*	*0.27*	*0.02*	*0.19*	*0.05*	*0.04*	*0.03*	*0.07*	*0.14*
Core Temp			*0.14*	*0.29*	*0.18*	*0.12*	*0.40*	*0.46*	*0.28*	*0.26*	*0.15*	*0.31*	*0.03*	*0.02*	*0.19*	*0.20*	*0.05*	*0.16*	*0.17*
pH				*0.19*	*0.13*	*0.25*	*0.39*	*0.00*	*0.29*	*0.25*	*0.47*	*0.21*	*0.43*	*0.12*	*0.43*	*0.42*	*0.44*	*0.45*	*0.44*
EC					*0.76*	*0.86*	*0.63*	*0.79*	*0.81*	*0.82*	*0.38*	*0.81*	*0.60*	*0.57*	*0.60*	*0.59*	*0.64*	*0.51*	*0.49*
Cl						*0.89*	*0.62*	*0.79*	*0.82*	*0.88*	*0.20*	*0.78*	*0.49*	*0.60*	*0.50*	*0.51*	*0.56*	*0.44*	*0.44*
NO_3-N							*0.62*	*0.74*	*0.90*	*0.93*	*0.31*	*0.78*	*0.68*	*0.64*	*0.63*	*0.62*	*0.74*	*0.56*	*0.55*
SO_4								*0.56*	*0.84*	*0.78*	*0.70*	*0.77*	*0.68*	*0.43*	*0.89*	*0.90*	*0.71*	*0.83*	*0.83*
Ca									*0.71*	*0.76*	*0.26*	*0.82*	*0.41*	*0.43*	*0.36*	*0.36*	*0.49*	*0.32*	*0.30*
Mg										*0.98*	*0.52*	*0.83*	*0.75*	*0.58*	*0.83*	*0.82*	*0.79*	*0.77*	*0.77*
Na											*0.42*	*0.84*	*0.69*	*0.61*	*0.74*	*0.75*	*0.77*	*0.68*	*0.67*
Si												*0.46*	*0.59*	*0.03*	*0.65*	*0.66*	*0.59*	*0.64*	*0.66*
K													*0.60*	*0.46*	*0.67*	*0.69*	*0.67*	*0.63*	*0.62*
Al														*0.40*	*0.77*	*0.75*	*0.94*	*0.81*	*0.76*
Fe															*0.47*	*0.47*	*0.49*	*0.42*	*0.34*
Co																*0.99*	*0.77*	*0.94*	*0.95*
Ni																	*0.76*	*0.92*	*0.93*
Cu																		*0.79*	*0.72*
Zn																			*0.97*

Table 3.7 – Pearson product-moment correlation analysis in the batter drainage system. Significance testing for all results in black are at $P < 0.05$ level. Results in grey show no significant correlation.

	Air Temp	Core Temp	pH	EC	Cl	NO_3-N	SO_4	Ca	Mg	Na	Si	K	Al	Fe	Co	Ni	Cu	Zn	Cd
Flow	*0.59*	*0.59*	*0.01*	*0.05*	*0.07*	*0.09*	*0.03*	*0.08*	*0.03*	*0.05*	*0.01*	*0.03*	*0.07*	*0.05*	*0.01*	*0.00*	*0.05*	*0.07*	*0.07*
Air Temp		*0.54*	*0.28*	*0.20*	*0.21*	*0.20*	*0.22*	*0.17*	*0.22*	*0.23*	*0.12*	*0.19*	*0.03*	*0.05*	*0.11*	*0.13*	*0.04*	*0.04*	*0.14*
Core Temp			*0.26*	*0.13*	*0.05*	*0.03*	*0.25*	*0.07*	*0.12*	*0.10*	*0.32*	*0.19*	*0.10*	*0.01*	*0.07*	*0.08*	*0.01*	*0.11*	*0.14*
pH				*0.84*	*0.82*	*0.81*	*0.82*	*0.81*	*0.82*	*0.83*	*0.47*	*0.82*	*0.83*	*0.66*	*0.77*	*0.79*	*0.79*	*0.75*	*0.35*
EC					*0.98*	*0.97*	*0.93*	*0.98*	*0.96*	*0.98*	*0.52*	*0.97*	*0.83*	*0.66*	*0.88*	*0.91*	*0.86*	*0.76*	*0.37*
Cl						*0.98*	*0.89*	*0.98*	*0.94*	*0.97*	*0.47*	*0.95*	*0.80*	*0.64*	*0.84*	*0.88*	*0.84*	*0.70*	*0.29*
NO_3-N							*0.89*	*0.98*	*0.96*	*0.98*	*0.53*	*0.96*	*0.84*	*0.66*	*0.89*	*0.92*	*0.90*	*0.77*	*0.35*
SO_4								*0.89*	*0.97*	*0.95*	*0.53*	*0.93*	*0.80*	*0.63*	*0.91*	*0.93*	*0.77*	*0.82*	*0.61*
Ca									*0.94*	*0.97*	*0.54*	*0.97*	*0.84*	*0.64*	*0.87*	*0.90*	*0.89*	*0.74*	*0.28*
Mg										*0.99*	*0.53*	*0.95*	*0.84*	*0.68*	*0.94*	*0.95*	*0.85*	*0.84*	*0.56*
Na											*0.52*	*0.97*	*0.83*	*0.67*	*0.92*	*0.94*	*0.85*	*0.80*	*0.47*
Si												*0.60*	*0.58*	*0.28*	*0.55*	*0.56*	*0.62*	*0.56*	*0.20*
K													*0.83*	*0.63*	*0.88*	*0.91*	*0.86*	*0.76*	*0.36*
Al														*0.65*	*0.90*	*0.90*	*0.94*	*0.92*	*0.44*
Fe															*0.69*	*0.70*	*0.64*	*0.69*	*0.43*
Co																*0.99*	*0.90*	*0.95*	*0.64*
Ni																	*0.91*	*0.93*	*0.61*
Cu																		*0.87*	*0.33*
Zn																			*0.70*

Table 3.8 – Full system control level results, modified from Pearson correlation analysis results for each scale of the test pile system (Core-Batter-Total). Results summarize the number of good correlations (> |0.7|) for a given parameter, divided by the total number of possible cases.

Full System Control	
Parameter	**Good Correlations**
Mg	*86%*
Ni	*84%*
Co	*82%*
SO_4	*76%*
K	*71%*
Zn	*71%*
Na	*69%*
NO_3-N	*63%*
Cu	*61%*
EC	*59%*
Ca	*57%*
Cl	*57%*
Al	*53%*
Cd	*53%*
pH	*25%*
Si	*12%*
Core Temp	*2%*
Air Temp	*0%*
Fe	*0%*
Flow	*0%*

Table 3.9 – Cross-environment control level results, modified from Pearson correlation analysis results for each test pile subsystem pair (Core-Batter-Total). Results summarize the number of good correlations (> |0.7|) for a given parameter which are consistent across subsystem environments, as a proportion of the total number of possible cases.

Cross-Environment Control	
Parameter	**Good Correlations**
Mg	*78%*
Ni	*72%*
Co	*68%*
SO_4	*60%*
Zn	*60%*
K	*51%*
Na	*50%*
Cu	*43%*
NO_3-N	*41%*
Al	*34%*
EC	*32%*
Ca	*31%*
Cd	*31%*
Cl	*31%*
Air Temp	*0%*
Core Temp	*0%*
Fe	*0%*
Flow	*0%*
pH	*0%*
Si	*0%*

Table 3.10 – Estimated total mass of waste rock material, including the total mass of S, Ni, Co and Fe divided into the core, batter and total pile systems. Masses are further defined based on the < 5 mm waste rock fraction, < 50 mm waste rock fraction, and full grain size spectrum waste rock fraction.

	Test Pile Composition																
	Construction		Full Pile (kg)					< 50 mm Mass (kg)					< 5 mm Reactive Mass (kg)				
	Aerial (m^2)	Volume (m^3)	Rock	S	Ni	Co	Fe	Rock	S	Ni	Co	Fe	Rock	S	Ni	Co	Fe
Core	*1.35E+03*	*1.82E+04*	*3.7E+07*	*1.9E+04*	*1.4E+02*	*3.5E+01*	*2.8E+04*	*1.2E+07*	*7.5E+03*	*5.5E+01*	*1.4E+01*	*1.1E+04*	*5.3E+06*	*3.8E+03*	*2.8E+01*	*7.0E+00*	*5.7E+03*
Batter	*1.65E+03*	*1.37E+04*	*2.8E+07*	*1.4E+04*	*1.0E+02*	*2.6E+01*	*2.1E+04*	*9.3E+06*	*5.7E+03*	*4.2E+01*	*1.0E+01*	*8.4E+03*	*4.0E+06*	*2.9E+03*	*2.1E+01*	*5.3E+00*	*4.3E+03*
Full Pile	*3.00E+03*	*3.19E+04*	*6.5E+07*	*3.3E+04*	*2.4E+02*	*6.1E+01*	*4.9E+04*	*2.2E+07*	*1.3E+04*	*9.7E+01*	*2.4E+01*	*2.0E+04*	*9.2E+06*	*6.7E+03*	*4.9E+01*	*1.2E+01*	*9.9E+03*

Table 3.11 – Estimated annual and cumulative release of S, Ni, Co and Fe from the < 5 mm grain size fraction of waste rock. Results are presented as release from the total test pile system, and subdivided into the core and batter subsystems.

	Sulfur Release					
	Full Pile (kg)	Percent Total	Core (kg)	Percent Total	Batter (kg)	Percent Total
2007	2.93E+01	0.4%	0.0E+00	0.0%	2.9E+01	1.0%
2008	3.36E+01	0.5%	1.5E+01	0.4%	1.8E+01	0.6%
2009	3.97E+01	0.6%	7.3E+00	0.2%	3.2E+01	1.1%
2010	6.67E+01	1.0%	6.2E+00	0.2%	6.1E+01	2.1%
2011	7.10E+01	1.1%	3.9E+01	1.0%	3.2E+01	1.1%
2012	1.00E+02	1.5%	3.1E+01	0.8%	7.0E+01	2.4%
Total	**3.41E+02**	**5.1%**	**9.9E+01**	**2.6%**	**2.4E+02**	**8.4%**

	Nickel Release					
	Full Pile (kg)	Percent Total	Core (kg)	Percent Total	Batter (kg)	Percent Total
2007	1.68E-01	0.3%	0.0E+00	0.0%	1.7E-01	0.8%
2008	2.95E-01	0.6%	2.2E-01	0.8%	7.4E-02	0.4%
2009	5.76E-01	1.2%	1.5E-01	0.5%	4.3E-01	2.0%
2010	8.80E-01	1.8%	1.3E-01	0.5%	7.5E-01	3.6%
2011	9.26E-01	1.9%	7.9E-01	2.8%	1.4E-01	0.7%
2012	1.54E+00	3.2%	6.7E-01	2.4%	8.7E-01	4.2%
Total	**4.39E+00**	**9.0%**	**2.0E+00**	**7.0%**	**2.4E+00**	**11.6%**

	Cobalt Release					
	Full Pile (kg)	Percent Total	Core (kg)	Percent Total	Batter (kg)	Percent Total
2007	3.21E-02	0.3%	0.0E+00	0.0%	3.2E-02	0.6%
2008	5.94E-02	0.5%	4.1E-02	0.6%	1.8E-02	0.3%
2009	1.11E-01	0.9%	2.9E-02	0.4%	8.2E-02	1.6%
2010	1.70E-01	1.4%	2.4E-02	0.3%	1.5E-01	2.8%
2011	2.15E-01	1.8%	1.7E-01	2.5%	4.3E-02	0.8%
2012	2.98E-01	2.4%	1.3E-01	1.8%	1.7E-01	3.3%
Total	**8.85E-01**	**7.2%**	**3.9E-01**	**5.6%**	**4.9E-01**	**9.4%**

	Iron Release					
	Full Pile (g)	Percent Total	Core (g)	Percent Total	Batter (g)	Percent Total
2007	2.14E+00	0.0%	0.0E+00	0.0%	2.1E+00	0.0%
2008	1.83E+01	0.0%	1.7E+01	0.0%	1.2E+00	0.0%
2009	2.42E+01	0.0%	9.8E+00	0.0%	1.4E+01	0.0%
2010	2.04E+01	0.0%	4.8E+00	0.0%	1.6E+01	0.0%
2011	3.28E+01	0.0%	2.2E+01	0.0%	1.1E+01	0.0%
2012	5.24E+01	0.0%	1.3E+01	0.0%	3.9E+01	0.0%
Total	**1.50E+02**	**0.0%**	**6.7E+01**	**0.0%**	**8.3E+01**	**0.0%**

Chapter 4: Conclusions

4.1 Research Summary and Conclusions

This study focussed on results from a large (50m x 60m x 15m, L x W x H), low-sulfide (0.053 wt. % S), experimental waste-rock pile constructed at the Diavik diamond mine in the Northwest Territories, Canada. The research site is located in a region of continuous permafrost which undergoes significant annual temperature fluctuations resulting in complete internal freeze-thaw cycling within the waste-rock pile. The test pile was heavily instrumented to monitor internal temperature, air content, water content, fluid flow, mineralogy, microbiology, pore-water geochemistry and drainage geochemistry with substantial temporal and spatial resolution.

Thermal monitoring revealed that annual freeze-thaw cycling continuously altered the mass of rock and internal structure of the pile which could undergo active weathering and permit water flow. Conditions of stable internal water flow and geochemistry were defined to delineate the influence of freeze-thaw cycling. The completion of six annual freeze-thaw cycles (2007 to 2012) revealed significant geochemical evolution of pore-water and drainage water characterized by a low pH front, a release of oxidation products and a stepwise progression through acid neutralization processes (depletion of available carbonates; equilibrium with respect to aluminium hydroxide phases and subsequent iron(III) hydroxide phases). The geochemical evolution of the pore water provided an approximate timeline for the establishment of quasi steady state flow and dynamic internal geochemical equilibrium. Results indicate that vertical profiles of pore-water evolution in waste rock systems react in similar ways to mine tailings systems, despite fundamental differences in flow systems in these two types of waste. Provided that similar physiochemical conditions exist, this study suggests that the geochemical evolution of pore water in mine tailing systems offer a suitable reference when waste-rock studies are

unavailable. In addition, the movement of a downward weathering front within matrix pore water suggests that reactive transport models employing Richard's equation might be applicable when modelling many unsaturated waste-rock systems.

Comparison of the geochemistry of migrating water that was collected in small-scale basal lysimeters within the test pile core and the overall basal drainage leachate allowed for an evaluation of the timing and retention of infiltrating water during each annual freeze-thaw cycle. In accordance with thermal data, results indicated that fluid flow and solute loading from the base of a waste-rock pile could be divided into discrete core and batter subsystems. Estimated mean concentrations of various solutes were significantly higher in the core compared to the batter. Annual geochemical trends of drainage water from the core of the test pile revealed high concentration 'spring flushes' which were largely explained by a combination of the build-up of oxidation products over the winter and fluid residence time. Annual geochemical trends of drainage water from the total test pile base revealed that early-season leachate was dominated by snowmelt and batter flow and late-season leachate was dominated by contributions from the core of the pile. A thermal model describing the active zone cycling within the experimental waste-rock system was consistent with observed trends in the total drainage geochemistry. Results show that field measurements or modeling of annual freeze-thaw cycles in waste-rock piles is required before predictive flow or geochemical modelling can be considered.

Pearson product-moment correlation analysis results from core, batter and total drainage leachate were used for the identification of shared element sources and for assessing the complexity and spatial continuity of the release, transport and attenuation mechanisms, which control the mobility of several trace and major elements in the test pile system. This study highlights the value that this type of statistical analysis provides in the identification of processes

which govern metal mobility in ARD systems as well as the identification of elements which would be valuable targets for reactive transport modelling studies in similar waste-rock systems (specifically Ni, Co, Mg and SO_4).

This study also demonstrates that waste-rock basal drainage loading can be quantitatively divided into core and batter subsystems by up-scaling data from representative core lysimeters to the full core area, and by using a mass-balance approach to calculate batter characteristics from total drainage and core drainage loading. Spatial loading data provides quantitative estimates of release from test pile subsystems on annual and cumulative scales. Despite minor contributions from the core of the test pile to drainage outflow, up to 50 % of many solute loads were derived from this zone. In addition, core contributions to the loading of elements with similar sources and mobility controls (*eg*. Ni and Co from pyrrhotite weathering) were consistently in close agreement. Results indicate that observations of spatial contributions to drainage loading not only provide a valuable estimate of loading distributions, but also assist in the identification of the source, release and transport mechanisms which are common amongst different trace and major elements in ARD systems. Overall, results highlight the necessity to divide drainage leachate modelling in cold climate waste-rock systems into discrete core and batter subsystems when evaluating the timing and magnitude of metal release into the environment. In addition, findings emphasize the need to include the annual distribution of snow and resulting snowmelt contributions to system water budgets. Future closure plans should consider the impact of physiographic factors such as wind speed and direction, waste-pile orientation, shape and vegetation cover on the distribution of snow and resulting infiltration.

Although oxidation has been shown to persist at sub-zero temperatures, element release estimates from this study indicate that the physical isolation of the core of a waste-rock pile

through progressive freezing will significantly decrease effluent concentrations and loadings. In the future, cold climate waste-rock pile designs should place emphasis on the role of thermal covers and the engineered aggradation of permafrost into waste-rock pile cores. Despite a frozen core, waste-rock piles will still form a shallow active layer in the summer, the thickness of which will depend on several factors; however drainage concentrations and loadings in this limited active zone should be substantially reduced. In addition, a frozen core will substantially decrease the total mass of material available to contribute to ARD processes, thus decreasing the long term environmental impact of the mine site. A comprehensive understanding of freeze-thaw cycling in waste-rock piles, derived from field observations combined with thermal modelling, provides a strong foundation for the application of future up-scaling, and reactive transport modelling of drainage leachate in cold climates.

References

Ahonen, L., Tuovinen, O.H., 1992. Bacterial oxidation of sulfide minerals in column leaching experiments at suboptimal temperatures. Appl. Environ. Microbiol. 58, 600-606.

Al, T.A., Blowes, D.W., Martin, C.J., Cabri, L.J., Jambor, J.L., 1997. Aqueous geochemistry and analysis of pyrite surfaces in suifide-rich mine tailings. Geochim. Cosmochim. Acta 61, 2353-2366.

Allen, R.G., Pereira, L.S., Raes, D., Smith, M., 1998. Crop evapotranspiration: Guidelines for computing crop water requirements. FAO Irrigation and drainage paper 56, Food and Agriculture Organization of the United Nations, Rome, Italy.

Amoah, N., Haymont, R., Campbell, G., 2011. Benefits of timely and valid geochemical characterization of mine waste for life of mine and closure planning: A case study of Newmont Boddington Gold Mine in Western Australia. Tailings Mine Waste - Proc. Int. Conf. Tailings Mine Waste , 253-262.

Amos, R.T., Blowes, D.W., Smith, L., Sego, D.C., 2009. Measurement of wind-induced pressure gradients in a waste rock pile. Vadose Zone J. 8, 953-962.

Anawar, H.M., 2013. Impact of climate change on acid mine drainage generation and contaminant transport in water ecosystems of semi-arid and arid mining areas. Phys. Chem. Earth 58-60, 13-21.

Bailey, B.L., Ph.D., University of Waterloo, 2013. Geochemical and microbiological characterization of effluent and pore water from low-sulfide content waste rock.

Bailey, B.L., Smith, L.J.D., Blowes, D.W., Ptacek, C.J., Smith, L., Sego, D.C., 2013. The Diavik Waste Rock Project: Persistence of contaminants from blasting agents in waste rock effluent. Appl. Geochem. 36, 256-270.

Balistrieri, L.S., Box, S.E., Tonkin, J.W., 2003. Modeling precipitation and sorption of elements during mixing of river water and porewater in the Coeur d'Alene River basin. Environ. Sci. Technol. 37, 4694-4701.

Beven, K., Germann, P., 1982. Macropores and water flow in soils. Water Resour. Res. 18, 1311-1325.

Blowes, D.W., Logsdon, M.J., 1998. Diavik geochemistry baseline report. Prepared by Sala Groundwater Inc. and Geochimica Inc. for Diavik Diamond Mines Inc. and submitted to the Canadian Environmental Assessment Agency, variously paged.

Blowes, D.W., Jambor, J.L., 1990. The pore-water geochemistry and the mineralogy of the vadose zone of sulfide tailings, Waite Amulet, Quebec, Canada. Appl. Geochem. 5, 327-346.

Blowes, D.W., Jambor, J.L., Hanton-Fong, C.J., Lortie, L., Gould, W.D., 1998. Geochemical, mineralogical and microbiological characterization of a sulphide-bearing carbonate-rich gold-mine tailings impoundment, Joutel, Quebec. Appl. Geochem. 13, 687-705.

Blowes, D.W., Ptacek, C.J., Jambor, J.L., Weisener, C.G., 2003. 9.05 - The Geochemistry of Acid Mine Drainage. In: Editors-in-Chief: Heinrich D. Holland and Karl K. Turekian (Eds.), Treatise on Geochemistry. Pergamon, Oxford, pp. 149-204.

Chi, X., Amos, R.T., Stastna, M., Blowes, D.W., Sego, D.C., Smith, L., 2013. The Diavik Waste Rock Project: Implications of wind-induced gas transport. Appl. Geochem. 36, 246-255.

Dawson, R.F., Morin, K.A., 1996. Acid mine drainage in permafrost regions: issues, control strategies and research requirements. MEND Project 1.61.2.

Dyer, J.A., Trivedi, P., Scrivner, N.C., Sparks, D.L., 2004. Surface complexation modeling of zinc sorption onto ferrihydrite. J. Colloid Interface Sci. 270, 56-65.

Dzombak, D.A., Morel, F.M.M., 1990. Surface Complexation Modeling: Hydrous Ferric Oxide. John Wiley & Sons, Inc., Canada.

Elberling, B., 2005. Temperature and oxygen control on pyrite oxidation in frozen mine tailings. Cold Reg. Sci. Technol. 41, 121-133.

Elberling, B., Søndergaard, J., Jensen, L.A., Schmidt, L.B., Hansen, B.U., Asmund, G., Balic-Zunic, T., Hollesen, J., Hanson, S., Jansson, P.-., Friborg, T., 2007. Arctic vegetation damage by winter-generated coal mining pollution released upon thawing. Environ. Sci. Technol. 41, 2407-2413.

Environment Canada, 2012. Monthly data report for Ekati A, Northwest Territories. 2013.

Fretz, N., M.Sc., University of British Columbia, 2013. Multi-year Hydrolic Response of Experimental Waste-Rock Piles in a Cold Climate: Active-Zone Development, Net Infiltration, and Fluid Flow.

Gunsinger, M.R., Ptacek, C.J., Blowes, D.W., Jambor, J.L., 2006a. Evaluation of long-term sulfide oxidation processes within pyrrhotite-rich tailings, Lynn Lake, Manitoba. J. Contam. Hydrol. 83, 149-170.

Gunsinger, M.R., Ptacek, C.J., Blowes, D.W., Jambor, J.L., Moncur, M.C., 2006b. Mechanisms controlling acid neutralization and metal mobility within a Ni-rich tailings impoundment. Appl. Geochem. 21, 1301-1321.

Haines, T.S., Lloyd, J.W., 1985. Controls on silica in groundwater environments in the United Kingdom. Journal of Hydrology 81, 277-295.

Hannam, S.E.S., M.Sc., University of Waterloo, 2012. Diavik Waste Rock Project: Geochemical and mineralogical investigations of waste-rock weathering.

Hiemstra, T., Barnett, M.O., van Riemsdijk, W.H., 2007. Interaction of silicic acid with goethite. J. Colloid Interface Sci. 310, 8-17.

ICOLD, 1996. A Guide to Tailings Dams and Impoundments: Design, Construction, Use and Rehabilitation.

Jambor, J.L., 1997. Mineralogy of the Diavik Lac de Gras kimberlites and host rocks. Prepared by Leslie Investment Ltd. For Diavik Diamond Mines Ltd and submitted to the Canadian Environmental Assessment Agency, 187 p.

Jamieson, H.E., 2011. Geochemistry and mineralogy of solid mine waste: Essential knowledge for predicting environmental impact. Elements 7, 381-386.

Johnson, D.B., Hallberg, K.B., 2005. Acid mine drainage remediation options: A review. Sci. Total Environ. 338, 3-14.

Jurjovec, J., Ptacek, C.J., Blowes, D.W., 2002. Acid neutralization mechanisms and metal release in mine tailings: A laboratory column experiment. Geochim. Cosmochim. Acta 66, 1511-1523.

Krentz, A., M.A.Sc., University of British Columbia, In Progress. Hydrology of Waste Rock Piles in Permafrost Environments.

Kyhn, C., Elberling, B., 2001. Frozen cover actions limiting AMD from mine waste deposited on land in Arctic Canada. Cold Reg. Sci. Technol. 32, 133-142.

Langman, J.B., In Progress. Early weathering evolution of sulfide in a low-sulfur, granitic, mine-waste rock in an Arctic environment, Northwest Territories, Canada.

Langman, J.B., In Progress. The Evolution of Sulfur and Nickel in Pyrrhotite with Weathering of a Low-Sulfide, Granitic, Mine-Waste Rock.

Lindsay, M.B.J., Condon, P.D., Jambor, J.L., Lear, K.G., Blowes, D.W., Ptacek, C.J., 2009. Mineralogical, geochemical, and microbial investigation of a sulfide-rich tailings deposit characterized by neutral drainage. Appl. Geochem. 24, 2212-2221.

Malmström, M.E., Destouni, G., Banwart, S.A., Strömberg, B.H.E., 2000. Resolving the scale-dependence of mineral weathering rates. Environmental Science and Technology 34, 1375-1378.

Marescotti, P., Azzali, E., Servida, D., Carbone, C., Grieco, G., de Capitani, L., Lucchetti, G., 2010. Mineralogical and geochemical spatial analyses of a waste-rock dump at the Libiola Fe-Cu sulphide mine (Eastern Liguria, Italy). Environmental Earth Sciences 61, 187-199.

Mayer, K.U., Frind, E.O., Blowes, D.W., 2002. Multicomponent reactive transport modeling in variably saturated porous media using a generalized formulation for kinetically controlled reactions. Water Resour. Res. 38, 131-1321.

Moncur, M.C., Ptacek, C.J., Blowes, D.W., Jambor, J.L., 2005. Release, transport and attenuation of metals from an old tailings impoundment. Appl. Geochem. 20, 639-659.

Neuner, M., Smith, L., Blowes, D.W., Sego, D.C., Smith, L.J.D., Fretz, N., Gupton, M., 2013. The Diavik Waste Rock Project: Water flow through mine waste rock in a permafrost terrain. Appl. Geochem. 36, 222-233.

Nichol, C., Smith, L., Beckie, R., 2005. Field-scale experiments of unsaturated flow and solute transport in a heterogeneous porous medium. Water Resour. Res. 41, 1-11.

Nordstrom, D.K., 1982. Aqueous pyrite oxidation and the consequent formation of secondary iron minerals. In: Kittrick, J.A., Fanning, D.F. and Hossner, L.R. (Eds.), Acid Sulfate WeatheringSoil Science Society of America, pp. 37-56.

Nordstrom, D.K., Alpers, C.N., 1999. Negative pH, efflorescent mineralogy, and consequences for environmental restoration at the iron mountain superfund site, California. Proc. Natl. Acad. Sci. U. S. A. 96, 3455-3462.

Parkhurst, D.L., Appelo, C.A.J., 1999. User's guide to PHREEQC (Version 2) - A computer program for speciation, batch-reaction, one-dimensional transport, and inverse geochemical calculations. 99-4259.

Paulson, A.J., Balistrieri, L., 1999. Modeling removal of Cd, Cu, Pb, and Zn in acidic groundwater during neutralization by ambient surface waters and groundwaters. Environ. Sci. Technol. 33, 3850-3856.

Pham, N.H., Ph.D., University of Alberta, 2013. Heat Transfer in Waste-Rock Piles Constructed in a Continuous Permafrost Region.

Pham, N.H., Sego, D.C., Arenson, L.U., Blowes, D.W., Amos, R.T., Smith, L., 2013. The Diavik Waste Rock Project: Measurement of the thermal regime of a waste-rock test pile in a permafrost environment. Appl. Geochem. 36, 234-245.

Shipitalo, M.J., Edwards, W.M., 1996. Effects of initial water content on macropore/matrix flow and transport of surface-applied chemicals. J. ENVIRON. QUAL. 25, 662-670.

Smith, L., 2006. Test Piles Project 2006 Construction Summary. A report prepared for Diavik Diamond Mines by FDA Engineering.

Smith, L.J.D., Bailey, B.L., Blowes, D.W., Jambor, J.L., Smith, L., Sego, D.C., 2013a. The Diavik Waste Rock Project: Initial geochemical response from a low sulfide waste rock pile. Appl. Geochem. 36, 210-221.

Smith, L.J.D., Blowes, D.W., Jambor, J.L., Smith, L., Sego, D.C., Neuner, M., 2013b. The Diavik Waste Rock Project: Particle size distribution and sulfur characteristics of low-sulfide waste rock. Appl. Geochem. 36, 200-209.

Smith, L.J.D., Moncur, M.C., Neuner, M., Gupton, M., Blowes, D.W., Smith, L., Sego, D.C., 2013c. The Diavik Waste Rock Project: Design, construction, and instrumentation of field-scale experimental waste-rock piles. Appl. Geochem. 36, 187-199.

Søndergaard, J., Asmund, G., Seitz, M., Glahder, C., 2012. Naturally elevated spring-time fluxes of zinc and other elements from a sulphide ore deposit area in Citronen Fjord, North Greenland (83°N). Cold Reg. Sci. Technol. 71, 90-94.

Søndergaard, J., Elberling, B., Asmund, G., 2008. Metal speciation and bioavailability in acid mine drainage from a high Arctic coal mine waste rock pile: Temporal variations assessed through high-resolution water sampling, geochemical modelling and DGT. Cold Reg. Sci. Technol. 54, 89-96.

Søndergaard, J., Elberling, B., Asmund, G., Gudum, C., Iversen, K.M., 2007. Temporal trends of dissolved weathering products released from a high Arctic coal mine waste rock pile in Svalbard (78°N). Appl. Geochem. 22, 1025-1038.

Sracek, O., Choquette, M., Gélinas, P., Lefebvre, R., Nicholson, R.V., 2004. Geochemical characterization of acid mine drainage from a waste rock pile, Mine Doyon, Québec, Canada. J. Contam. Hydrol. 69, 45-71.

Stockwell, J., Smith, L., Jambor, J.L., Beckie, R., 2006. The relationship between fluid flow and mineral weathering in heterogeneous unsaturated porous media: A physical and geochemical characterization of a waste-rock pile. Appl. Geochem. 21, 1347-1361.

Strömberg, B., Banwart, S.A., 1999. Experimental study of acidity-consuming processes in mining waste rock: Some influences of mineralogy and particle size. Appl. Geochem. 14, 1-16.

Tonkin, J.W., Balistrieri, L.S., Murray, J.W., 2002. Modeling metal removal onto natural particles formed during mixing of acid rock drainage with ambient surface water. Environ. Sci. Technol. 36, 484-492.

Wagner, K., Smith, L., Beckie, R., 2006. Hydrogeochemical characterization of effluent from mine waste rock, Cluff Lake, Saskatchewan.

Yanful, E.K., Riley, M.D., Woyshner, M.R., Duncan, J., 1993. Construction and monitoring of a composite soil cover on an experimental waste-rock pile near Newcastle, New Brunswick, Canada. Canadian Geotechnical Journal 30, 588-599.